Bone Mineral Density and Fracture Risk Assessment for Patients Undergoing Total Hip Replacement

by

Þröstur Pétursson

Thesis of 60 ECTS credits
Master of Science in Biomedical Engineering

December 2013

Bone Mineral Density and Fracture Risk Assessment for Patients Undergoing Total Hip Replacement

Þröstur Pétursson

Thesis of 60 ECTS credits submitted to the School of Science and Engineering
at Reykjavík University in partial fulfillment
of the requirements for the degree of
Master of Science in Biomedical Engineering

December 2013

Supervisor:

Paolo Gargiulo, Phd
Assistant Professor, Reykjavík University, Iceland

Halldór Jónsson Jr, MD, Phd
Professor, University Hospital of Iceland, Iceland

Ólafur Eysteinn Sigurjónsson, Phd
Assistant Professor, Reykjavík University, Iceland

Examiner(s):

Sigurður Brynjólfsson
Professor, University of Iceland, Iceland.

Bone Mineral Density and Fracture Risk Assessment for Patients Undergoing Total Hip Replacement

Þröstur Pétursson

60 ECTS thesis submitted to the School of Science and Engineering
at Reykjavík University in partial fulfillment
of the requirements for the degree of
Master of Science in Biomedical Engineering.

December 2013

Student:

_____

Þröstur Pétursson

Supervisor(s):

_____

Paolo Gargiulo

_____

Halldór Jónsson Jr

_____

Ólafur Eysteinn Sigurjónsson

Examiner:

_____

Sigurður Brynjólfsson

Healthy citizens are the greatest asset any country can have

Winston Churchill

Abstract

Total hip replacement is one of the most successful practiced orthopaedic treatments, restoring hip function and relieving patients of pain. During the surgery the femoral head and the bearing surface of the acetabulum are removed and replaced with a prosthetic stem and a socket respectively. There are two types of total hip replacement; one uses bone cement to fix the components (cemented) and one uses a press-fitting technique without cement (cementless).

Cementless stems are preferred for two reasons. First, they induce bone growth and make permanent bond with bone. Second, when the stems ultimately fail, the cementless stems are far easier to remove and the success of revisions is better. However, not everyone can handle the cementless procedure. Amongst the important criteria to choose the implant type are age and gender. Today there are no quantitative pre-operative procedures to choose the correct implants for patients.

Thirty-nine total hip replacement patients were enrolled in this study which introduces a novel procedure relying on computer tomography image aquisition to measure bone mineral density of patients and create finite element models used to calculate a fracture risk index. The goal is to answer the question whether the femur can handle the press-fitting surgery.

The results indicate that although the bone mineral density tends to decrease with age, there are some patients that deviate from this trend; they have to be identified and the correct implant selected for them. The fracture risk index results indicate that fracture risk is not dependent on bone mineral density, age or type of implant. However, bone mineral density measurements are able to indicate bone quality of patients.

Although the fracture risk index does not reflect real risk of failure, the results indicate that all patients are different. The bone mineral density measurements demonstrate bone quality beyond age and gender.

Keywords: Bone Mineral Density, Fracture Risk, Total hip Replacement, Finite Element Analysis, Bone Cement

Úrdráttur

Heildarmjaðmaliðskipti eru meðal farsælustu bæklunaraðgerða sem gerðar eru, en hún hjálpar sjúklingum með liðhrörnum að endurheimta hreyfigetu og linar verki í mjöðm. Aðgerðin felur í sér að skera höfuð lærleggsins af og fjarlægja eyðilagt brjósk augnkarls mjaðmarinnar og koma ígræðlingi fyrir í lærleggnum og bolla í augnkarlinum. Það eru tvær týpur af heildarmjaðmaliðskiptum, önnur notar beinsement til þess að festa íhlutina en hinni er þrýst inn með hamarshöggum án beinsements.

Það eru tvær ástæður fyrir því að betra er að nota ekki beinsement. Í fyrsta lagi ýtir sú aðferð undir innvöxt beins og veldur það fastri tengingu milli ígræðlings og beins. Í öðru lagi, þegar ígræðlingurinn losnar og það þarf að skipta um hann, er talsvert auðveldara að skipta ef ekki var notað beinsement. Þó eru ekki allir sem geta fengið ígræðling án beinsements, því það reynir á lærlegginn að koma honum fyrir. Læknar velja hentugari týpuna fyrir aðgerðina en aldur og kyn hafa mikil áhrif. Í dag eru engar magnbundnar aðferðir í notkun til að velja rétta tegund ígræðlings.

Þrjátíu og níu heildarmjaðmaliðskiptasjúklingar tóku þátt í þessari rannsókn sem kynnir aðferð sem byggir á tölvusneiðmyndum af sjúklingum til þess að mæla beinþéttleika og búa til bútalíkön sem notuð eru til þess að reikna brothættustuðul lærleggs fyrir aðgerð. Markmiðið er að svara því hvor gerðin af ígræðlingi hentar betur fyrir hvern sjúkling.

Niðurstöðurnar sýna að beinþéttni minnkar með aldri, en þó eru nokkrir sjúklingar frávik. Þessa sjúklinga þarf að finna og tryggja að þeir fái réttan ígræðling. Brothættustuðullinn sem reiknaður var virðist ekki gefa til kynna tengls við beinþéttleika, aldur eða týpu ígræðlings. Beinþéttnimælingarnar gefa hins vegar góða mynd af gæðum beins.

Þó brothættustðullinn endurspegli ekki raunverulega mynd af brothættunni, gefa niðrustöðurnar til kynna fjölbreytni sjúklinga. Beinþéttnin sem reiknuð var gefur vísbendingar um ástand beinsins umfram aldur og kyn.

Lykilorð: Heildarmjaðmaliðskipti, Beinþéttni, Brothættustuðull, Bútalíkön, Beinsement.

Acknowledgment

I would like to thank my supervisor Paolo Gargiulo, assistant professor at the University of Reykjavik, for the opportunity he presented to me, to work on this project. He has played a massive part in supporting me through this work.

I would also like to thank Halldór Jónsson Jr., at the National University Hospital of Iceland, for his contribution in making this study a reality. He was always ready to assist and his help sometimes went well beyond already great expectations.

I would like to thank Benedikt Magnússon, a co-worker and friend for the time we have spent together developing the ideas of this study.

Furthermore I would like to thank Gígja Magnúsdóttir and Grétar Halldórsson at Landspitali Gransásdeild for giving their time to work on this project with us.

This work was supported by the Scientific Research Fund of the National University Hospital of Iceland and the Rannís Innovations Fund.

List of Tables

List of Figures

Contents

1. Introduction

1.1. Motivation and Clinical Background

Total Hip Replacement (THR) is one of the most successful practiced orthopaedic treatments, restoring hip function and relieving patients of pain by replacing pathological hip joints with artificial ones. There are two components in THA, femoral and acetabular. During surgery, the femoral head is removed and a prosthetic stem is inserted into the femoral canal (the femoral component). Additionally, the articular surface of the acetabulum is removed to hold a metal cup with a plastic liner (acetabular component) where the head of the femoral stem goes into. There are two types of THR: One that fixes the femoral and acetabular components with cement (cemented THR), and one that uses no cement (Cementless).

In cemented THR, the stem and the acetabular cup are held in place with acrylic bone cement but cementless prosthetic components use the tensile elasticity of the bone as a method of fixation. There are two reasons why cementless stems should be the first choice for patients. First, eventually all THR will fail, usually after more than 10 years. When they fail, loosening of the stem is amongst the most prevalent causes. The quality of fixation of cemented stem tends to degrade over time [1] while cementless stems on the other hand, are press-fitted into the femoral canal, causing expansion of it. This introduces high tensile stresses on the femur that hold the stem in place. With time, cementless stems induce bone growth and make permanent bond with bone, which is the main cause for why cementless stems often perform better on the long-term than cemented stems [2, 3]. Secondly, when the stems fail, they have to be replaced. Removing cementless stems is very easy in comparison with cemented stems. When the bone cement is removed, some amount of bone tissue can follow, further weakening a weak bone but also, the stem-bone interface is less capable of receiving another implant. However, not all femurs can handle the press-fitting surgery of implanting cementless stems; the bone has to be strong enough. This has to be examined before surgery to choose the correct implant.

Eventually, if people live long enough, everyone will need a THR surgery. The hip joint is a load-bearing joint, which is constantly receiving high loads. These loads lead to gradual degradation of articular surfaces, causing functional impairment and pain. This degradation is termed arthrosis and at 65 years of age, ~80% of people have recognizable hip arthrosis on x-ray image, of which 25-30% shows symptoms [4]. In 2012, 264 patients underwent primary THR in Landspítali Hospital [5]; that means five hip joints are replaced

every week of the year on average. The cost of every operation is close to one million ISK so it is manifest that a lot of expenses lie in THR. In 2012, 27 revision THRs were made in Iceland. The average cost of revision surgeries is at least double the cost of primary ones.

Currently there are no absolute criteria on how to choose the correct type of prosthesis for THR. Despite the plethora of techniques available it is still the feeling of physicians that plays the big role in the decision, along with female gender, age (the indicators of bone quality) and visual x-ray analyses. There is a clear need for quantitative methods to securely choose the correct implant for individual patients.

This study introduces a method relying on computed tomography (CT) images to build three-dimensional models of femoral bones and performing Finite Element Analysis (FEA) to calculate a Fracture Risk Index. Additionally, Bone Mineral Density (BMD) is calculated on the proximal femur to increase the depth of the evaluation of bone quality. This way, the risk of fracture can be estimated pre-operatively and the question answered if individual patients are likely to tolerate the press-fitting surgery of cementless stems.

This work is part of a larger study on fracture risk analysis in THA patients also based on spatial and temporal gait data, electromyography (EMG), bone- and muscle density and quality of life (QOL) questionnaire. The aim is to use measured parameters to create a clinical evaluation score system for THA planning and monitoring recovery of patients after surgery. Figure 1 shows the events of the project on a time axis.

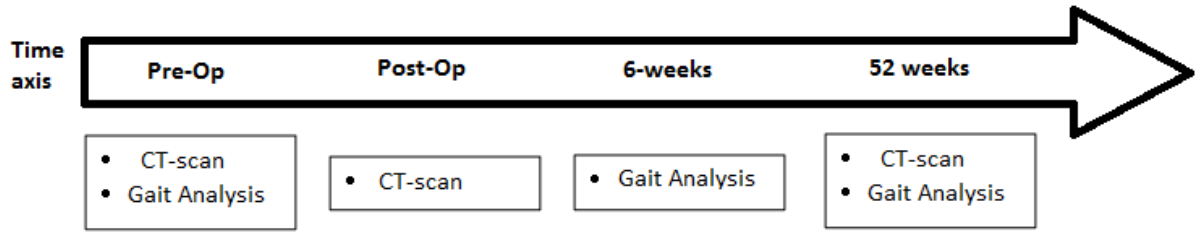

Figure 1: Project timeline. Before surgery, patients are CT-scanned and undergo a gait assessment with EMG. Soon after the operation, they are CT-scanned again. Then 6 weeks later they are called in for gait analysis again. 52 weeks later they are CT-scanned and undergo a gait analysis with EMG.

1.2. Objective of the Thesis

The objective of this study is to design a novel approach to provide a quantitative tool to choose the type of implant before THR surgery. The goal is to import these methods into clinical use and optimize pre-operative decision-making of implant type, and thereby reduce the rate of revisions followed by a cemented implant, which are highly complicated, very expensive procedures and have limited success.

1.3. Thesis Overview

In chapter 2.1 the anatomy and biomechanical properties of bones and the hip joint will be described. Chapter 2.2 will then take on the nature of total hip replacements, the main differences between cemented and cementless techniques and introduce the main prosthetic components. Chapter 2.3 will cover the currently employed pre-operative planning of THR. Chapter 2.4 includes an introduction to the finite element method and how it is used in THR applications. Chapter 3 is the materials and methods employed in the present study and chapter 4 displays the results. Chapters 5 and 6 consist of discussions and conclusion respectively. At the end, the future directions of the project are discussed.

2. Theoretical Framework

2.1. Bones and the Hip Joint

2.1.1. Introduction

Bone is a quite complex and dynamic connective tissue. It has two major roles: first, together all the bones in the body form the skeleton, which provides mechanical support and protects neural structures. Secondly, they store important minerals, particularly Ca2+, necessary to maintain mineral homeostasis and vital organ function.

Bone tissue is composed of (on a weight basis) inorganic- (60%) and organic (30%) phases and water (10%) [6]. On a volume basis the proportions are 40, 35 and 25% respectively. The inorganic part of bones are an impure form of naturally occurring calcium phosphate, usually referred to as *hydroxyapatite:* $Ca_{10}(PO_4)_6(OH)_2$ [7]. The organic part is collagen.

Bones differ from other connective tissues in the way that they are very stiff and strong. They work in a very small range of strain, yet they are very sensitive to strain level. They respond to strain by adapting their structure to be more able to receive the loads causing the strain. Bone is *viscoelastic*, meaning the mechanical properties depend on deformation grade, and *anisotropic*, meaning the displacement depends on direction of applied forces. The material properties stem from the fact that they are a composite; hydroxyapatite in a collagen lattice. Bones also differ in the way that they grow by adding layers of bone tissue on a cell-laden surface, unlike other connective tissues that grow interstitially.

In this chapter the properties of bones will be described. The discussion of different bone types and hierarchical levels will start at nanoscale and work towards macroscopic structures. From there the bone cells will be covered, continuing to how they are involved with bone building and remodelling. At last bone mechanical properties will be discoursed on, with the focus on long bones and especially the human femur. The objective of this chapter is to introduce functional structure and anatomy of bones and how they remodel themselves when put under load. With this knowledge and the important terminology laid down in this chapter, comprehension of the next chapters, on total hip arthroplasty and prosthetic technology will be easier.

2.1.2. Hierarchical Levels of Bone

Bone has many hierarchical levels and it is essential to be familiar to the properties and shape of the different component phases to understand the mechanical properties of bone tissue. On the smallest phase (sub-nanostructure) there are collagen molecules and bone crystals (hydroxyapatite mineral crystals) arranged in collagen fibrils (figure 2). On a nanostructural scale, those collagen fibrils comprise collagen fibres, synchronized to make up lamellae in lamellar bone (sub-microstructure). In each lamella, collagen fibres are arranged in parallel with each other in layers that are aligned alternately. The lamellae are concentric around the *Haversian canal* which confine vessels and bone nerves. The concentric layers of lamellae form a microstructure called *osteon*. These osteons are cylindrical with a diameter of 10-500 μm and 1-3 mm in length and they are aligned in quasi-parallel to the long axis of bones [8]. The highest hierarchical level of bones divides into two main bone types: *cortical-* and *trabecular* bone. Cortical bone is dense and consists of aligned osteons while trabecular bone is highly porous with spongy appearance in which lamellae arrange in small struts called *trabeculae.*

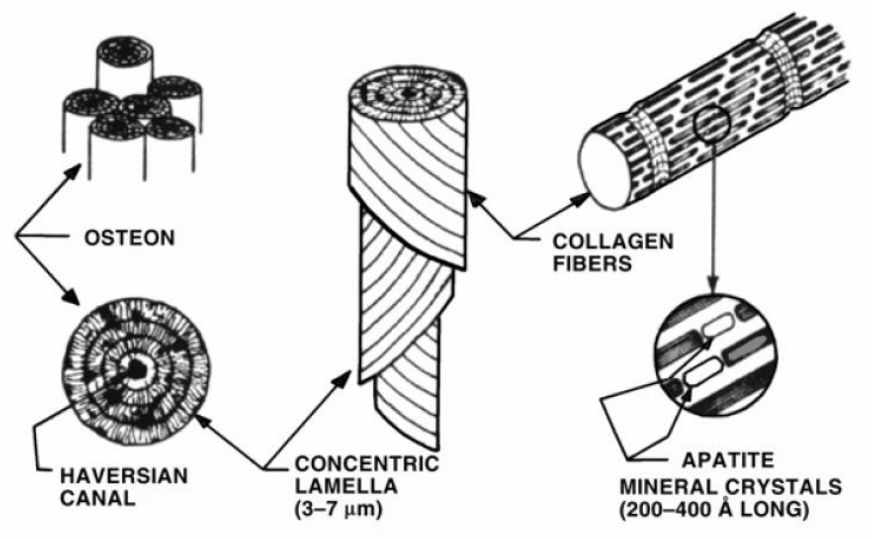

Figure 2: Structure of bone tissue from nano to microscale. Adapted from [9]

The Structure of Trabecular Bone

Trabecular bone, which is usually in the confines of cortical coverings, is more metabolically active then cortical bone and is remodelled more often. It consists of trabeculae that are similar in shape as osteons of cortical bones, consisting of concentric lamellae. The functional units of trabecular bone are called packets and they are semilunar in shape. Trabecular bone is made of a meshwork of rods, 0.08-0.14 mm in diameter and ~1 mm in length, and plates, up

to 0.5 mm thick and several millimetres in their long dimension [10]. There rarely are blood vessels inside the trabeculae; they instead thread in and out of the large spaces between individual trabeculae. Figure 3 displays three different types of trabecular bone meshwork, differentiating on the ratio and structure of rods and plates.

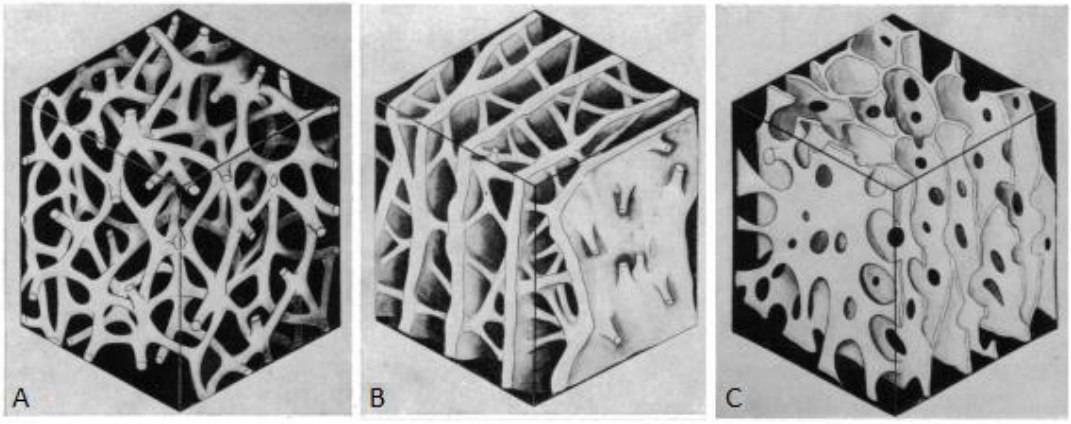

Figure 3: Different types of trabecular bone. A) Meshwork consisting entirely of rods. This is the most delicate type of trabecular bone and is typically found in the deeper parts of long bone ends. B) Meshwork of plates separated by rods. This type has a various density and is typically found in the lower end of the femur. C) Meshwork consisting entirely of plates. The plates form a mesh and enclose tubular spaces orientated along the direction of stress. This arrangement is distributed in the skeleton found for example adjacent to articular surfaces in the lower tibia. Adapted from [10]

The Structure of Cortical Bone

Cortical bone is dense and solid and as the name suggests it forms a cortex around the bone marrow. Osteons of cortical bones are called Haversian systems. Cortical bone can be divided into three types: lamellar-, osteonal- and woven bone.

Lamellar bone

Lamellar bone consists of laminae; small units that are about 200 μm thick and arranged concentrically [11] (figure 4). Between the laminae is a system of vessels that are essentially two-dimensional. Every lamina is divided into three zones. The first zone is a very dense and well organized bone tissue. This zone reaches from the surface of the inter-laminae vessels and about one-third the length across the lamina to the next one. The second zone is equal in range as the first one, and is badly organized bone tissue. This zone is split in two by the third zone, called the bright line. The lamina is symmetrical about this line.

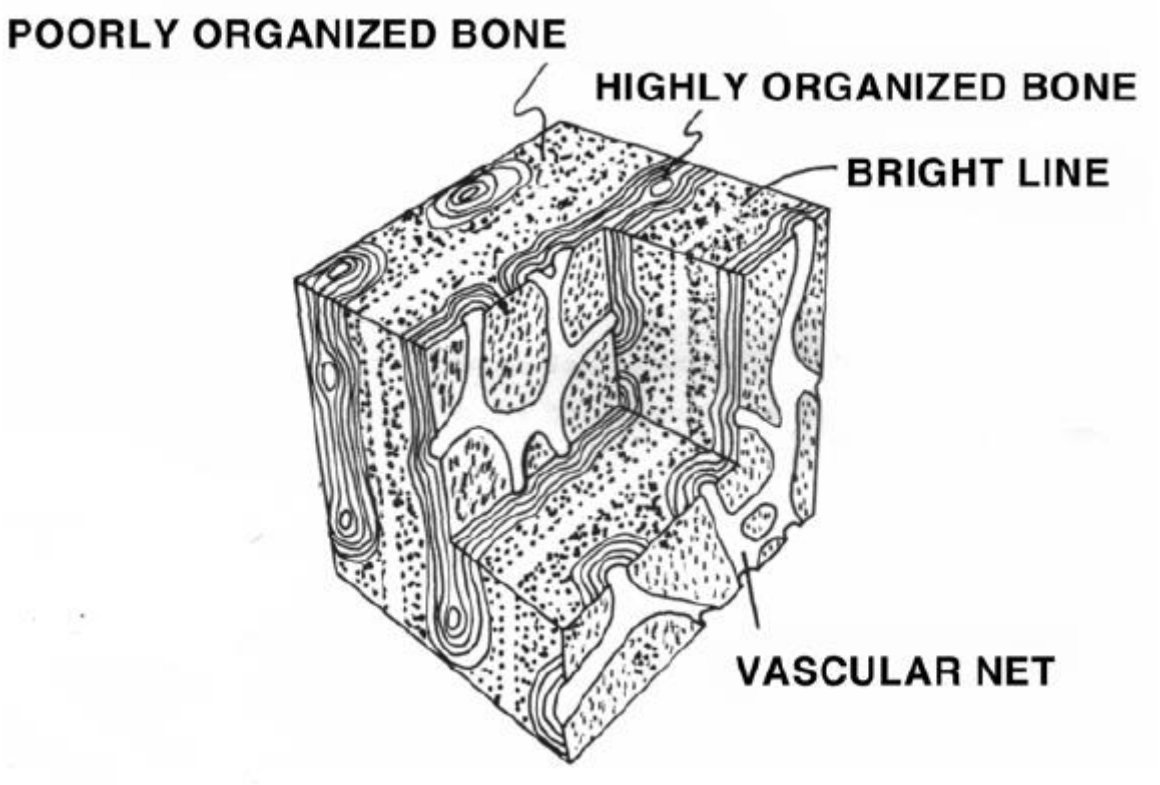

Figure 4: Typical layer-structure of lamellar bone. Adapted from [12]

Osteonal Bone

Osteonal bone essentially consists of cylindrical elements called osteons. There are two types of osteons: *primary* and *secondary* osteons. Primary osteons are the structure around vessels that are developed when the bone is initially formed. Secondary osteons are formed after the tissue has mineralised; they are more of interest than primary osteons because in human adult bone, osteons are primarily made up of secondary osteons. Osteons which are about 200 micrometres in circumference and 1-2 cm long are organised to house a system of small arteries, arterioles and capillaries (figure 5). The blood in the osteonal canals is transported along the long axis of long bones. So-called *Volkmann canals* connect the osteonal canals and in them blood is transported perpendicular to the long axis. The Volkmann canals are named after the German physiologist Alfred W. Volkmann (1800-1877) who discovered them [13]. Osteons, of osteonal bone, and lamellae, of lamellar bone, are the same material, only arranged in a different way.

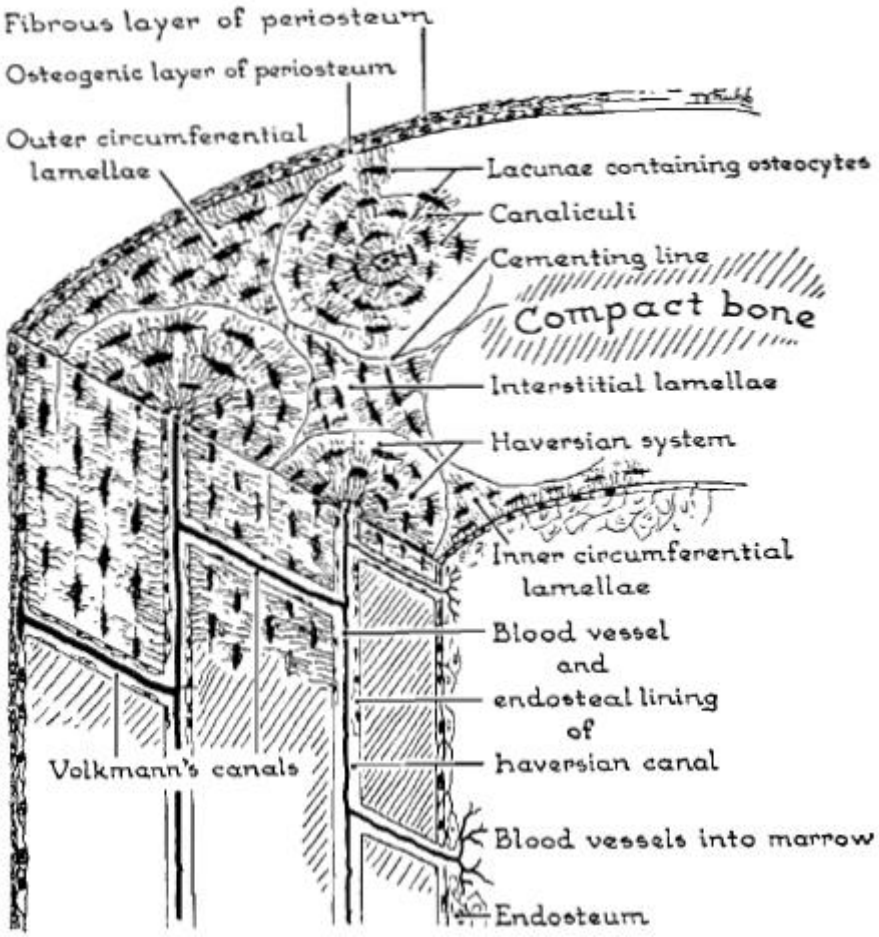

Figure 5: Basic structure of cortical bone. Adapted from [14]

Woven Bone

Woven bone is found in both cortical- and trabecular bones in young, growing animals and in adults after bone injuries. Bones of new-borns are mostly made of woven bone but it transforms into lamellar bone during maturation, and at maturation a part of lamellar bone transforms into osteonal bone. What distinguishes woven bone from the other bones is the ratio of collagen to mineral. This ratio is almost fixed in lamellar and osteonal bone but varies greatly in woven bone; hyper-mineralization can often be observed in woven bone. Woven bone can form very quickly when it does, with no uniform orientation of collagen fibres.

2.1.3. Anatomy of the Femur

As mentioned before, there are two main types of bones on a macroscopic level: cortical and trabecular bone. The smooth outer layer of the cortical bone is called *periosteum* (figure 6) which consists of active cells that enlarge the girth of bones in remodelling; it is laminated, vascularized and forms bone's outer coating. On the periosteum, bone formation typically exceeds resorption, so diameter of long bones tends to increase with age. The top layer of

periosteum consists of collagenous fibres and fibroblasts. This fairly impermeable fibre-film sticks to bone and is always under tension. The canal in the middle of long bones is called the *medullary canal*. The surfaces of these canals are called *endosteum*, which mainly consists of laminated cells. In the endosteum, bone resorption typically exceeds formation so the medullary canal normally expands with age. The mid-shaft of long bones is called *diaphyseal* region and the *epiphyseal* region is at the ends, where trabecular bone is inside the cortical shell. The m*etaphysis* connects the epiphysis and diaphysis. Longitudinal bone growth occurs at *growth plates*, where cartilage proliferates, in the epi- and metaphyseal areas [13]. In the mid diaphysis, the narrowest part of the femur is called the *isthmus*.

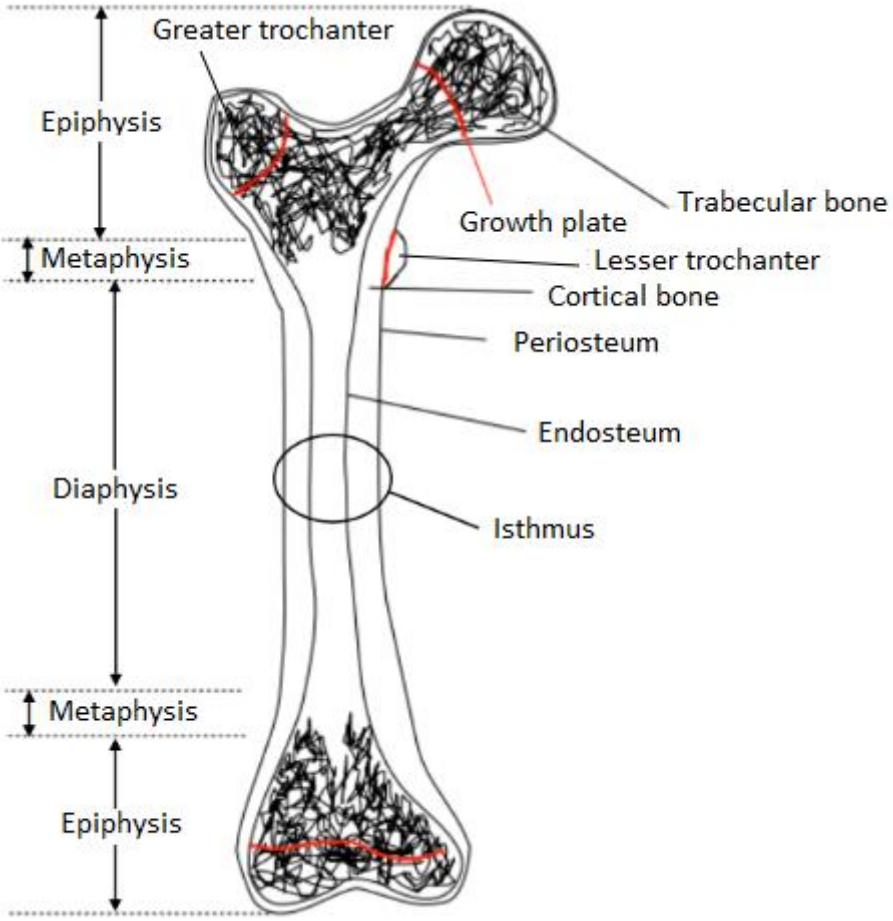

Figure 6: Gross anatomy of the femur.

2.1.4. Anatomy of the Hip Joint

The hip joint is a synovial ball-and-socket joint with the properties of one: as a joint cavity, the touching surfaces are covered with articular cartilage; it has a synovial membrane producing synovial fluid and it is covered with a ligamentous capsule [15].

The acetabulum consists of three bones, *ilium*, *ischium* and *pubis*. Those three bones are connected with cartilage until they fuse together between 13-23 years of age [16]. When looking inside the "cup" of the acetabulum, a horseshoe-like cartilage can be observed, called *labrum* (figure 17). The head of the femur, fitting into the cup, is also covered with articular cartilage, providing extremely low friction and is held in the socket by a ligament, the *ligamentum of Teres*. Connecting the shaft and the head of the femur is the femur neck, forming an angle of 125° +- 5° in the average individual [17].

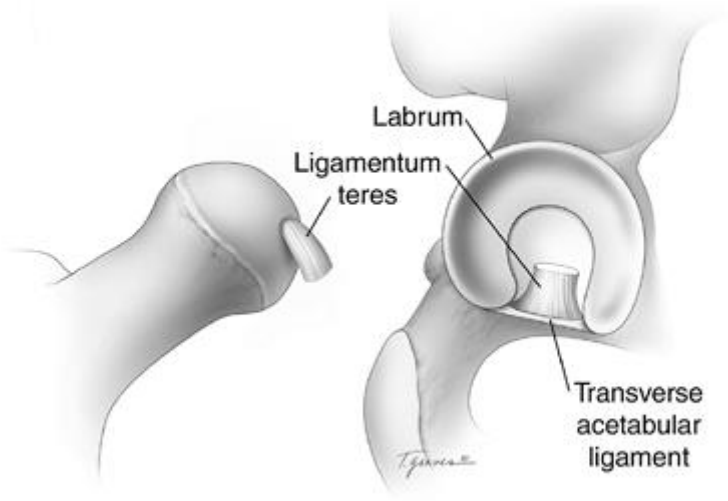

Figure 7: Articular surfaces of the hip joint. Adapted from [18]

2.1.5. Bone Cells

Bone cells within the bone tissue work together to keep the skeleton intact. Their work includes, new bone development, bone maintenance and regulation of minerals. The five kinds of bone cells found both in growing and grown skeleton will be covered in the following sub-chapters.

Osteoprogenitor Cells

There are two types of osteoprogenitor cells, *preosteoblasts* and *preosteoclasts*. Preosteoblasts are mesenchymal cells which can differentiate into *osteoblasts* through the process of mitosis. Similarly, preosteoclasts differentiate into *osteoclasts*. These daughter cells will be covered in the next paragraphs. The osteoprogenitor cells usually lie in the inner layers of periosteum, endosteum, osteonal canals and Volkmann canals. Preosteoblasts are most active during bone growth but some parts of them also reactivate after bone fracture during repair. They also differentiate into osteoblasts during the perpetual remodelling of

bone [19]. Preosteoclasts have relatively newly discovered functions, besides giving rise to osteoclasts, for example hinder the activity of osteoblasts [20].

Osteoblasts

Osteoblasts are specialized mesenchyme-derived cells that have the functions of adding and maintaining bone tissue. They secrete un-mineralized collagenous bone matrix, called *osteoids*. The osteoids then mineralize into new bone. Osteoblasts also work on calcification of bone by regulating calcium and phosphate flux in and out of bone [21]. In figure 7 osteoblasts (and osteocytes) can be seen on a microscopic image.

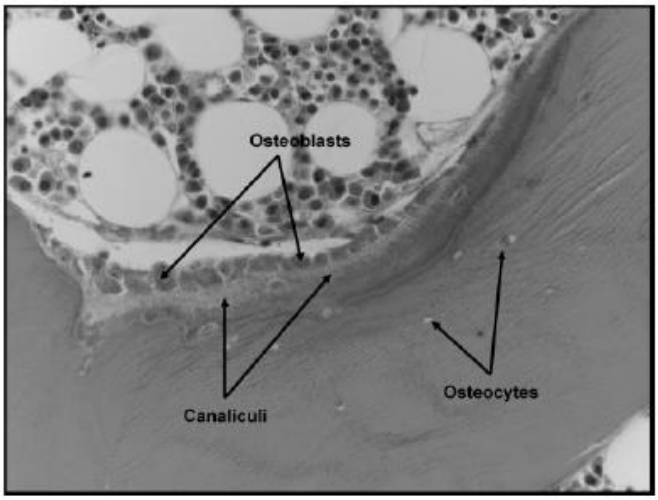

Figure 8: Image showing osteoblasts and osteocytes with canaliculi canals also visible. Adapted from [22]

Osteoclasts

Osteoclasts are cells that destroy bone tissue to precipitate bone remodelling or cause bone loss in pathological cases. Their range of function reaches beyond removing bone tissue; they also secrete cytokines that have various regulating-abilities in bone remodelling [23]. Osteoclasts are most often found in so called *Howship's lacunae* (figure 9) which are, according to Encyclopaedia Britannica, pits on the bone surface, formed after bone resorption [24].

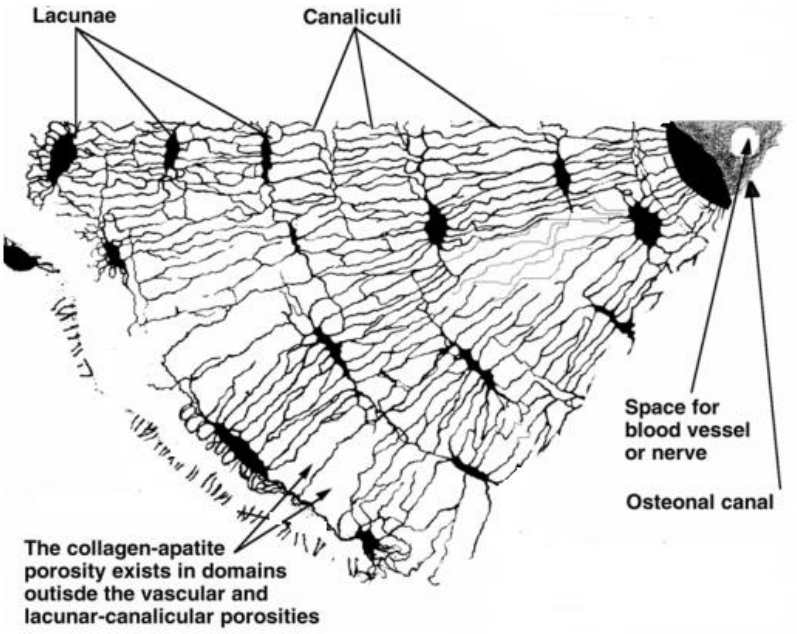

Figure 9: A pie-shaped section of an osteon. Adapted from [13]

Bone-Lining Cells

Bone lining cells draw their name from the fact that they are thin and long as they line up to cover most bone surfaces. They are assumed to be derived from osteoclasts and preosteoclasts [13]. Bone lining cells play a big role in modulating formation of osteoclast and preparing the bone surface so the bone eating cells can attach to it [25].

Osteocytes

Osteocytes are converted osteoblasts that are left behind when the bone surface grows outwards, encased in the mineralised matrix from their own secretion [13]. According to Encyclopedia Britannica, osteocytes can both deposit and resorb bone tissue. They also participate in bone remodelling by sending signals to other osteocytes via cytoplasmic processes within *canaliculi* (figure 7), as a response to even slight deformation caused by skeletal muscles [26]. Through this mechanism, bone gets stronger when it is properly loaded (as in physical exercising) or weaker when it is under-stressed (by inactivity). The next sub-chapter will cover bone remodelling in more detail.

2.1.6. Bone Remodelling

Bone remodelling is the process of continuous bone shape changes as a response to physiological influences or mechanical forces. The skeleton gradually adjusts its structure to be better able to receive frequent loads.

Continuous degradation from bone-eating osteoclasts and adding from bone-building osteoblasts prevents and removes fatigue induced micro-damages and adapt the structure of bones. The function of osteoblasts and osteoclasts are controlled by various factors such as hormones and cytokines along with local signalling molecules which respond to stress tensors [27, 28].

Taking the femur as an example, during walking, forces act on it; for example compressive hip contact ground reaction forces and tensile forces from the muscles attached to the femur. The applied forces do not solely build up and maintain the bone mass but they also control structural adaptation of the bone. The structural adaptation of bone as a response to loads is described by Wolff's law, articled by the German anatomist and surgeon Julius Wolff in but in 1892 he wrote: "every change in form and function of a bone, or in its function alone, is followed by certain definite changes in its internal architecture and equally definite secondary alteration in its mathematical laws" [29]. This simply means that bone changes its structure to be better able to withstand frequently applied forces. Similarly, we lose bone mass in under-stressed situations, as is sometimes the case when a prosthesis is introduced to the human body. Normal stresses are then substituted for synthetic material-induced stresses that can lead to under-stressed areas around the prosthetic implant. This phenomenon is called *stress shielding.* In the case of total hip replacement, where the femur head is replaced with a prosthetic stem which is inserted into the medullary canal, stress shielding can for example occur on the proximal femur when the stresses bypass that part and are carried down to the isthmus, the narrow part of the femur [30].

2.1.7. Biomechanics of Bone

When materials are put under stress they respond with deformation. *Strength* and *hardness* of materials tell us how they deform. Due to its combination of inorganic and organic materials, bone is amongst the strongest and most rigid structures of the body; the organic material provides bone with flexibility and the inorganic provides resilience. Bones have some behavioural properties worth mentioning: They are *anisotropic***,** which means that their deformation depends on the direction of the applied load. Bone can for example receive higher loads in the longitudinal direction then transversely, as a result of structural adaptation. Bones are also *viscoelastic***;** their behaviour depends on the speed and length of applied loads.

This sub-chapter will discuss the biomechanical properties of cortical and trabecular bone separately, but first, important mechanical terminology will be introduced.

Stress

Consider a body *B* (figure 9). It has a closed surface *S* within *B*. Let Δ*S* be a small surface area element on *S*. The direction of this small element is indicated by a unit normal vector **v**. The side orientated in the same direction as the normal is often referred to as the positive side and the other side negative. The part lying on the positive side exerts a force **ΔF** on the other part. Introducing the assumption that *ΔS* tends to an infinitesimally small size, the ratio **ΔF**/Δ*S* tends to the definite limit d**F**/*dS* with an acceptable variability. Since *ΔS* tends to a very small size, the moment of the force acting on it vanishes in the limit. The limiting vector can be written as

$$\boldsymbol{T}_{\boldsymbol{v}} = d\boldsymbol{F}/dS \qquad (1)$$

The transcript ν is used to denote that the normal **v** indicates the direction of the surface. **T** is called *traction* or the *stress vector* and represents force per unit area.

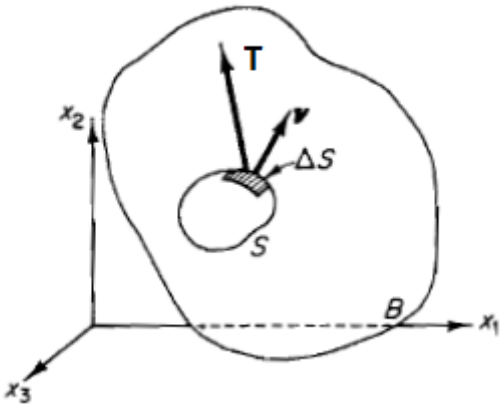

Figure 10: Traction on a surface element. Force T acting on an infinitesimal surface element in body B, with normal v. Adapted from [31]

In continuum mechanics **stress** indicates the inner forces that particles in a body react on each other. Macroscopic stress on a body is really a sum of inner forces and collisions of particles in the body. If we take a rod, with cross-sectional area of $A\ [m^2]$ and $F\ [N]$ as the force that is applied at the ends of it, then the stress is calculated as:

$$\sigma = \frac{F}{A}\ [Pa] \qquad (2)$$

The unit N/m^2 is called Pasqual and is denoted *Pa*. The general notation of stress components is as figure 10 demonstrates; there the stresses for each direction in the 3D Cartesian space are

shown, acting on the surfaces of the cube. τ_{11}, τ_{22} and τ_{33} are called *normal stresses* which can be either compressive or tensile. The other stress vectors are *shear stresses***.** Shear stresses change the angle of objects, while normal stresses change their extent. Compressive stresses reduce extent of bodies in the direction they work in while tensile stresses elongate bodies in their working direction. It can be shown that knowing the component of a stress tensor $\boldsymbol{\sigma}$ with respect to Cartesian coordinates, the stress vector acting on a surface element with unit outer normal vector *v* (figure 8), can be written:

$$\boldsymbol{T} = v\boldsymbol{\sigma} \tag{3}$$

Besides surface tractions, *body forces* act on the total volume of the element. They may be applied to the bulk material, like gravity, or to the surface of the element like contact forces or external pressure. In figure 11, a body force acting in the direction of x_1 is drawn. Body forces can be divided into three components depending on direction. It can be shown that for a body in equilibrium, the stress components must satisfy:

$$\frac{\partial \tau_{11}}{\partial x_1} + \frac{\partial \tau_{12}}{\partial x_2} + \frac{\partial \tau_{13}}{\partial x_3} = -b_1 \tag{4}$$

$$\frac{\partial \tau_{21}}{\partial x_1} + \frac{\partial \tau_{22}}{\partial x_2} + \frac{\partial \tau_{23}}{\partial x_3} = -b_2 \tag{5}$$

$$\frac{\partial \tau_{31}}{\partial x_1} + \frac{\partial \tau_{32}}{\partial x_2} + \frac{\partial \tau_{33}}{\partial x_3} = -b_3 \tag{6}$$

where b_1, b_2 and b_3 are Cartesian components of body forces, per unit volume, acting on the body.

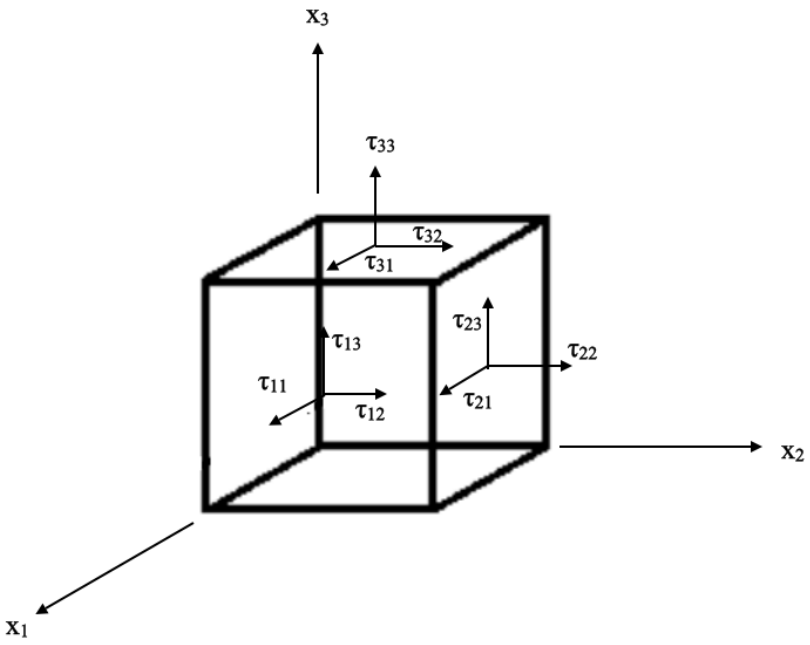

Figure 11: General notation of stress components.

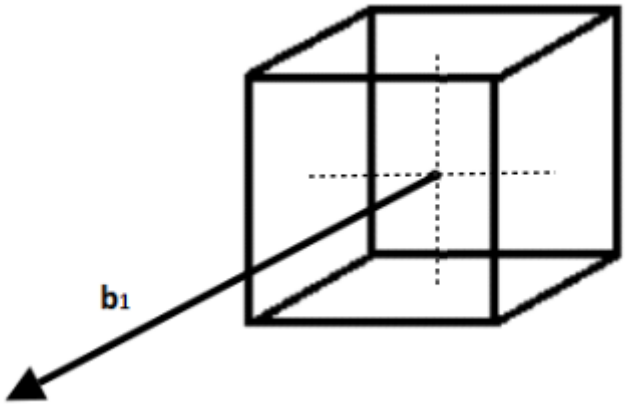

Figure 12: Body force acting inside an infinitesimal element.

Strain

Strain is a measure of deformation caused by stresses; it indicates the displacement of particles in a body. The ratio of the change in length of a body to its original length is called *stretch ratio*:

$$\varepsilon = \frac{l - l_0}{l_0} \qquad (7)$$

and is a measure of strain. For most engineering materials subjected to uniaxial infinitesimal stretching, the equation

$$\sigma = E \cdot \varepsilon \tag{8}$$

is valid for a certain range of stress, specifically until reaching the *yield stress*. In this relation, E is called *Young's modulus*. The equation is called *Hooke's law* and the materials that obey it are called Hookean materials. Similarly to equation 8, for a Hookean material subjected to an infinitesimal shear strain, the relationship

$$\tau = Gtan(\theta) \tag{9}$$

is valid until yield is reached. It is important to note that the yield strain is different for compression, tension and shear.

These situations describe simple deformation, but in nature, most deformations are much more complex. Therefore a general method of strain treatment of bodies is needed. It is achieved through so-called Cauchy's infinitesimal strain tensor, and it is written:

$$\varepsilon_{ij} = \frac{1}{2}\left[\frac{\partial u_i}{\partial x_j} + \frac{\partial u_j}{\partial x_i}\right] \tag{10}$$

where ε_{11}, ε_{22} and ε_{33} are normal strains while the others are shear strains. For an example, in the case of shear strain, where the angle of the object is changed, the angle change in each 2D direction can be divided into two parts (for each 2D axis), resulting in the infinitesimal strain equation above:

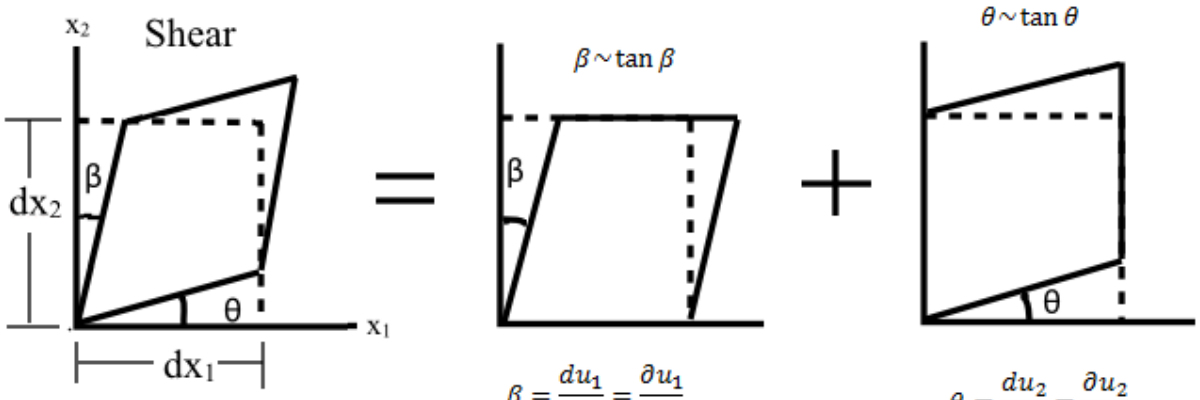

$$\beta = \frac{du_1}{dx_2} = \frac{\partial u_1}{\partial x_2} \qquad \theta = \frac{du_2}{dx_1} = \frac{\partial u_2}{\partial x_1}$$

$$\varepsilon_{ij} = \frac{1}{2}\left[\frac{\partial u_1}{\partial x_2} + \frac{\partial u_2}{\partial x_1}\right]$$

Infinitesimal shear strain means that the change in angle is very small. Therefore the notation $\beta \sim \tan\beta$ can be considered valid. This is a simple example, when dealing with complicated structure can be simplified by dividing whole bodies into small element like the rectangle in this example. This method is called the finite element method.

Strength and Hardness

When investigating behaviour of materials under stress, a graph where stress is plotted against strain is often used to record the relationship. Figure 13 shows a typical stress-strain graph; these graphs are different for the same material depending on direction of loading. In the elastic region of the stress-strain curve there is a linear relationship between strain and stress, and the slope is the modulus of elasticity or Young's modulus. When bone, or any material, is deformed inside this region it is recovered fully when it is relieved of load. If the bone is deformed beyond the yield limit the tissues start to cede, introducing micro-breaks. Beyond the yield point materials will not fully recover and if the load is persisted it eventually breaks. Material strength indicates how much load it can receive before it breaks. It is often measured in energy storage before fracture; that is the area under the stress-strain curve [32]. The elastic modulus is a measure of material hardness. Hard materials respond to load with small deformation and tend to be fragile, that is, they break at the end of the elastic region. When materials over-deforms beyond yield point into the plastic region, it is said flexible.

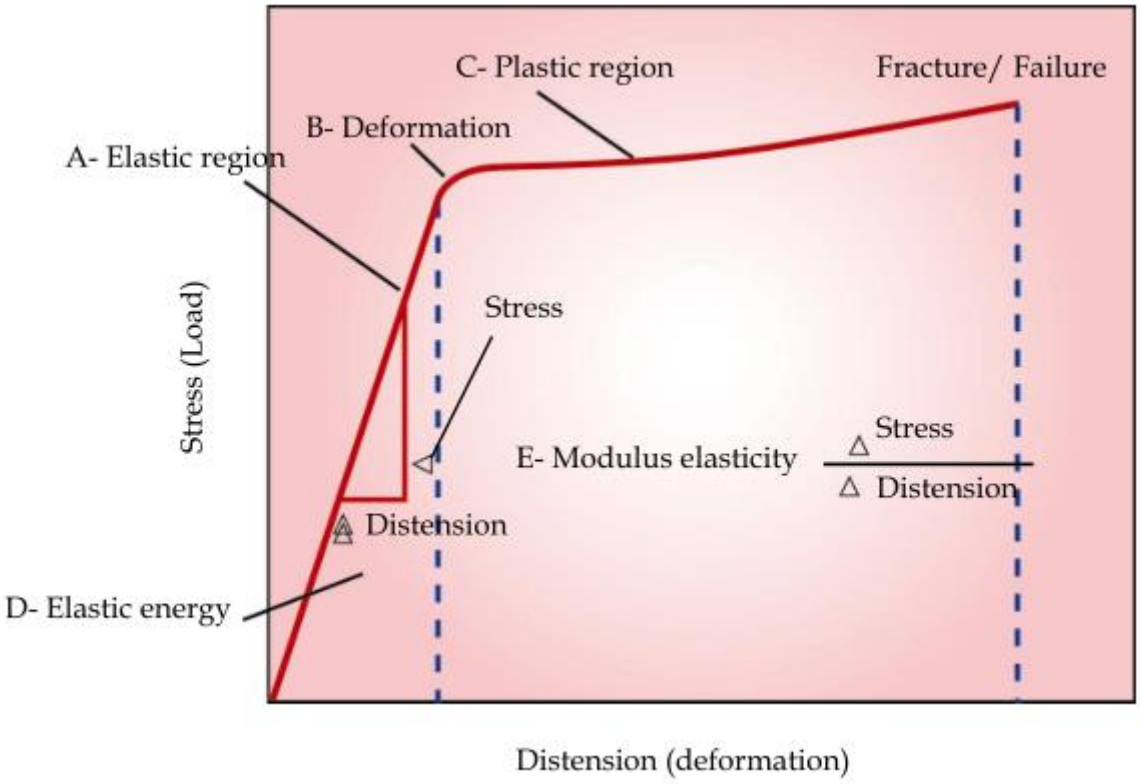

Figure 13: A stress-strain curve with the most important readings labelled. Adopted from [31]

Poisson's Ratio

Another important measure of behaviour of materials is the Poisson's ratio, named after Siméon Poisson (1781-1840), a French mathematician and physicist. Poisson's ratio describes how materials change their extent when loaded. It is the negative ratio of transverse to axial strain:

$$\upsilon = -\frac{\varepsilon_{axial}}{\varepsilon_{transverse}} \qquad (11)$$

For example, if a load is put on a cube and it is compressed in one direction it tends to expand in the other directions. Similarly if materials are stretched in one axis, they become narrower along the other axis (figure 14).

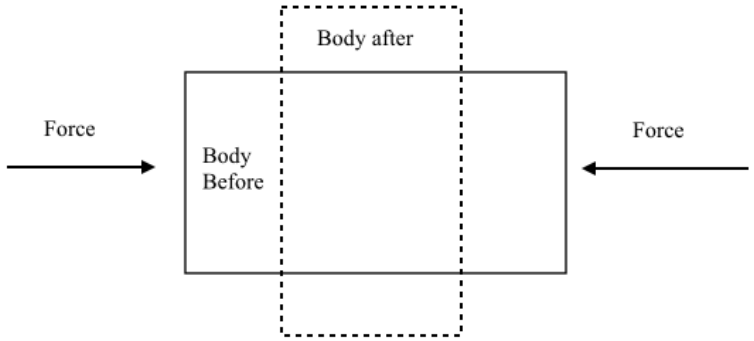

Figure 14: Interpretation of Poisson's ratio. When a body compressively stressed in one direction, it tends to expand in the other direction. The behaviour can be mapped with Poisson's ratio.

Modes of Loading

After covering the most important mechanical terms used in this study, the types of macroscopic loading modes serves as a summary. There are various loads which the skeletal system can be subject to. Figure 12 shows these types of loading on a human femoral bone. The equation in the chapters above can basically be implemented in ways to describe these types of loadings.

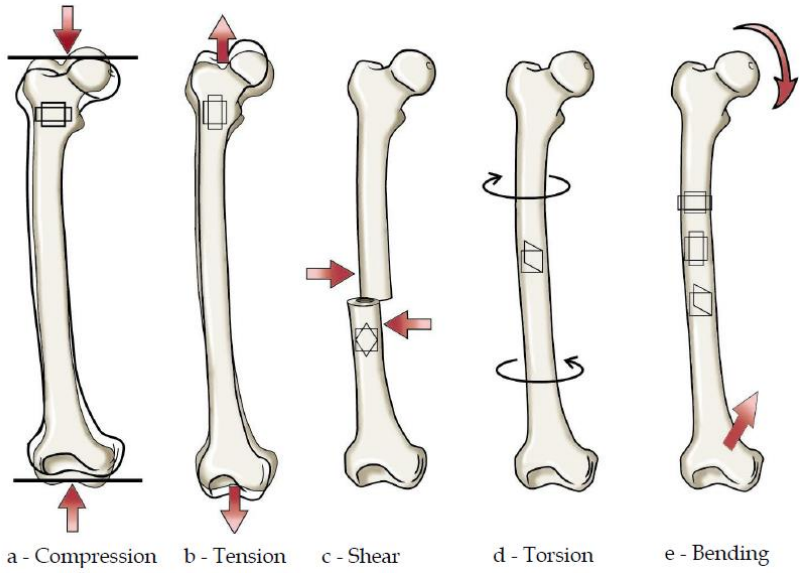

Figure 15: Different loading modes shown on a human femoral bone. a) Compression causes shortening and extension. b) Tensile strength causes narrowing and elongation. c) Shear strength, causes change in angle before fracture. d) Torsion creates angular distortion. e) Bending includes all the changes seen in compression, tension and shear. Adapted from [33]

As stated before, compression and tension are results of normal stresses that reduce or increase the extent of bodies in the direction they work in, respectively. Shear stresses change the angle of bodies; shear forces work parallel to the cross section. Torsion is the twisting of objects due to applied torque. During torsion shear stresses emerge perpendicular to the

radius. When a long bone is bent, one side will compress, while the other will elongate due to tension.

Mechanical Properties of Cortical Bone

As already stated, bones are anisotropic, so strength and elasticity are different depending on the direction of applied forces. Cortical bone has more strength and stiffness along the longitudinal axis than along the transverse axis, because it is more used to receive high vertical loads that apply in normal activities such as gait (table 2 and 3). Additionally, cortical bone is stronger in compression than in tension. The Poisson's ratio for cortical bone is in the range 0.2-0.5 with average value around 0.3 [34]. Figure 16 manifests the anisotropy of cortical bone, where a stress-strain curve is plotted for four different loadings on the femoral shaft. These graphical interpretations indicate that the femoral shaft is more flexible in the longitudinal direction than in the transverse, howbeit, it indicates more stiffness in the longitudinal direction.

Table 1: Anisotropic properties of human femoral cortical bone. Adapted from [35]. * Standard deviations are in parenthesis.

Longitudinal Modulus (MPa)	17.900 (3900)*
Transverse Modulus (MPa)	10.100 (2400)
Shear Modulus (MPa)	3.300 (400)
Longitudinal Poisson's ratio	0.40 (0.16)
Transverse Poisson's ratio	0.62 (0.26)

Table 2: Anisotropic ultimate stresses of human cortical bone. Adapted from [35]. * Standard deviations are in parenthesis.

Longitudinal (MPa)	
- Tension	135 (15.6)*
- Compression	205 (17.3)
Transverse (MPa)	
- Tension	53 (10.7)
- Compression	131 (20.7)
Shear (MPa)	65 (4.0)

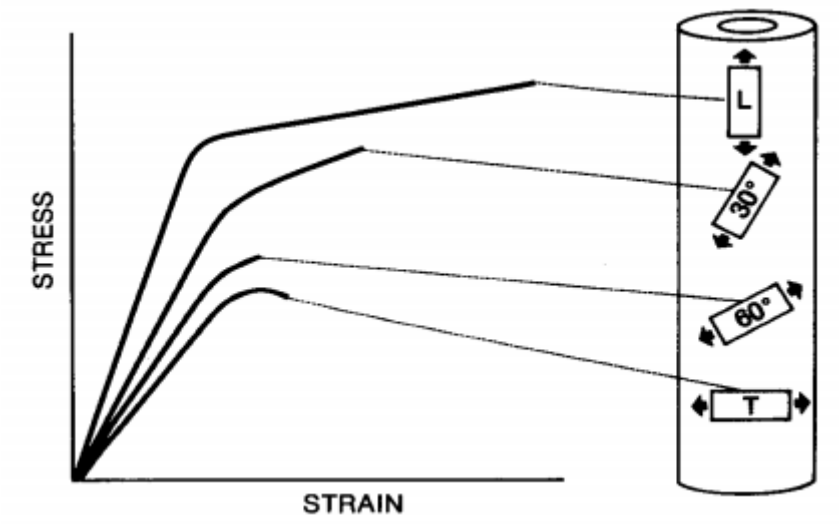

Figure 16: Anisotropy of the femoral shaft in tension. The stress-strain curve indicates more stiffness and flexibility along the longitudinal direction and less stiffness and more brittle fracture transversely. Adapted from [36]

Cortical bone is linearly elastic until reaching yield point and fails at low strains. If it is loaded close to yield, then unloaded and reloaded again there will be some residual permanent strain, so load cycles of high enough value (or enough cycles) can produce fatigue damages.

Unlike ultimate stress, which is higher in compression then tension, ultimate strain is higher in tension then in compression. Table 2 reflects that shear strength of cortical bone is low, but it is weakest in transverse tension. An example of transverse tension is when a hip stem of too large size is press-fitted to far into the diaphysis of the femur.

Often the average properties of cortical bone are presented, however there are many things that can affect its behaviour. Although not very variable between individual humans, small increment in mineralization can increase Young's modulus and strength (figure 17). Ageing also has a considerable impact on cortical bone properties. Tensile ultimate stress has been reported to decrease around 2% per decade [37]. Tensile ultimate strain shows 10% decrease per decade; it alters from being as high as 5% for people in their thirties to being as low as 1% for people over 80 years. So the energy that cortical bone can receive before failing is quite dependent on age.

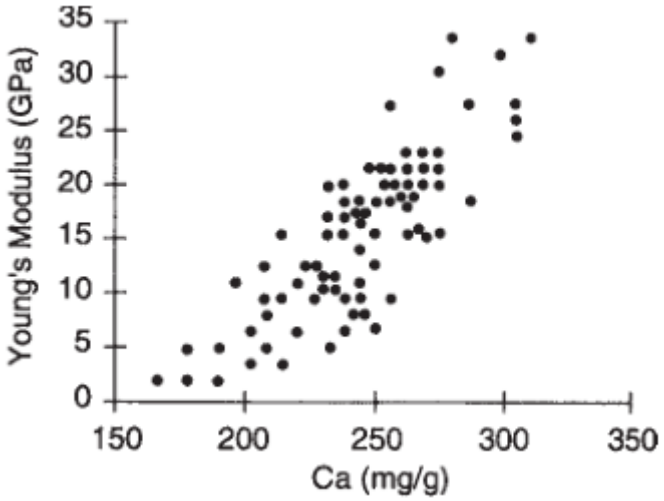

Figure 17: Young's Modulus plotted against calcium content of cortical bone, taken from 18 different species. Adapted from [38].

As mentioned earlier cortical bone is viscoelastic, howbeit, the rate of loading only has a moderate effect on modulus and strength. For a change of six orders of magnitude in load rate the modulus changes by a factor of two and strength by a factor of three [39]. Since most physiological activities occur in a narrow strain range the strain rate effects can often be neglected.

The behaviour of cortical bone also depends on level of damage. If the bone is loaded past its yield point, the load released and then reapplied, the Young's modulus is lower than before [40]. Furthermore, fatigue decreases the Young's modulus of cortical bone due to increase in energy dissipation in each load cycle [41]. Histological damage in cortical bone increases with age and is more pronounced in women than men [42]. Histological damages on bone are often pooled under the name *microdamage*. The term microdamage covers the damage patterns of longitudinal and transverse microcracks, diffuse damage and cross-hatched shear band patterns [43]. When the cortical bone matrix suffers from permanent microdamage it induces physiological response and bone cells fix the matrix before the lead to unrecoverable damage.

A lot of micromechanical models for elastic and strength properties of cortical bone have been developed. What drives the ambition behind those studies is the fact that the properties of bone are anisotropic and change with age and under pathological conditions. Thus these conditions have to be mapped from proper mathematical modelling of bone.

Mechanical Properties of Trabecular Bone

Trabecular bones are usually linearly elastic until yield point although being nonlinearly elastic even at short strain range [44, 45].

Trabecular bone is a highly porous cellular solid and its mechanical properties depend on porosity and architecture of trabeculae. This porous solid can absorb substantial quantity of energy before failure; in compression the yield is about 1%, but beyond that limit it can reach strain values of 50% while keeping its ability to receive loads [43].

Elastic and strength properties of trabecular bone vary with age and health, anatomic site and loading direction and mode. Young's modulus can range from 10 MPa - 20 GPa [43, 46] and the values can vary 100-fold on a single epiphysis and three-fold depending on direction [47, 48]. Diseases such as osteoporosis and osteoarthrosis are known to have considerable impact in behaviour of trabecular bone, due to decrease in bone mineral density. Bone mineral density influences strength and Young's modulus [49].

Anisotropy in trabecular bone strength and stiffness increases with age and decreasing density [50, 51] but the strength is also dependent on load direction, being highest in compression and lowest in shear [52]. In this context it is interesting to note that density has little effect on the yield and ultimate strains of trabecular bone [53, 54].

Recent development in imaging techniques, such as micro-CT, has increased the knowledge on mechanics of bone tissue. With the ability of 3D structural indices the Poisson ratios for trabecular bone have recently been reported to be variable between 0.01 - 0.35 [55]. For femoral heads the ratio is usually little above 0.3 [56].

When trabecular tissue is loaded, unloaded and loaded again, the elastic modulus is decreased, as is the case with cortical bone [57].

Concerning time-depending properties of trabecular bone, strain rate has only moderate effect; the behaviour is only slightly viscoelastic when tested in vitro [58]. Otherwise, little is known about time-dependent properties of trabecular bones.

2.1.8. Conclusion

In this chapter, structure of bone at micro- and macroscopic levels has been discussed. Additionally the biomechanical properties of bones have been introduced and how bones respond to different types of loading. With this information collected, along with the terminology introduced, the focus will move towards total hip replacement and how bones react to THR implants.

2.2. Total Hip Replacement and Prosthetic Technology

2.2.1. Introduction

During THR, metallic, polymeric and/or ceramic components are used to replace pathological femoral heads and the bearing surfaces of the acetabulum. THR is widely used in treatment of advanced hip joint damages and pain. For decades it has provided a very successful symptomatic and functional treatment for pathologies such as osteoarthrosis, inflammatory arthritis, fracture etc.

The success of primary THR is well documented in literature and has been reported with survival rates of around 90% at 15-year follow-up [59, 60, 61]. However, unfortunately not all THR surgeries are successful and eventually have to be replaced, arguably sooner than they should be.

Hip arthrosis is one of the most common orthopaedic diseases and the leading cause for need of THA [62]. At 65 years of age, 80% of people have recognizable hip arthrosis in an x-ray image but only 25-30% show symptoms [4].

Advances in the field of THRs are taking place at a constantly accelerating rate. As the understanding of the diseases leading to the need of THR increases, improvements in implant design, materials and surgical techniques can be expected.

The most common complications of THA are hip joint dislocation, fractures, wound infection, stem loosening, phlebothrombosis and embolism, periarticular calcification, malposition of components and leg length discrepancy [63]. Most of these complications can directly lead to premature revisions; however, the focus of this study will be on intra-operative fractures.

This section will discourse upon the challenges of total hip replacement, the differences between types and the main types of prostheses used in THR.

2.2.2. Components and Configurations of Total Hip Replacement

Components of Total Hip Replacement

In figure 18, all the components used in THR are shown and then the following text describes those components. Table 4 then summarises them with respect to materials used for each one.

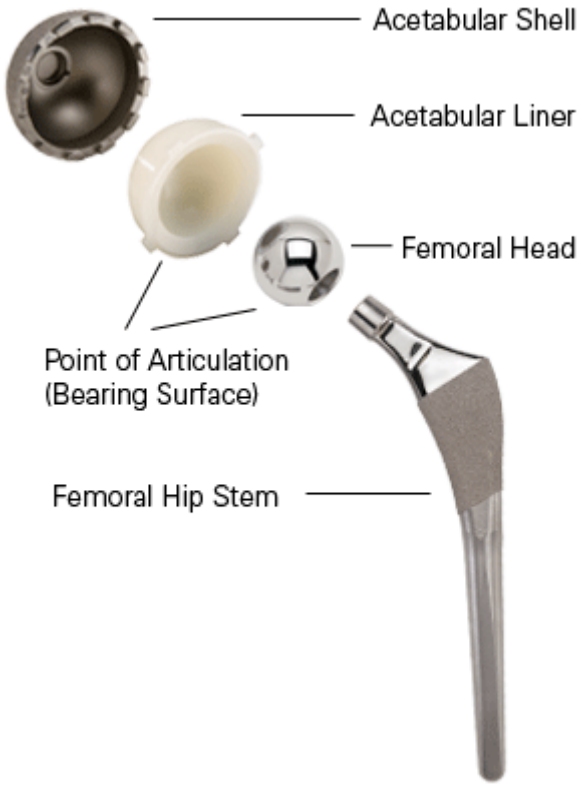

Figure 18: Components of total hip replacement. Adapted from [64]

Stem

The damaged head of the femur is replaced with a metal *stem*. The stem is most often Cobalt-Chromium- or a Titanium alloy and can be fixed inside the medullary canal either with use of cement or press-fitting technique.

Ball

On top of the stem, a metal or ceramic *ball* is placed. This ball serves as replacement for the femoral head.

Socket

The damaged articular surface of the acetabular cup is removed and replaced with a metal *socket* and similar to the stem, this component can be fixed with or without bone cement. When a proper fixation is hard to achieve, screws can be used to hold it in place.

Liner

Between the prosthetic socket and the ball at the end of the stem, a cup *liner* is placed. The only movement allowed is at the interface between the ball and the liner. The most used liner is made of Ultrahigh Molecular Weight Polyethylene (UHMWPE). For convenience, from now on, it will be referred to as *polyethylene*.

Table 3: The most common materials components in THR are made of. Adapted from [65]

Component	Material class	Most used material
Femoral stem	Metal	CoCrMo and Ti-alloys
Femoral head	Metal	CoCrMo and stainless steel
	Ceramic	Alumina (pure or zirconia-toughened) and zirconia
Acetabular liner	Polymer	UHMWPE
	Metal	CoCrMo
	Ceramic	Alumina (pure or zirconia-toughened) and zirconia
Acetabular socket	Metal	Titanium and stainless steel

Articular Surfaces in THR

Below are descriptions of the most used articulation configurations of THR. The list is not exhaustive, as many different configurations have been (and are) under investigation.

Metal or Ceramic Ball on Polyethylene Liner

This is the most common configuration of the sliding interface in THR. The adoption of polyethylene by Charnley (after bad experience with other materials) truly marks the beginning of the great success of THR still experienced today. Polyethylene is a very tough material, has a good chemical and abrasion resistance and a very low friction. Despite the qualities polyethylene possesses, wear is a big issue. It is now known that particulate debris generated from hard-on-soft articulating surfaces initiates adverse tissue responses leading to bone resorption [66, 67]. This can cause osteolysis and loosening of components. Ceramic ball on polyethylene liner has been reported with better survivorship and less wear than metal ball on polyethylene [68, 69].

Metal or Ceramic Ball on Crosslinked Polyethylene Liner

Radiation crosslinking coupled with thermal treatment of polyethylene has recently been proved to increase wear resistance of polyethylene and thus decreasing the rate of loosening of the stem [70, 71, 72]. Understanding the mechanism of crosslinking is not of great importance and will therefore not be detailed here.

Metal Ball on Metal Cup

Generation of wear debris caused by polyethylene has renewed the interest in metal-on-metal hip prosthesis. Second generation metal-on-metal articulation in THR were reported to have considerably lower wear than metal ball on polyethylene liner articulation [17, 72]. The earliest types of metal-on-metal prostheses used in THR were made of stainless steel; however due to high rate of prosthesis fracture, Cobalt-Chromium has taken its place. Despite the advances in wear that metal-on-metal offers, great concerns have risen over this configuration. There is no way to fully avoid metal debris and in recent years Co-Cr particles have been speculated to cause adverse reaction is some patients, damaging bone and causing pain [73, 74].

Ceramic Ball on Ceramic Liner

Ceramic ball used with a ceramic liner has likely the best wear resistance of all the configurations. There are three types of ceramic material used in THR: *Alumina*, with high compression strength, high hardness, high resistance to abrasion and chemical attacks; *Zirconia*, exhibiting lower hardness than alumina but higher fracture toughness; and *Alumina-Zirconia composite*, with improved ageing behaviour and reduced brittleness of zirconia and alumina individually. Despite the advantages that ceramic-on-ceramic offers, they have become less interesting due to reports indicating that audible squeaking can occur [75]. Additionally they are very hard, and offer little shock absorption and can experience unexpected mechanical failures [76]. The failures may stem from the fact that ceramic materials have lower strength and toughness under tension and bending, but those are the loading modes in which cracks initiate and propagate [77].

2.2.3. Total Hip Replacement

There are two types of THR; one of them uses bone cement as a method of fixation and is referred to as cemented THR. Cemented hip replacements date back to 1960s when Sir John Charnley introduced a low-friction hip component for THR, using bone cement [78]. In the

1980s another type of THR emerged, without cement. This cementless type relies on the elastic properties of the proximal femur as a method of fixation. This method was supposed to prevent stem loosening in active patients by inducing bone growth instead of shielding the femur from natural stresses. The remainder of this sub-chapter will be dedicated to the two types of THR.

Cemented Total Hip Replacement

Sir John Charnley first introduced the cemented total hip arthroplasty in 1960. The technology included acrylic bone cement to fix prosthetic stems inside the femur (figure 19). Through the years, this method has proved itself as a very successful treatment for pathological hip joints. In cemented THA, a bone cavity is created by reaming trabecular bone from inside the medullary canal of the femur. Then a plug is inserted into canal, down to the isthmus to keep the bone cement from flowing towards the knee. When the stem is inserted, the bone cement is pressurised to flow into the trabecular bone, helping to provide a strong cement-bone interface. The fixation relies on a stable interface between stem and cement as well as a solid biomechanical bond between bone and cement. The cement has no adhesion properties, it only forms a micromechanical interlock with bone. The cement provides stability of the stem and stresses acting on the femur are transmitted down the metal prosthesis through the cement mantle [78]. Optimal thickness of the cement mantle between stem and bone is at least 2 mm [79]. Additionally, the acetabulum is reamed with circular reamers of a predefined outer diameter. This way the articular surface is removed and the acetabulum deepened enough to be able to securely fix the acetabulum cup with bone cement. Finite element studies of cemented stems have shown that the highest stresses occur at the bottom of the stem and around the calcar (the remaining femur neck at the medial side) [780, 81]. In the early generations of cemented stems, there was a concern about the fixation, because loosening was a big issue. Since then, fixation has improved, but up to this day, evidence indicates that it is still a problem in younger, more active patients [82].

Bone cement is usually made of polymethylmethacrylate (PMMA). It is rather ductile, with elongation of 0.8-2.5% and a modulus between 1.1 and 4.1 GPa (Hip replacement, 2002). PMMA is weakest in shear and tension but strongest in compression.

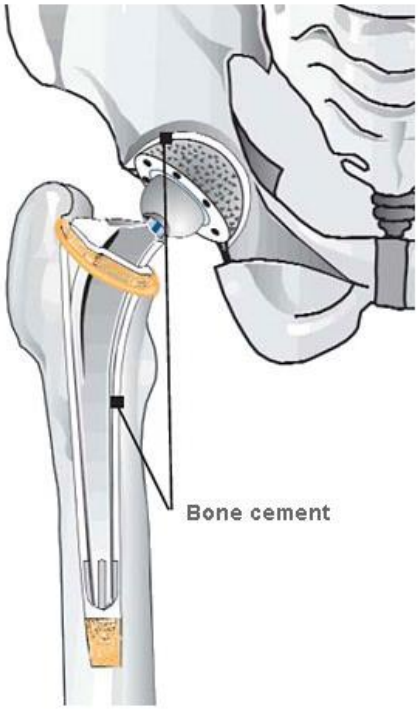

Figure 19: Image of implanted cemented THR components. Adapted from [83]

Cementless Total Hip Replacement

In the early 1990s, concerns over the fixation of cemented stems intensified. The main interest was improved cementing techniques and cementless fixation (figure 20). Fixation, thigh pain and wear were early problems of the young cementless stems. These concerns have greatly decreased up to day, as several cementless techniques are proving to be as good if not better than its cemented counterpart [18]. In the chapter „Press-Fit Femoral Components“ in *the Adult Hip* [84] there are three stages of fixation: *primary- secondary-* and *intermediate fixation*.

- *Primary fixation* is achieved in the operation, with press-fitting. In press-fitting the femoral cavity is made a little narrower than the stem. When the stem is press-fitted, the cross-sectional area of the femur increases. This change in cross-section is called *assembly strain* and is the reason for why the stem stays in place immediately after the surgery. If the assembly strain is too low, the stem will be loose, and if it is too high, the femur can break.
- *Secondary fixation*: The fracture of trabecular bone around the stem during surgery induces a healing response, which leads to the adjacent trabecular bone to grow onto (and into if the stem is porous coated) the stem. This solid fixation is

called *osseointegration*. Twelve weeks after the surgery, it is likely that no press-fitting remains and the osseointegration replaces the primary fixation.

- *Intermediate fixation*: During the period between press-fitting and osseointegration, a relaxation of the press-fitting is happening. This can lead to loss of fixation or apposition of new bone leading to osseointegration. The design of the implant will determine the fate of the fixation during this period. Coating the stem will induce the rate of osseointegration. Cementless stems tend to migrate in the intermediate period, but the stem design must ensure a stable enough fixation so osseointegration can occur.

For the acetabular components, the acetabular cup is reamed to be a bit smaller in diameter than the prosthetic component, so elastic properties of the bone hold it in place. The surgeon chooses how much press-fit is necessary; if the reamer is too small or the acetabular component too large, pelvic fracture can occur.

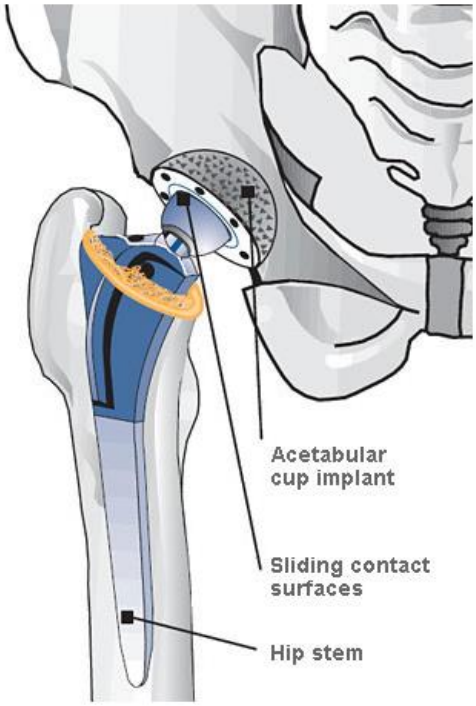

Figure 20: Image of implanted cementless THR components. Adapted from [83]

Hybrid Total Hip Replacement

Hybrid configuration in THR refers to when one component has cemented fixation and the other cementless. Until recently, hybrid THR usually included a cemented stem and cementless acetabular cup, thus the inverse configuration is referred to as reverse-hybrid THR. The reason for why reverse-hybrid THR was less frequently used was the well

documented success of cemented femoral stem while cementless stems have only recently been documented as good or better. However, according to recent reports, reverse hybrid THR has been performing well and in the future it might become more popular than hybrid THR [85, 86].

2.2.4. Cemented- or Cementless Total Hip Replacement?

Studies have shown that rapid, substantial and constant improvements in health-related quality-of-life can be achieved with both cemented and cementless THR [87, 88]. However, there are some documented differences between the two.

In 2012, 264 primary THAs were performed in Landspítali University Hospital; 159 cemented and 105 cementless. Table 5 shows the number of THRs performed with respect to implant type and their average therapy- and department costs. The therapy cost consists of operation theatre costs, surgeon salary, emergency room costs, research costs and outpatient department costs. The department cost consists of doctors' and nurses' salaries, medication and meals [5]. The therapy cost was similar; around 500.000 ISK per patient, but the department cost was a little higher for the cemented ones (351.000 ISK vs. 255.000). In 2013, until June, 119 THR operations have been performed (72 cemented and 47 cementless). The costs are in similar format as in 2012. In 2012, 27 revisions were made (16 cemented, 5 cementless, 6 hybrid), and in 2013, until June, 7 revisions (6 cemented, 1 cementless). As the table shows, the cost of revision surgeries is two times more expensive than the primary ones.

Table 4: Therapy and department cost (in ISK) of total hip replacements for 2012 and half of 2013. Numbers from [5]

		Type	Number	Therapy cost	Dpt cost
2013 (jan-june)	Primary	Cem	72	575.526	313.542
		Unc	47	550.470	288.291
		Mixed			
		Total	119		
	Revision	Cem	6	1.390.132	450.736
		Unc	1	1.750.555	503.552
		Mixed			
		Total	7		

		Type	Number	Therapy cost	Dpt cost
2012	Primary	Cem	159	517.230	351.139
		Unc	105	500.415	255.362
		Mixed	0		
		Total	264		
	Revision	Cem	16	1.264.650	681.468
		Unc	5	922.617	263.780
		Mixed	6	1.645.090	383.030
		Total	27		

The differences between the outcomes of cemented and cementless THR have been studied extensively. Cementless stems have been reported to be more frequently revised due to periprosthetic failure during surgery and the first two post-operative years [89], which might be explained by some minor fissures produced during the surgery [90]. However, the acetabular components appear to be the reason for most revisions of cementless prostheses. According to recent studies, cemented cups show superior results compared to cementless cups [85]. Revisions of cementless stems are, on the other hand, much easier than for cemented; the bone cement tends to stick to the bone and tear parts of it out of the medullary canal when removed. This further weakens the bone. Cementless stems generally appear to have slightly superior survival rates to cemented ones, especially for patients under 75 years [82, 91]. Survival rates for some cementless stems have been reported to be close to 99% after 20 years [2, 3]. *Stress shielding* is one of the reasons for premature revisions, it describes the redistribution of stresses that occur when the femoral head is replaced with a synthetic material; the load then bypasses the proximal femur and is carried through the stem into the diaphysis [30]. Stress shielding on the proximal femur is more frequent with cemented stems, since the only fixation of cementless stems is in the proximal femur they induce bone ingrowth, especially when they are porous-coated [1].

The recommendation for cementless THA depends on the patient's bone quality; the femur has to be able to tolerate the stresses derived from the press-fitting method of the surgery. Thus cementless stems are implanted in younger and more active patients while cemented prostheses are used in older patients with weaker bone. Therefore it should not surprise that cementless stems have been found to show superior outcomes in younger patients [82, 92, 93].

Looking at short term clinical outcome, most studies favour cemented stems [94] and the cementless type has been associated with slightly more thigh pain [95]. However, some studies conclude that cementless prostheses quality tends to gradually diminish with time and one of the advantages of cementless stems is its potential to permanently bond with the femur bone [96]. Table 6 gives a summary of the comparison between cemented and cementless THR discussed in this section.

Currently there are no an absolute criteria for choosing between the cemented and cementless THR. Orthopaedic surgeons decide between the two types and since women have lower BMD and it tends to decrease with age, those are the important criteria today. Although age and gender are known to give a good idea about the quality of bone and muscle quality, individual differences can be vast [97].

Table 5: Summary of comparison between cemented and cementless THR.

Cemented THR	Cementless THR
Advantages	**Advantages**
Better short-term outcomes	Better long-term outcomes
Cemented cups perform better.	Bone in-growth – permanent fixation
	Easier to remove
Disadvantages	**Disadvantages**
Quality tends to gradually decline with time	More often revised due to periprosthetic fracture
Harder to remove	Inferior survival rates of acetabular cups
Inferior survival rates of stems	

Revision of Total Hip Components

Despite the success of THR, there are some that fail, requiring revision surgery. Outcomes of revision surgeries are far worse than for primary revisions [98] with corresponding increase in cost.

The removal of cementless stems is most often easy while cemented stems can be more difficult. During extraction of cement from the femoral cavity, parts of the bone can be loosened. Further bone loss can be devastating when the bone quality is already of bad quality.

PMMA is cohesive rather than is adhesive, so it must interdigitate with trabecular bone to obtain appropriate fixation. When cemented stems loosen, migration of the stem within the canal leads to smoothening of the endosteal surface. This inhibits interdigitation and subsequently leads to weaker bond between stem and bone, thus cemented revision surgeries have a limited survival rate [99].

Due to the aforementioned problems with cemented revision stems, cementless are usually preferred. Several possibilities for cementless revision stems are available when the bone stock is poor; extensively porous coated stems with isthmus fixation are popular [18]. Since, most often, conditions for proximal fixation after failures are unfavourable, longer stems are often used to achieve distal fixation instead.

2.2.5. Prosthetic Technology

The design goal of all total hip arthroplasty prosthesis should be to relief patients from pain and restore hip joint function through restoration of load-bearing ability of articular surfaces. Other qualities all prosthesis should possess are:

- Biocompatibility – they should not cause adverse responses of surrounding tissues
- Resistance to wear, degradation and corrosion – they should keep their initial state for best service
- Similar properties to the structures they are intended to replace – if their properties are very different from the structure they replace, it can have negative effects on the surrounding tissues

There are three types of total hip replacement implants used in Iceland at the moment; two types of cemented stems (CPT Hip Stem and Spectron EF Hip Stem) and one cementless (Spotorno Hip Stem).

Cementless (CLS) Spotorno Hip Stem

The Spotorno stem was launched in Italy in 1984, based on the idea of proximal anchorage and long lasting stability due to osseointegration. It has maintained most of its original design, although it has been technically improved through the years. As of 2007, roughly 500,000 implants have been documented world-wide with the CLS hip system [100]. The stem can be seen in figure 24.

Figure 21: The Spotorno CLS stem. Adapted from [100].

The CLS Spotorno stem is made of a titanium alloy, more precisely Ti-6Al-4V, consisting of 88-91% titanium, 5.5-6.5 Aluminium, 3.5-4.5 Vanadium and less than 1% Carbon, Hydrogen, Iron, Nitrogen and Oxygen [101]. This roughly blasted titanium alloy prosthesis is largely osteophilic, meaning it induces osseointegration. Some of the mechanical properties of the Ti-6Al-4V alloy are shown in table 7.

Table 6: Material properties of Ti-6Al-4V alloy [102]

Properties	Values
Density	4.43 g/cm3
Ultimate Tensile strength	950 MPa
Tensile Yield Strength	880 MPa
Elongation at break	14%
Young's modulus	113.8 GPa
Compressive yield strength	970 MPa
Poisson's ratio	0,342
Shear strength	550 MPa

The main advantages of Titanium alloys in orthopaedics are [103]

- They have a relatively low modulus of elasticity compared to others
- They have superior biocompatibility and corrosion resistance
- Their wear and fatigue attributes are positive

However they report some disadvantages, the most significant being low shear strength. Aldinger et al. [104] reported an average 15-year follow-up of 240 patients with 257 CLS implants. The survival was 88% at 17 years. Survival with femoral revision for aseptic loosening as an end point was 94%. Proximally small osteolytic lesions were found on 15% of femurs with no incident of distal osteolysis. Müller et al. [2] followed 94 patients with 107 CLS stems for a mean of 17 years. Stable fixation was observed in 98.5% hips, and the stem survival (with non-traumatic loosening) after 17 years was 100%. High-grade stress shielding was seen in 14% of the hips and thigh pain in 20 hips. CLS was concluded to allow excellent long-term results in THA.

Collarless Polished Tapered (CPT) Cemented Hip Stem

The collarless, polished tapered cemented stem was introduced into clinical practice in England in the late 1980s [105]. The CPT stem is double-tapered, with a highly-polished surface and has a rectangular geometry proximally (figure 25). The design of the stem is based on the fact that the bone cement is a viscoelastic material and under constant load, deforms. The polished, tapered design ensures that the stem sits firmly when the cement

deforms, and optimizes the transfer of compressive stresses rather than shear forces [106, 107].

Figure 22: Three Collarless Polished Tapered stems with different offset values. Adapted from [107]

The CPT stem is made of Co-28Cr-6Mo; 58-59% Cobalt, 26-30% Chromium, 5-7% Molybdenum, 1% Manganese, 1% Silicon, 1% Nickel, 1.5% Iron and less than 1% of Carbon and Nitrogen. Some of the material properties of Co-28Cr-6Mo are listed in table 8.

Table 7: Material properties of medical grade Co-28Cr-6Mo. [101]

Properties	Values
Young's modulus	210 GPa
Tensile strength	1399-1586 MPa
Yield Strength	896-1200 MPa
Elongation at break	12%

According to Long and Rack [103] the main advantages of using Co-18-Cr-6Mo for implants are the excellent corrosion- and wear resistance, additionally fatigue strength is high.

The disadvantages are that they have a high Young's modulus (almost twice that of Titanium-based alloys), meaning it is very different from the modulus of bone. [108] conducted a research where 191 CPT stems were followed for average of 15.9 years in 175

patients. 11% of the patients needed some sort of revision procedure, of which 4% stems. Mean subsidence of 2.1 mm was noted. [105] did a clinical follow-up of 111 patients (122 hips) for at least 10 years. The mean subsidence was 1.95 mm and only three patients stem loosening occurred. However there was a high incidence of severe heterotopic ossification, affecting 22%, leading to ankylosis in some cases. [109] reported on 100 CPT receiving patients and after more than 5 years reported over 50% of the patients suffering from second degree of resorption or more, although none had fourth degree.

The Spectron EF Hip

Spectron cemented hip was introduced in USA in 1983. The femoral neck geometry is circulotrapezoidal to provide increased range of motion. Anterior/posterior grooves increase rotational stability without increasing stresses in the cement. The cross section is trapezoidal to minimise tensile stresses and longitudinally tapered to evenly distribute the stresses throughout the length of the prosthesis (figure 26).

Figure 23: Spectron EF Hip Stem. Adapted from [110]

The Spectron stem is made out of forged Cobalt-Chromium (the same medical grade Co-Cr as the CPT stem). Gerellick et al [111] compared the Spectron cemented stem with the Charnley cemented stem, which was a very popular hip stem. In the study, 206 Charnley prostheses were compared to 204 Spectron stems. During the 10 years of monitoring, 15 patients

required revision procedure, of which 7 Spectron. Four Spectron implants required revision due to aseptic loosening, all of which were the fault of the acetabular components. A 10-year survivorship of 95.9% (±3.0%) was reported for the Spectron stem. The study concluded that Spectron provided an excellent treatment for elderly patients. Issack et al published results in 2003 [112] where they introduce a mean follow-up of 16 years of 120 THR surgeries with Spectron stem. The mean age at the time of surgery was 68.5 years. Sixteen year survivorship of the stem with aseptic loosening as an endpoint was 90.3% (±4.4%).

2.2.6. Conclusion

In this chapter, numerous things have been identified. Amongst those things is the fact that likely the best articulation surface in THR is achieved with a ceramic prosthetic head on crosslinked polyethylene, although hard evidence are lacking. Similar costs have been associated with cemented and cementless THR in Landspítali University Hospital over the past two years; although slightly higher for cemented patients. The revision surgeries are, on the other hand, about two times more expensive than primary ones. Revising cemented stems is much harder than cementless stems and after removing a cemented stem, it is often impossible to acquire a good bone-stem interface. Despite the fact that there are many things that can affect the success of THR prostheses, cementless stems have generally been reported to have better long-term survival than cemented ones. The CLS stem has been reported with up to 99% survival after 17-20 years. The cementless acetabular cups are the reason for most failure of cementless THR. Therefore it will be interesting to see future reports on long-term follow-up of hybrid THR, with cementless stems and cemented cups. Furthermore, how the survival of cross-linked polyethylene will hold up.

2.3. Clinical Assessment of Total Hip Replacement Patients

2.3.1. Introduction

Pre-operative planning of THA is of paramount importance to obtain good results and meet the expectations of patients. Planning helps the surgeons to approach the operation visually before making a cut and therefore minimize the occurrence of wrongly placed implants and other complications such as intraoperative fracture.

This section will discuss intraoperative fractures, current trends in pre-operative planning for THA and the focus of recent studies on the subject.

2.3.2. Intra-operative Periprosthetic Fractures

One of the major possible complications of total hip arthroplasty is fracture of the femur, often referred to as periprosthetic fracture, and it has received great attention in literature, where researchers are always looking for ways to reduce this risk. Although not exclusive to cementless femoral components, the incidence of intra-operative periprosthetic fracture is higher than with cemented. Studies have shown incidence of fracture for cementless stems from as low as 1% up to over 20%, and usually less than 1% for cemented [113, 114, 115, 116]. The main reason for intraoperative fractures is the press-fitting in primary THA and bone loss in revisions. Female gender and increased age have been reported to be independent factors that influence fracture risk [117]. Osteoporosis is, however, believed to confound these factors. Rheumatoid arthritis and other comorbidities have been shown to increase fracture risk but similarly, osteopenia confounds those factors [118]. These results indicate that each patient should be thoroughly evaluated pre-operatively.

2.3.3. Current Pre-operative Planning

The success of total hip arthroplasty is based on the ability of doctors to provide a prosthetic stem that renews the biomechanics of the hip. No one implant is suitable for every patient because no two femurs are identical; therefore many sizes and types exist.

Saluja & Bargar in 2002 [119] described four stages of pre-operative planning for THA currently employed, they are: *History of conditions and physical examination*, *radiographic evaluation*, *implant selection* and *radiographic templating*.

History and physical examination

The doctor examines the type and severity of the hip arthritis. It is also important to investigate the etiology of the hip disease because every abnormality can cause anatomical and biological characteristics, which need to be addressed. Additionally a comprehensive physical examination is performed, where for example, leg length discrepancy (LLD) is measured. In figure 27 a traditional fill-in form of physical examination before THA surgery can be seen.

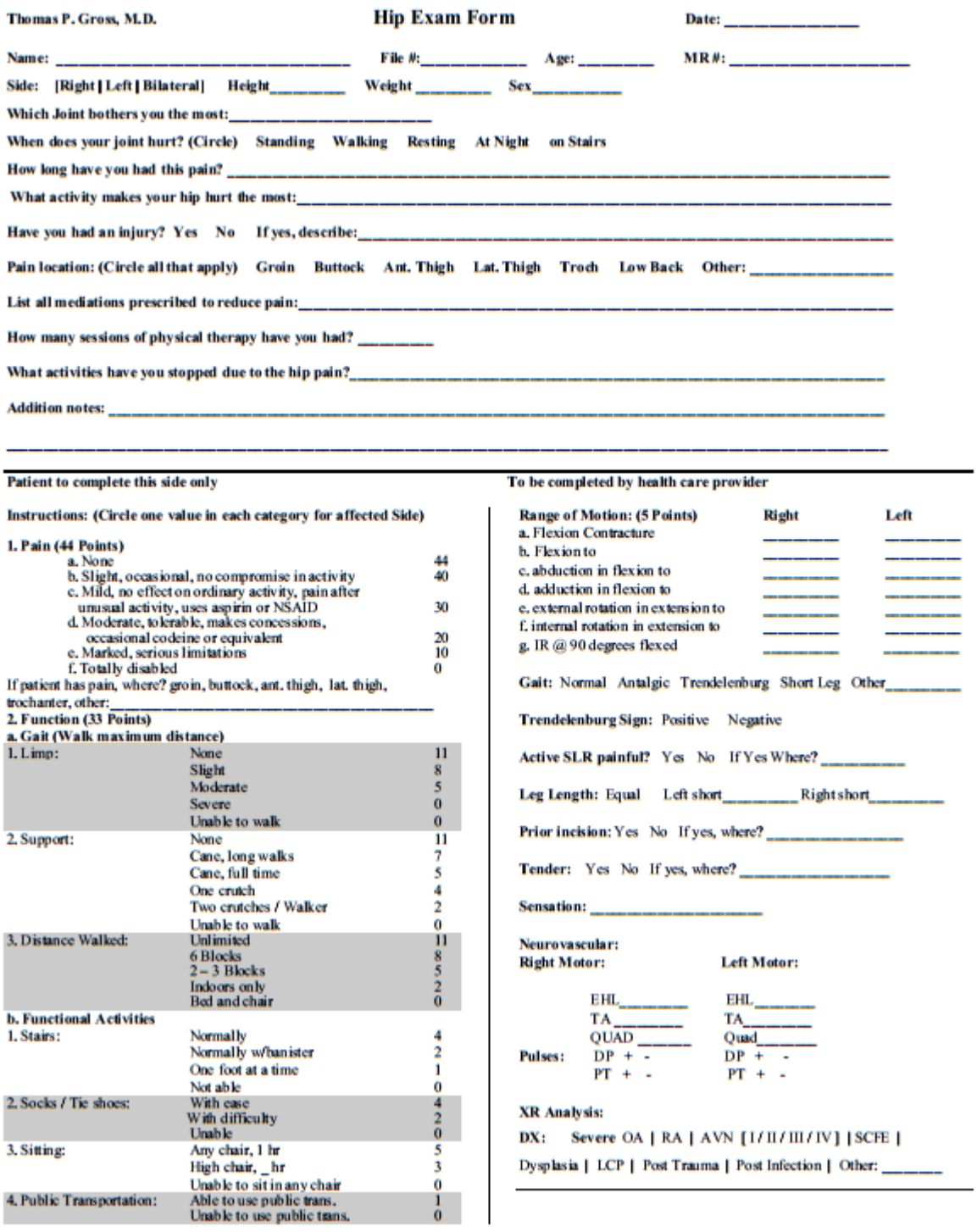

Thomas P. Gross, M.D.

Hip Exam Form

Date: _____

Name: _____ File #:_____ Age: _____ MR#: _____

Side: [Right | Left | Bilateral] Height_____ Weight _____ Sex_____

Which Joint bothers you the most:_____

When does your joint hurt? (Circle) Standing Walking Resting At Night on Stairs

How long have you had this pain? _____

What activity makes your hip hurt the most:_____

Have you had an injury? Yes No If yes, describe:_____

Pain location: (Circle all that apply) Groin Buttock Ant. Thigh Lat. Thigh Troch Low Back Other: _____

List all mediations prescribed to reduce pain:_____

How many sessions of physical therapy have you had? _____

What activities have you stopped due to the hip pain?_____

Addition notes: _____

_____

Patient to complete this side only

Instructions: (Circle one value in each category for affected Side)

1. Pain (44 Points)

a. None	44
b. Slight, occasional, no compromise in activity	40
c. Mild, no effect on ordinary activity, pain after unusual activity, uses aspirin or NSAID	30
d. Moderate, tolerable, makes concessions, occasional codeine or equivalent	20
e. Marked, serious limitations	10
f. Totally disabled	0

If patient has pain, where? groin, buttock, ant. thigh, lat. thigh, trochanter, other:_____

2. Function (33 Points)

a. Gait (Walk maximum distance)

1. Limp:	None	11
	Slight	8
	Moderate	5
	Severe	0
	Unable to walk	0
2. Support:	None	11
	Cane, long walks	7
	Cane, full time	5
	One crutch	4
	Two crutches / Walker	2
	Unable to walk	0
3. Distance Walked:	Unlimited	11
	6 Blocks	8
	2 – 3 Blocks	5
	Indoors only	2
	Bed and chair	0

b. Functional Activities

1. Stairs:	Normally	4
	Normally w/banister	2
	One foot at a time	1
	Not able	0
2. Socks / Tie shoes:	With ease	4
	With difficulty	2
	Unable	0
3. Sitting:	Any chair, 1 hr	5
	High chair, _ hr	3
	Unable to sit in any chair	0
4. Public Transportation:	Able to use public trans.	1
	Unable to use public trans.	0

To be completed by health care provider

Range of Motion: (5 Points)	Right	Left
a. Flexion Contracture	_____	_____
b. Flexion to	_____	_____
c. abduction in flexion to	_____	_____
d. adduction in flexion to	_____	_____
e. external rotation in extension to	_____	_____
f. internal rotation in extension to	_____	_____
g. IR @ 90 degrees flexed	_____	_____

Gait: Normal Antalgic Trendelenburg Short Leg Other_____

Trendelenburg Sign: Positive Negative

Active SLR painful? Yes No If Yes Where? _____

Leg Length: Equal Left short_____ Right short_____

Prior incision: Yes No If yes, where? _____

Tender: Yes No If yes, where? _____

Sensation: _____

Neurovascular:

Right Motor:		Left Motor:
	EHL_____	EHL_____
	TA_____	TA_____
	QUAD _____	Quad_____
Pulses:	DP + -	DP + -
	PT + -	PT + -

XR Analysis:

DX: Severe OA | RA | AVN [I / II / III / IV] | SCFE |

Dysplasia | LCP | Post Trauma | Post Infection | Other: _____

Figure 24: A form for documenting basic history physical examination findings. Adapted from [120]

Radiographic evaluation

This step includes evaluation of the hip on a good-quality radiograph. The radiographs are usually in anterior-posterior view, to measure the femoral neck angle, lateral offset and overall comparison between the two legs.

Implant selection

There are number of factors that contribute to the decision of implant type; whereof age and activity are one of the most important. Younger, higher-demand patients, usually receive cementless implants while the older, low-demand patients receive cemented prostheses. Bone quality is also important. Canal Flare Index (CFI) as Noble [121] describes is sometimes used as an indicator for implant choice; it is the ratio of canal width 20 mm proximal to the lesser trochanter to the width at the isthmus (Figure 28). A ratio of 3.0-4.7 is considered normal. When the ratio is less than 3.0 the femur is said to have stovepipe configuration and when the ratio is above 4.7 the femur is said to have champagne flute configuration. Stovepipe configuration is usually convenient for cemented implant while the champagne flute suits uncemented better. Sometimes the femur is anteverted, so a custom-made prosthesis might be needed - all anatomical distortions need to be identified. The severity of arthrosis needs to be evaluated on a radiograph; the more severe, the less the femur is suitable for uncemented implants, due to less bone mineral density.

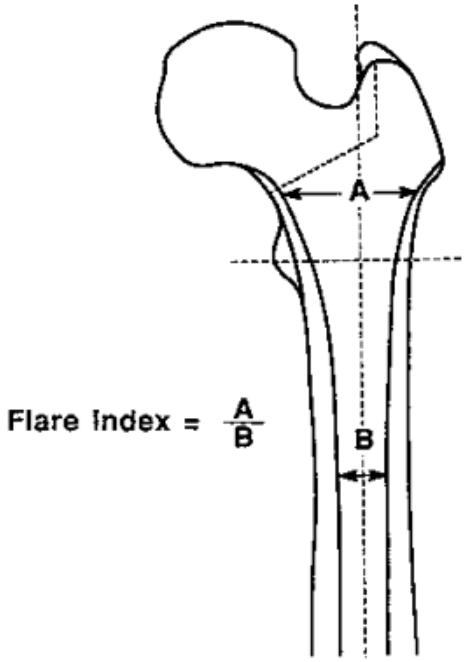

Figure 25: Canal flare index, the ratio of the proximal and distal width of the femoral canal. Adapted from [119]

Radiographic templating

When the implant type has been selected, the size and femoral neck resection needs to be estimated. A line is drawn on the radiographic image between similar points on each femur with the acetabulum as a reference. This way the LLD can be estimated, and fixed during the surgery. Pelvic obliquity is also considered for the LLD analysis. The femoral components are then templated on an anterior-posterior

radiograph. Uncemented stems are templated in the way that they totally fill the femur while cemented stems are given more room, since there has to 2-3 mm for the bone cement between stem and bone. The offset is determined in consideration with LLD, and the neck resection is marked on the radiograph. Pre-operative planning is important for the success of THA [122, 123]. However some studies conclude the need for better methods to estimate bone morphology and quality [124]. To minimize the rate of revision THR surgeries, all the suitable and available technologies have to be properly utilized for more substantial pre-operative planning of THR.

Studies on Pre-operative Assessment

A lot has been published on pre-operative planning for THA. Templating is reported to have significant effect on the outcome of THA, increasing its success [122, 123, 125]. Templating contributes to correct positioning of the femoral and acetabular components during surgery. Comparing digital and analogue templating, digital templating techniques seem to be overtaking the analogue ones [126, 127, 128]. Following the digitalism of templating are techniques using Computed Tomography which are used increasingly in pre-operative planning and navigation for THA. 3D templating, with CT-based procedures, seems to offer more reliable planning for prosthesis size and orientation [129, 130]. Eingartner [131] remarks that two types of navigation is currently used,: image guided procedures (Pre-operative CT and intra-operative fluoroscopy) and kinematic navigation. He argues that improved accuracy could be shown, compared to conventional templating [132, 133].

The current preoperative planning mostly includes stem positioning with templating and navigation, however the current trends lack quantitative planning and sensitive tools to decide on the implant type and patient's outcomes.

2.3.4. Conclusion

Most of the efforts of studies on pre-operative assessment for THR have been on templating techniques, which have been reported to have positive effect on the success of placement of THR implants.

Bone mineral density tends to decrease with age and usually is lower in females. Therefore gender and age are amongst the most important criteria for choice of implant. However, comorbidities such as osteoporosis confound this trend; therefore there is urgent need for quantitative, patient-specific pre-operative analysis of bone quality to choose the correct type of implant more securely.

2.4. The Finite Element Method

2.4.1. Introduction

Modelling complex bodies can be a difficult task and calculations time consuming. In the mid-20th century an approach in mechanics emerged, based on division of complex elements into many smaller, simpler elements to approximate a more complex differential equation over a large domain. This method is referred to as the finite element method (FEM) and analyses based on this method called finite element analyses (FEA).

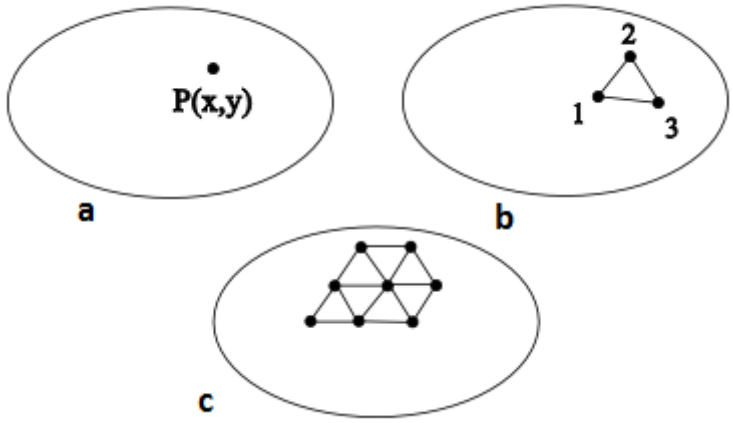

Figure 26: a) A two-dimensional domain of a field variable. b) Three nodes comprising a finite element inside the domain. c) Additional elements added, comprising a mesh.

To explain how finite element analysis works, it is best to look first at figure 26a. In the figure there is a volume of a material (or a domain). For simplification, the object is considered to be two-dimensional, with a single field element $\phi(x,y)$, where x and y are axes values of the Cartesian coordinate system. This field element need to be defined at every point P(x,y) inside the domain. That means that at every existing point inside the domain, some governing equation needs to be satisfied. However, due to the fact that most material domains are complex there is a need for methods based on numerical techniques and digital computation. FEA is a good tool for this kind of analysis. In figure 26b there is now, inside of the domain, a subdomain, with three points connected to each other. Together these points form a finite element, and the points are called element nodes. In finite element analysis, the governing equation is satisfied at the nodes and then interpolation functions are used to interpolate the values between nodes to acquire values of the field element at non-nodal points. Figure 26c shows more elements linked together to form a mesh inside the domain. By dividing complex bodies into smaller elements like this and acquiring approximate

solutions, it is much easier to calculate of distribution of field variable values inside their domain.

2.4.2. Assignment of Material Properties to Finite Element Models

As mentioned before, bones are anisotropic, viscoelastic. They are also highly inhomogeneous; therefore research is often focused on investigating assignment of material properties to finite element models of bones. Since stresses on bones cannot be measured in-vivo, several different CT-based models have been generated in the field of biomechanics. First, CT-imaging principles need to be addressed.

In CT-imaging, X-rays are sent through the material under investigation, from all directions (in a spiral). The incident X-rays travel through the body and are attenuated differently depending on the density and thickness of objects in its way. The difference between the incident and the detected X-rays are used to project a two-dimensional image of the objects. Together, all the X-ray projections, from all the directions, are calculated to build a three-dimensional image of the region of interest (ROI). The values assigned to each volume element (voxel) in a CT-image are given in Hounsfield Units (HU). HU indicate the X-ray attenuation represented by voxels in the CT image. HU are calculated:

$$HU = \frac{\mu_{voxel} - \mu_{water}}{\mu_{water}} \qquad (12)$$

where μ is an attenuation coefficient. This means that CT images are calibrated with reference to water attenuation.

There is a relationship between HU of a CT-image and the actual bone density. Some researchers have investigated the relationship between HU and BMD[1] [134, 135]. Accuracy of material properties assignment has also been studied extensively. Taddei et al [136, 137] compared the accuracy of density-based inhomogeneous models with two-material model, where cortical and trabecular bones were separately considered homogenous. Both methods were compared with experimental data on wet cadaveric specimens. The results were that assigning inhomogeneous material properties had better accuracy. Some researchers have investigated the effect of how many elements are used to comprise the FE models on their strain energy calculation [138]. This is important since the number of elements in the FE model controls time-length of running simulations. Other studies have focused on comparing

[1] BMD is a measure of density of minerals (such as calcium) in bones.

the quality of different density-based inhomogeneous equations for assigning material properties of femoral bones [139]. The general equation relating Young‘s modulus to the density has the form:

$$E = a + b\rho^c \qquad (13)$$

where *a*,*b* and *c* are model parameters, *E* is the Young‘s modulus and ρ is the density of bone, either *ash density* or *apparent density*. Apparent density is the ratio of bone tissue mass in a specimen to the bulk volume, while the ash density is the total mineral content divided by bulk volume.

It is evident that the accuracy of models has great effect on the value of the results. However, there is no way to include all the features of bone behaviour in a single model, so the analyst has to decide what is of most interest at each time and how time-consuming it can be.

2.4.3. Other Applications of Finite Element Models in Total Hip Replacement

In one way or another, for THR applications, most researchers have been using FEM to simulate the *strain distribution* in the prosthetic stem, cement or bone tissue. Some have used FEA to investigate the cement condition; different stress distribution for different cementing conditions [140] and others to research the debonding between cement and the bone or femoral prosthesis [81, 141]. Concerning femoral stem design, finite element methods have often been employed, both for analysing and comparing different design features [142, 143] and in designing new femoral stems, addressing known issues leading to failure [144, 145, 146]. Increasing number of researchers are investigating micromotion and stability of cementless stems, concluding that material properties of the stem and friction between stem and bone significantly influence the stress distribution and initial stability [147, 148, 149, 150]. Since stress-shielding is amongst the leading cause for stem loosening, many studies have taken on this subject. Lengsfeld et al, [151] for example, made finite element models of THA patients approximately 12 years post-surgery, identifying large strain density differences between operated- and non-operated femurs for most subjects. Other studies take on other causes of failure of femoral and acetabular components with the help of FEA, such as wear [152], dislocation manoeuvres [153] and fatigue. Most fatigue analysis based on FEA, for

THA applications, concern the polyethylene acetabular cup [154, 155, 156] since polyethylene wear debris has been implicated in osteolytic lesion development [157].

With increasing technical advancement in biology and biomechanics, more complex models of mechanical and biological processes can be investigated, understood and used in simulations. More complex and accurate 3D models and simulations lead to the possibility to design more reliable femoral- and hip components for THA.

2.4.4. Conclusions

The objective of this chapter was to explain the basic principles of the finite element method and demonstrate how it can be used to model living structure. Furthermore, to demonstrate how assigning material properties to finite element models can help to approximate the behaviour of living tissue. In the next chapter, methods of the finite element analysis of this study will be introduced. Some parts of those methods are developed from studies like the ones mentioned above.

3. Materials and Methods

In figure 27 the workflow of this study is presented. The first step was to recruit patients undergoing THA for the first time (without total knee arthroplasty) and call them for a pre-operative CT-scan. Next, the CT-images of the patients were segmented, where regions of interest are separated from the rest. From the segmented two-dimensional images three-dimensional models could be built. Directly from the models, the bone mineral density was calculated with a conversion from HU values. For the finite element analysis, a finite element mesh was made from the 3D models. Then boundary conditions were added to the model resulting in strain distribution on the proximal femur. From selected strain values, the Fracture Risk Index was calculated.

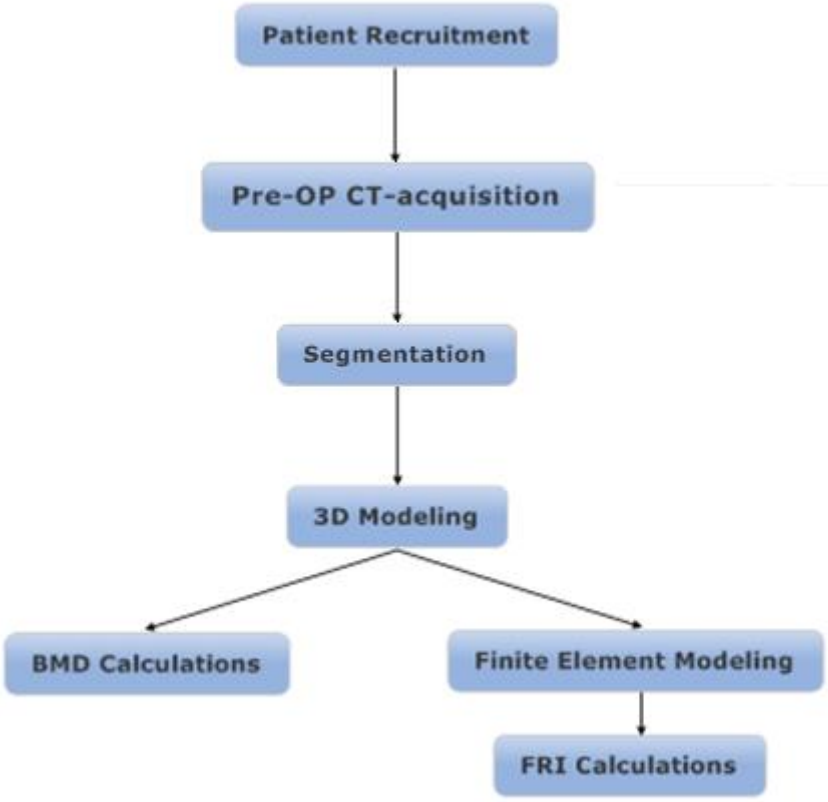

Figure 27: Overall workflow of the study

3.1. Patient Recruitment

Thirty-nine patients were voluntarily enrolled in the study (23 females and 16 males). Eighteen patients received cemented and 21 received cementless implant. The implant type was decided according to the evaluation of the surgeons; mainly based on age, gender and

general clinical conditions. The average age at the time of operation was 60.2 years (54.7 yrs for males and 64.0 yrs for females, p=0.0186; 54.0 yrs for cementless and 67.4 yrs for cemented, p>0.01). Patients with total knee implants, previous hip implants or received implants during the research period, were excluded. Table 8 gives an overview of the participants.

Table 8: Overview of all the patients in the study.

Participants		
21 Cementless (54.8%)	18 Cemented (46.2%)	
Average Age	Average Age =	p>0.01
54.0 (± 10.65) years	67.4 (± 6.60) years	
23 Females (59.0%)	16 Males (41.0)%	
Average Age	Average Age	
64.0 (± 8.68) years	54.7 (± 13.67) years	p=0.0186

3.2. CT Acquisition

All participants in the project were scanned with a 64 Philips Brilliance spiral-CT machine (figure 28) before, 24 hours after and 52 weeks after surgery. However, for the purpose of this study, only pre-operative and 24 hour data were used. The scanning region extends from iliac crest to the middle of the femur (figure 29). The image protocol included slice thickness of 1 mm, slice increment of 0.5 mm and the tube intensity was set to 120 KeV. The slice increment determines how much the gantry moves forward each circle and if it is shorter than the slice thickness, overlapping occurs. Overlapping increases quality due to the fact that more photons pass through per unit volume. This imaging protocol allowed an accurate 3D reconstruction of the proximal femur.

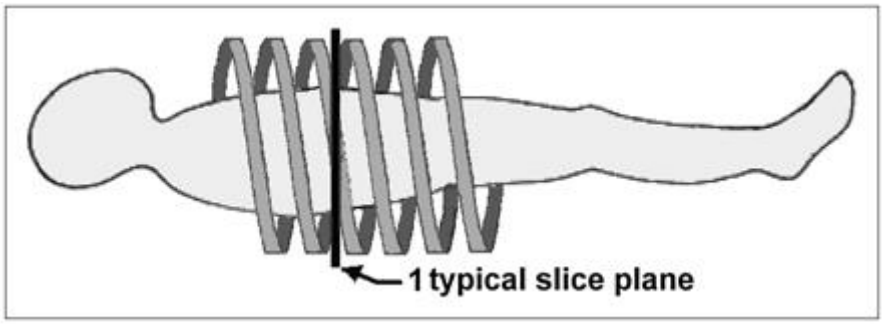

Figure 28: Explanatory drawing of a spiral-CT camera movement. Adapted from [158]

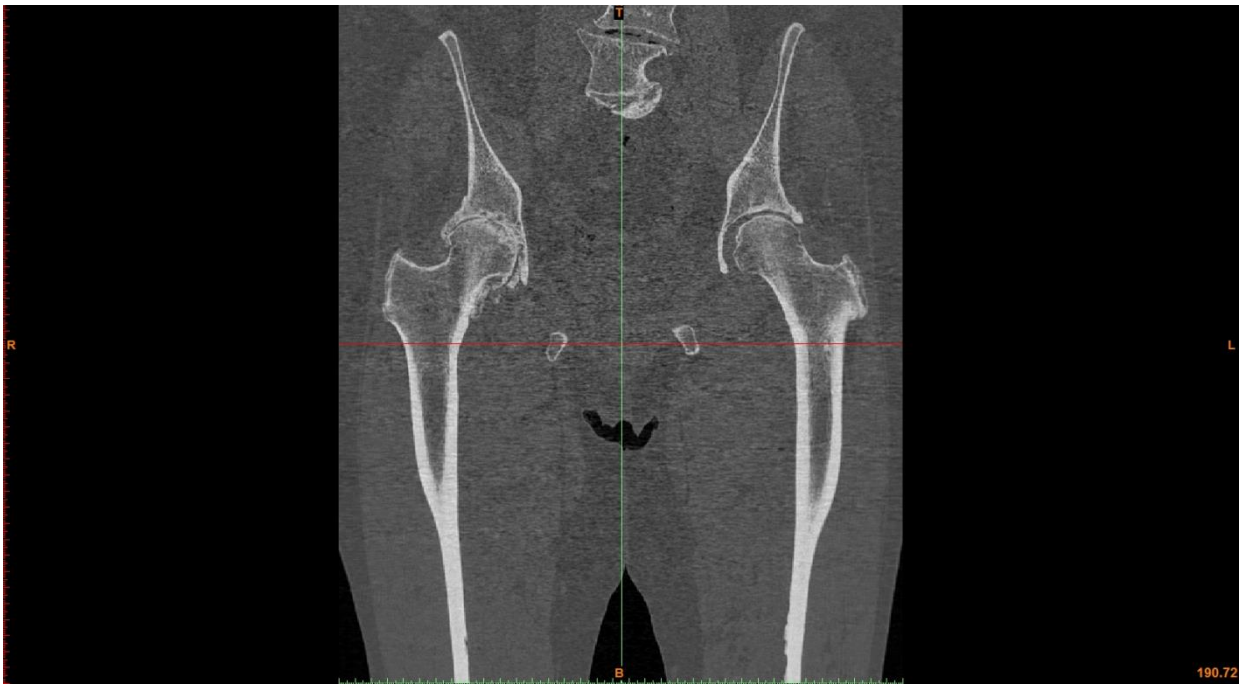

Figure 29: Coronal view of an CT image slice used in the study.

3.2.1. CT Calibration

Prior to the study, the CT machine was calibrated to acquire a relationship between HU and BMD. The relationship was not a completely linear. The resultant relationship can be seen in figure 30. The resultant equation, giving the relationship between HU and BMD was:

$$BMD\ \left[{}^{g}/_{cm^3}\right] = (-8 \cdot 10^{-8})HU^2 + (0{,}0006)HU + 0{,}9456 \qquad (14)$$

Linear regression analysis resulted in a correlation coefficient $R^2 \sim 0.99$.

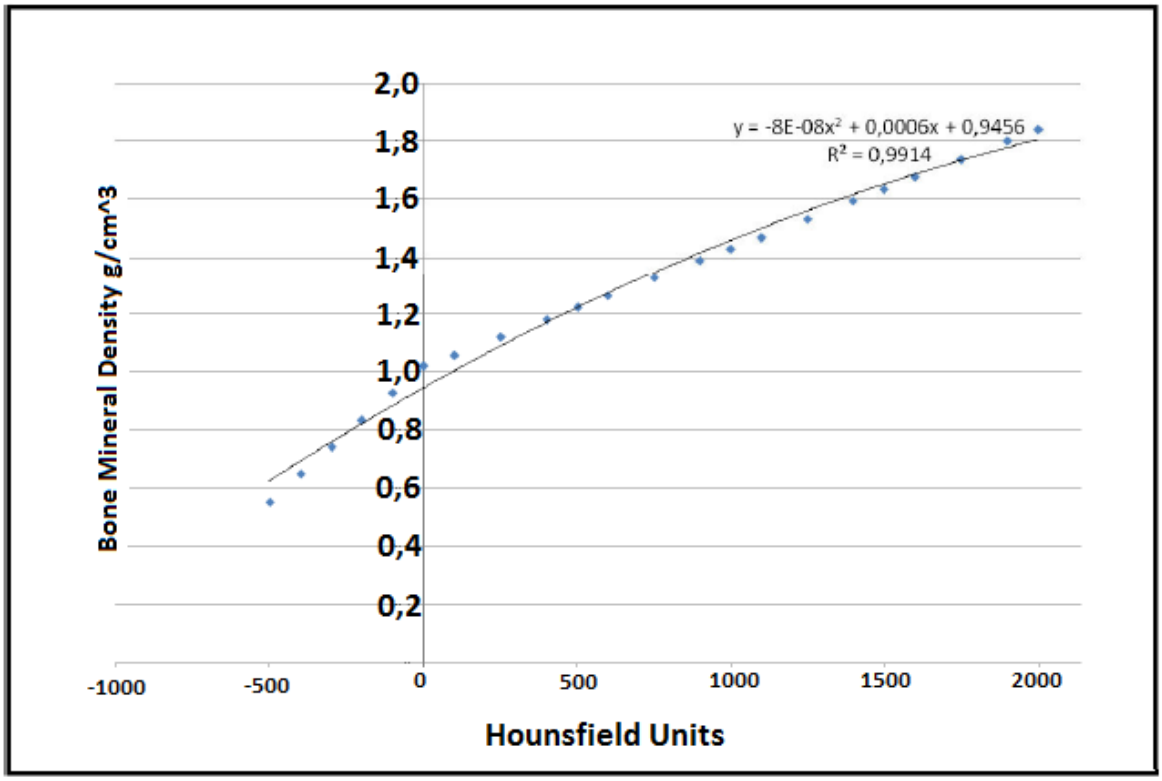

Figure 30: Density plotted against Hounsfield Units to calibrate the CT-machine. The line of best fit is shown as well as its equation

3.3. Segmentation

In order to build the 3D models of the CT-data were imported into Mimics [159]. There, by selecting known HU thresholds for bone along with some minor manual refinements, the image elements belonging to the femur were collected in a mask (figure 31A). Then a 3D model was calculated of this mask (figure31B). With polyplanes, the femoral head was cut off, similar to the surgery (figure 31C). From this model, a new mask was created (figure (31D).

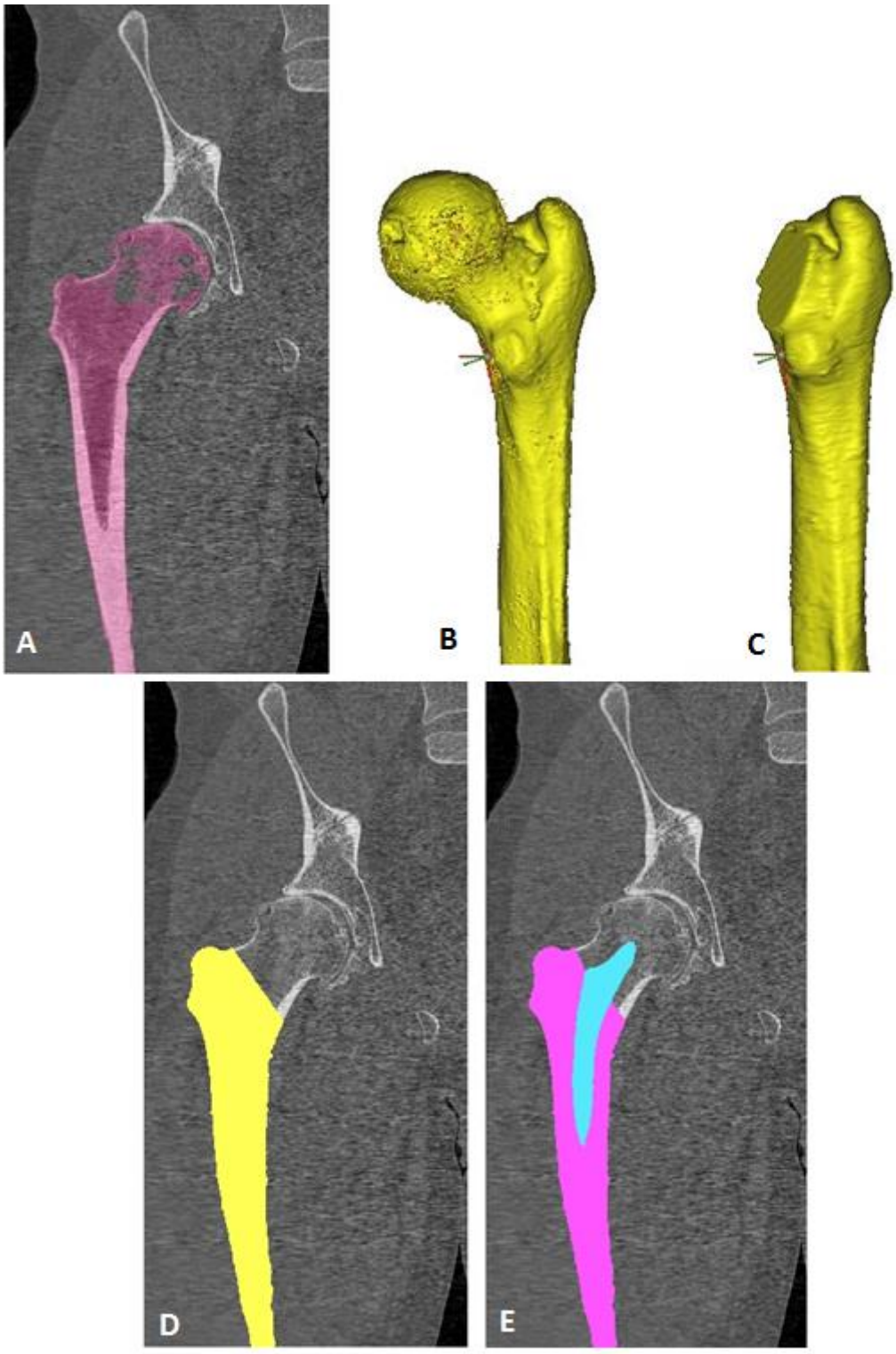

Figure 31: The progress of modelling. A) A mask of the whole femur. B) A 3D model of the femur from A. C) The model after the femoral head has been cut off. D) A mask calculated from the model in C. E) The mask after the stem has been inserted.

3.4. Fracture Risk Index Calculations

3.4.1. Finite Element Modeling

Since this data is obtained from the pre-operative CT-scans, the stem is not on the images. Therefore, the stem has to be exported from the 24 hours post images into the pre-operative. For the cementless patients, their own stem is imported into the pre-operative data, however, for the cemented patients a stem of appropriate size has to be exported from post-operative data of one of the cementless patients. The stem then has to be positioned in the way that it does not touch the cortical bone at any place. When the stem mask has been properly positioned (figure 31D) inside the mask of the femur, a non-manifold model can be created, where every pixel in the model only belongs to one mask. From the two masks in figure 31D, a non-manifold model was created were the stem and the femur volumes do not overlap (figure 32A). Using 3-matic, a software module accompanied with Mimics, the non-manifold model is meshed, that is, it is divided into numerous small tetrahedral elements (figure 32B). This is the finite element model.

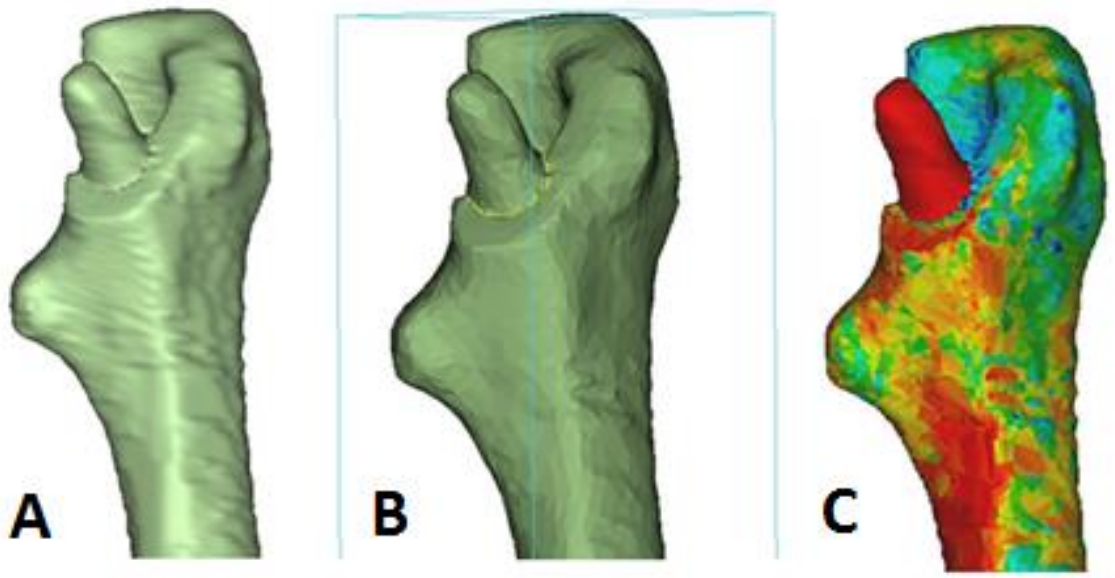

Figure 32: A meshed model of a femur, showing the tetrahedral elements inside the model.

The elements of the FE model need to be given material properties that describe their behaviour. Forty different values of material properties are given to the elements, so those who have similar HU values are pooled together under one value. For simplification, the femur was considered isotropic and using the aforementioned HU to BMD conversion, the Young's modulus of the elements was obtained using an equation introduced in [134]:

$$E = 10500 \cdot {\rho_{ash}}^{2.29} \quad (15)$$

where ρ_{ash} is the bone mineral density from equation 14. This equation yields E in MPa if ρ_{ash} is provided in g cm^{-3}. This formula was used to represent both trabecular and cortical bone. In figure 32C a FE model of a femur can be seen when the material properties have been added. The colour represents the Young's modulus; red colour means high modulus, while green and blue mean less modulus; the stem is given one Young's modulus and is all red compared to the femur, which is given 40 different values of Young's modulus and none reach the value of the stem.

Additionally a Poisson's ratio of 0.33 was assumed for the whole bone mask. Material properties of the implant were added according to table 5. Each model consisted of 70-90.000 elements.

3.4.2. Fracture Risk Calculations

The FE model of the femur, containing the material properties, is imported into Ansys Mechanical APDL [160]. There a static structural analysis was performed on the model. The objective of the simulations was to simulate the forces introduced on the femur during the press-fitting surgery of cementless stems. When the stem is pushed into the medullary canal most tensile stresses can be expected to arise at the medial- and lateral side of the proximal end, since the flare of the stem is the steepest at the top. After experiments with a hammer used in cementless THR surgeries, a force of 1000 N was decided to be added in each direction at the proximal canal (figure 33). This force is considered to represent the cumulative force introduced intra-operatively.

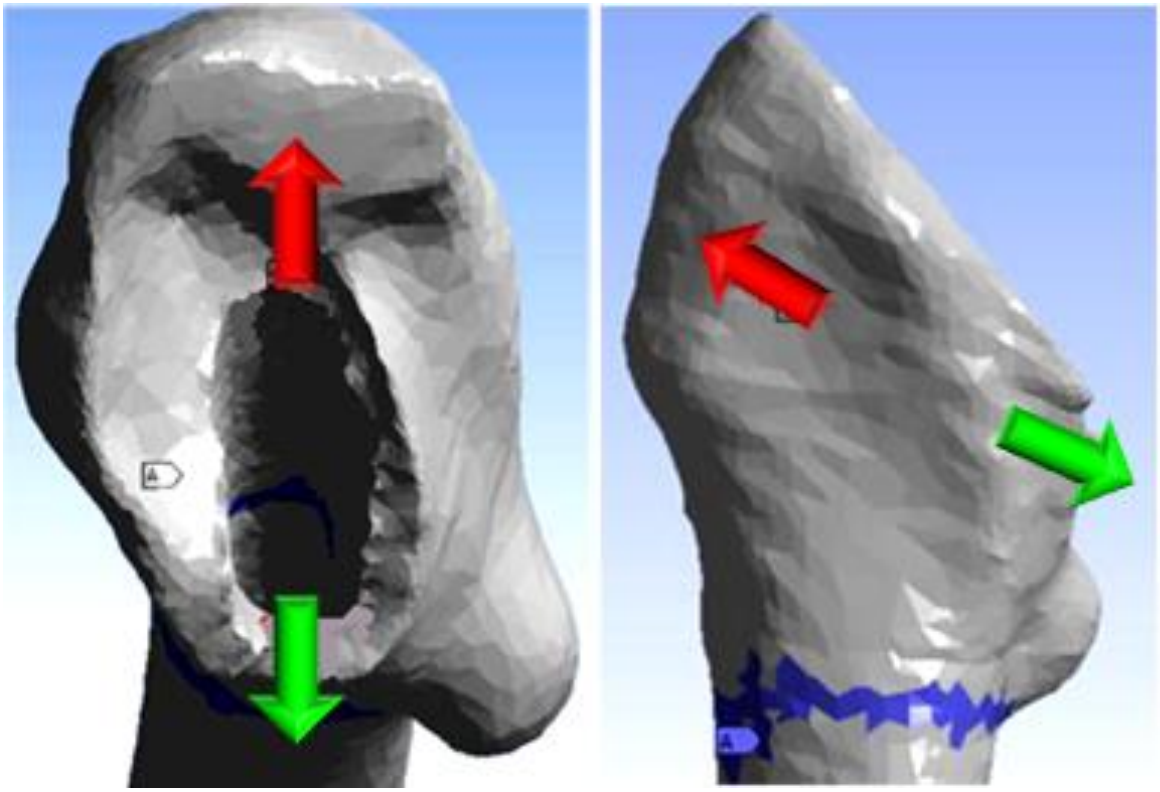

Figure 33: Boundary conditions used for the simulations in Ansys. The arrows represent the forces while the blue color represents the fixed elements.

Strain distribution of the proximal femur is of interest in these simulations and therefore a fixed support was added below the lesser trochanter. This was done to exclude displacements below, thus minimising the risk of bending of the shaft. The results of the simulation are in the form of von Mises strain distribution. The von Mises strain is an equivalent of all strains, both normal and shear strains, and while this equivalent strain is under the yield the material is not considered failed, according to the von Mises criterion. The von Mises strain distribution is used to calculate the risk of fracture; chosen values are compared to a known yield strain from literature. Ultimate strength of bones is known to be dependent on bone mineral density of bones [43, 161] and usually ranges from 0.6-1.2%. Since the density does not vary a great deal in the region of interest a value of 0.9% was considered to represent a catastrophical failure of the bone. The fracture risk index was calculated:

$$FRI(\%) = \frac{\varepsilon_{max}}{\varepsilon_{yield}} \cdot 100\% \qquad (16)$$

where ε_{max} was the von Mises equivalent strain of the selected elements. Values for ε_{max} were selected from standardised areas, and the one value chosen to represent each area was the average of ten close-by measurements. The FRI was calculated in the areas seen in figure 34.

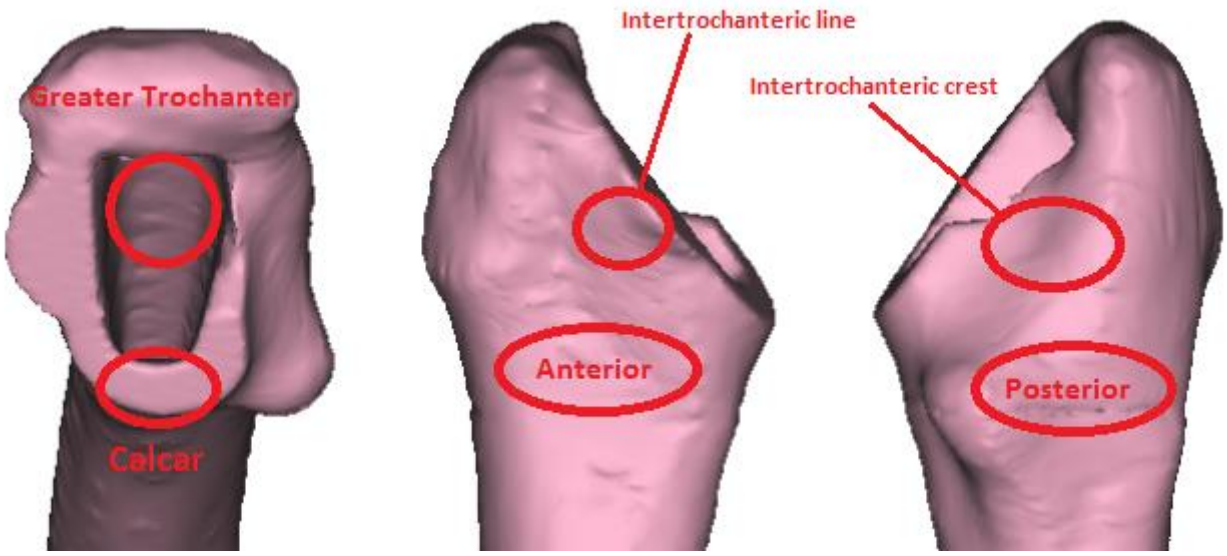

Figure 34: Location of strain readings used to calculate fracture risk index.

Since the yield stress of bone is dependent on the density, an example test was done, as a alternative way of realising the risk of fracture. This method included calculating the stress in each element of the finite element model and graphing it against density. First the relationship between yield stress and bone mineral density is plotted. The relationship is described in [161]:

$$for\ \rho_{ash} < 0.317:$$
$$Yield\ \text{Stress [MPa]} = 137 = \rho_{ash}^{1.88} \quad (17)$$

$$or\ \rho_{ash} \geq 0.317:$$
$$Yield\ \text{Stress [MPa]} = 114 = \rho_{ash}^{1.72} \quad (18)$$

Then the stress results from the simulation are used to plot a scatter where elements are given red colour if their simulated stress reaches their calculated yield stress, otherwise they are given green colour.

3.5. Bone Mineral Density Calculations

Using the mask of the femur seen in figure 31D, a 3D model was calculated; without the stem. In the same manner as when the head of the femur was cut off, a cut is made to separate the femoral shaft and the proximal femur, at the middle of the lesser trochanter. Then the upper part is used to calculate a new mask, containing the image elements that are included in the BMD measurements. From this mask, the average HU values are extracted and converted to

BMD with equation 14. In figure 35 the region used to calculate the BMD is shown as blue. The other two (white) parts have been separated from this mask. Additionally, in the figure, inside the femur head, osteolytic parts can be observed.

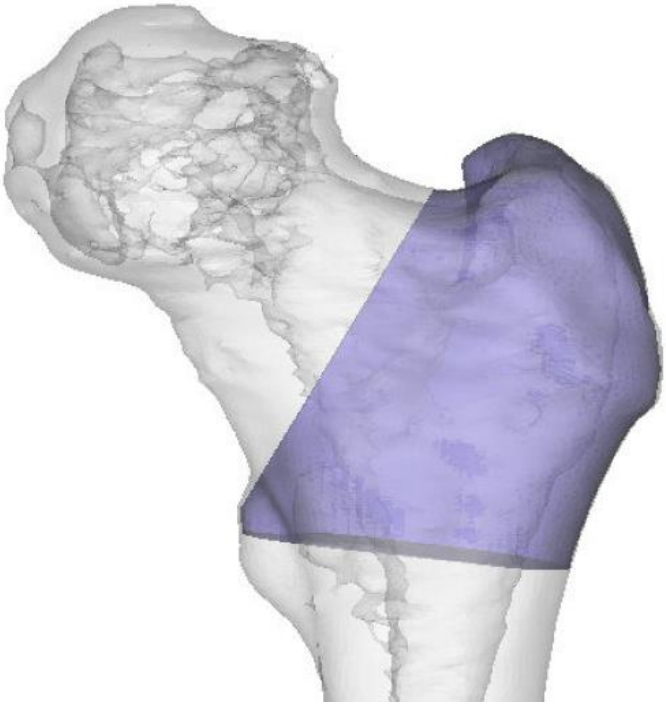

Figure 35: The region of the proximal femur used to evaluate the bone mineral density of patients.

4. Results

4.1. Fracture Risk Index

Fracture Risk Index was calculated for 38 of the 39 enrolled patients. The results from one of the patients can be seen in figure 36. There the force direction is indicated with red arrows and the surface elements colored blue are those who are fixed in the model. The highest fracture risk on the image was on the calcar and the greater trochanter area. It was similar for the rest of the patients where highest FRI was observed for 73.7% of the patients and the greater trochanter for the rest, or 26.3%.

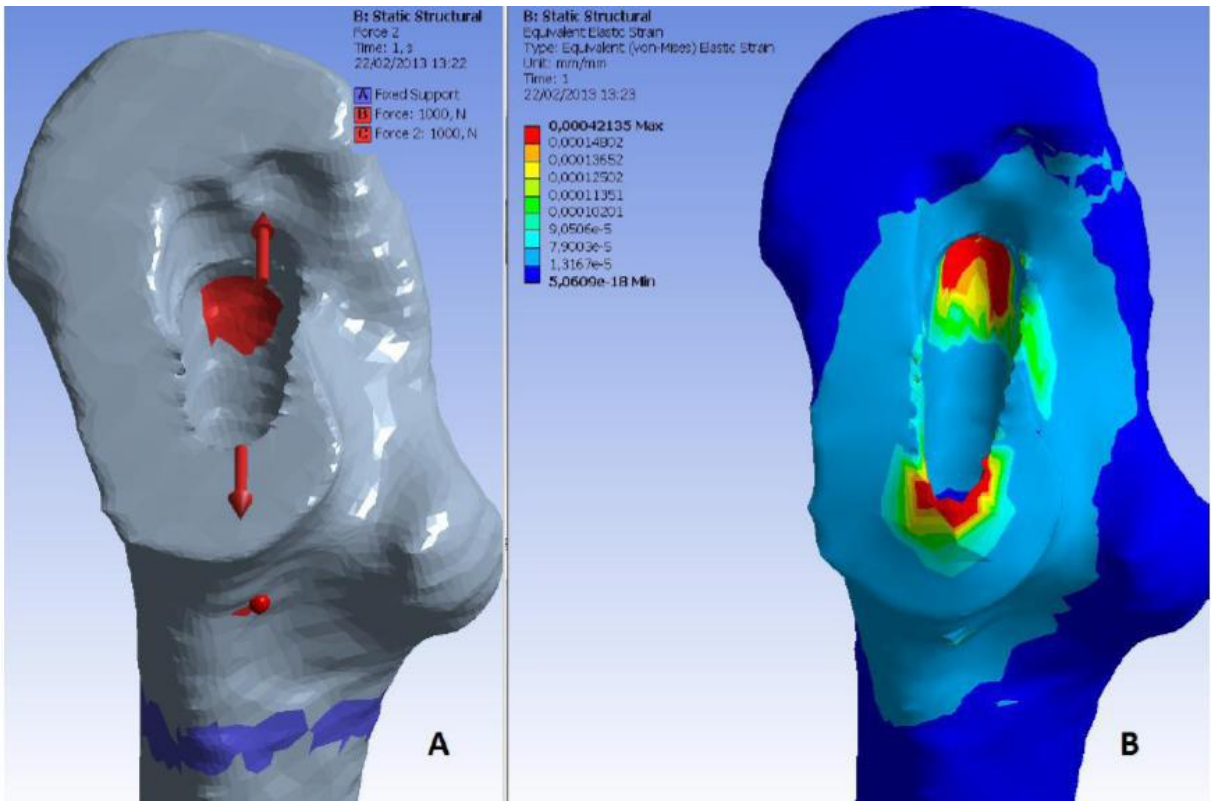

Figure 36: A) The boundary conditions used in the simulations, the red arrows are the forces used and the blue color indicates where the fixed support was added. B) The von Mises strain distribution around the femoral opening, where strain is represented with color from blue to red for low to high respectively.

The average FRI was 1.293% (±0.78%) for the cementless patients while 0.976% (±0.58%) for the cemented; the difference did not reach significance (p=0.27). A power analysis gave the results that 96 patients are needed in order to acquire a statistically significant difference between the groups, assuming 0.8 power and given that the difference between the two means and standard deviation is maintained. The results are graphed in figure 37.

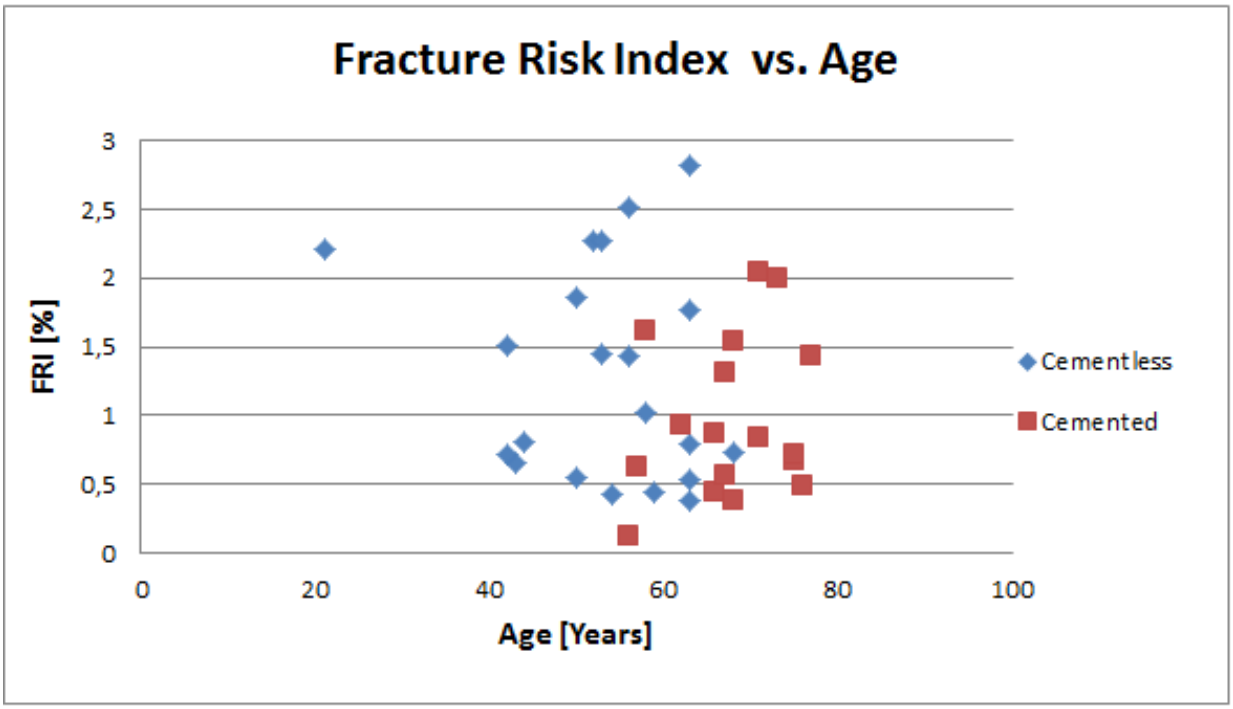

Figure 37: Fracture Risk Index plotted against age, for cemented and cementless patients seperately.

Comparing gender and type, the average FRI for female cementless patients was 1.181% (±0.82%) while for female cemented patients 0.966% (±0.62%) (p=0.49). The average FRI for male cementless patients was 1.415% (±0.76%) and 1.00% for cemented male patients (±0.54%) (p=0.25). The results can be seen in figure 38.

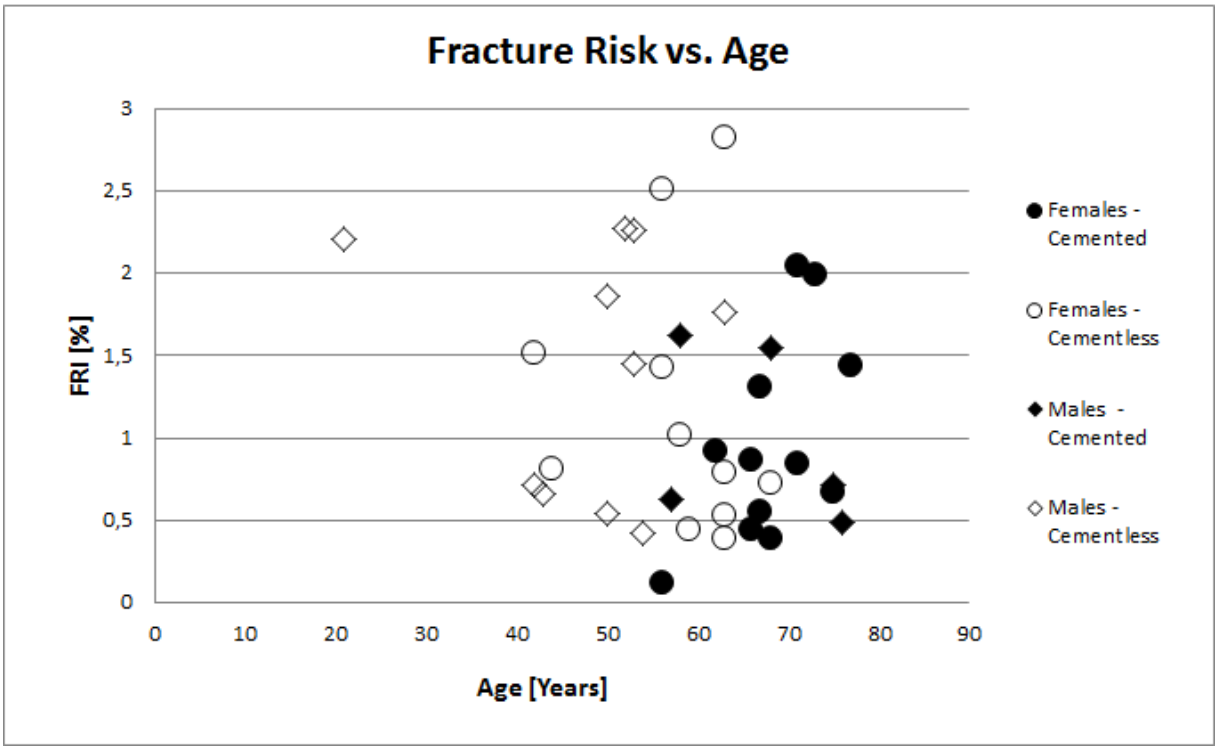

Figure 38: Fracture risk index plotted agains age in years for four groups of patients, grouped according to gender and type of implant.

Table 9 contains the average FRI for all the participants, categorised after type of implant and gender. The p-values are given in the last column.

Table 9: An overview of average age and FRI for different groups, in the cohort. The last column displays the p-values from two-headed T-tests.

Fracture Risk Index				
21 Cementless		**17 cemented**		
Average Age = 53.14 years		*Average Age = 67.82 years*		*p < 0.01*
Average FRI = 1.29%		*Average FRI = 0.98%*		*p = 0.16*
11 females (52.4 %)	*Average Age = 57.73*	**12 females (70.6 %)**	*Average Age = 68.25*	*p < 0.01*
	Average FRI = 1.18%		*Average FRI = 0.97%*	*p = 0.49*
10 males (47.6 %)	*Average Age = 48.10*	**5 males (29.4 %)**	*Average Age = 66.8*	*p < 0.01*
	Average FRI = 1.42%		*Average FRI = 1.00%*	*p = 0.25*
23 Females		**15 Males**		
Average Age = 63.22 years		*Average Age = 54.33 years*		*p = 0.036*
Average FRI = 1.07 %		Average FRI = 1.28 %		*p = 0.38*

A test was conducted to see if the forces on the femoral canal were doubled the Fracture Risk Index would also increase twofold. The results can be seen in figure 39 and they indicate that by doubling the forces, the FRI also increases by twofold.

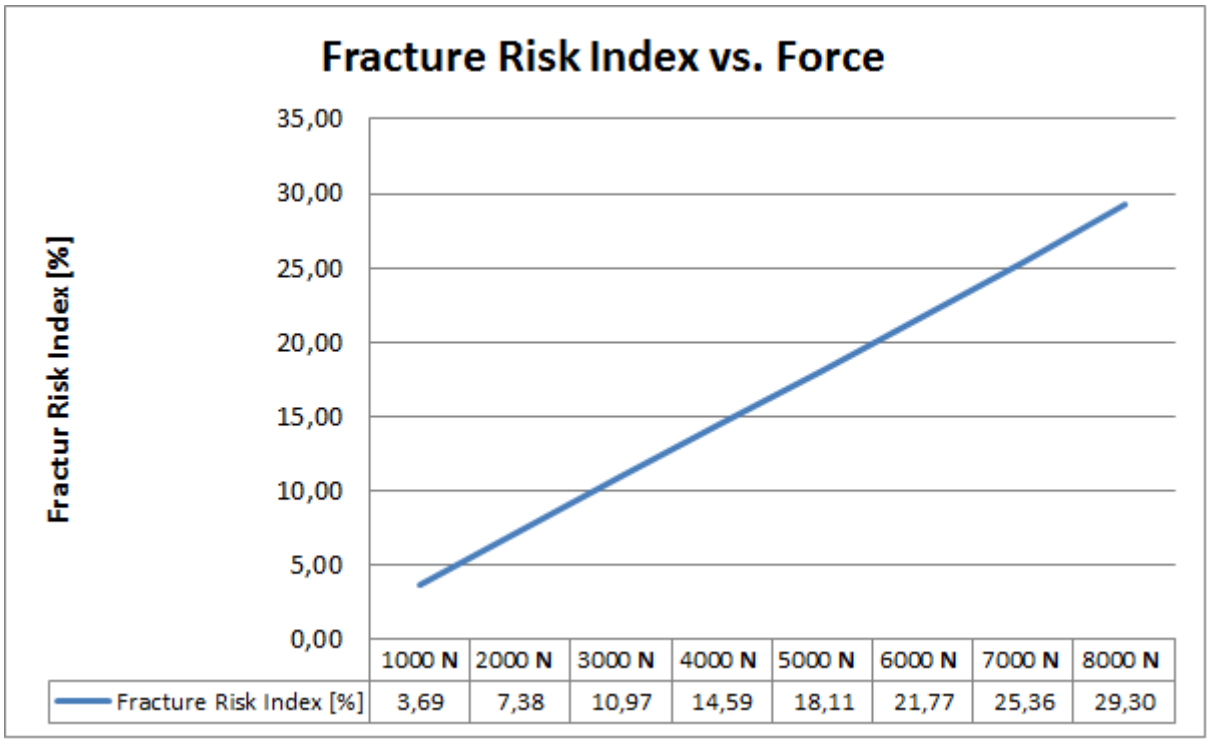

Figure 39: Fracture Risk Index Increase as force in increased.

The results from the simulation where the yield stress of the elements comprising the finite element model were considered to be dependent on their density are shown in figure

40A. The black scatter line represents the yield stress which is dependent on the mineral density of the bone. Then the stress is calculated for all the elements and plotted against their bone mineral density. If the elements are above the black line, they can be considered failed otherwise they can be considered safe. In figure 40B the elements are plotted in 3D to comprise the model of the femur with the stem inside again. On this model the red elements represents the failed elements while the blue are safe elements.

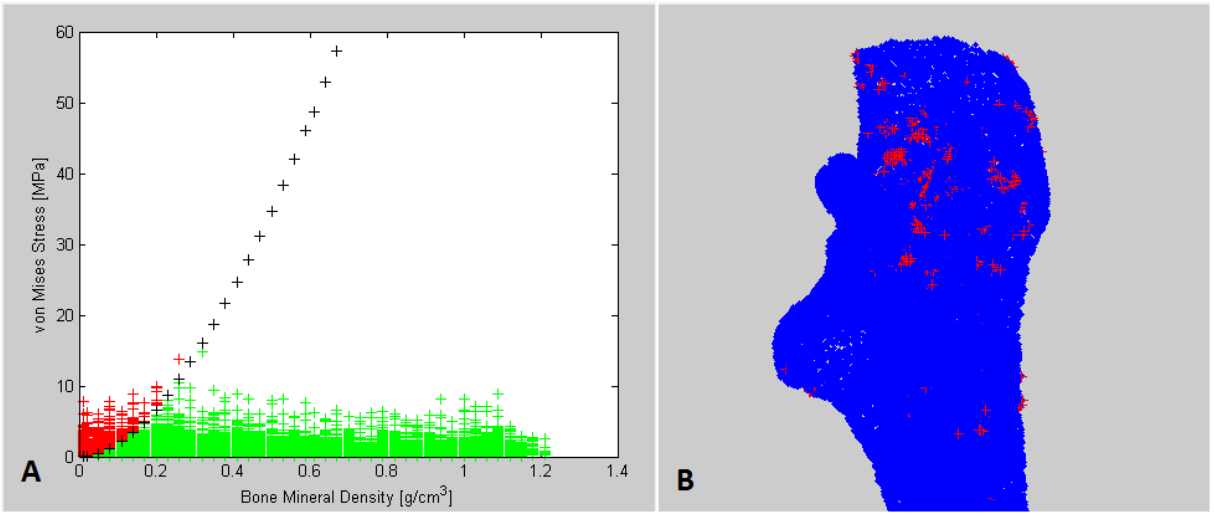

Figure 40: A) von Mises stress of every element plotted against its bone mineral density. The black-crossed line represents the relationship between ultimate strength (Mpa) of bone with bone mineral density. The red dots represent the emelent that will fail and the green dots represents the elements that will not fail according to the failure criterion. B) the elements are plotted in 3D to comprise the model again. The red dots represent the failed elements, while the blue are safe.

4.2. Bone Mineral Density

Bone Mineral Density was calculated for 33 of the 39 enrolled patients. The overall results are plotted in figure 41. A line of best fit has been added resulting in a Pearson correlation coefficient of R = -0.468.

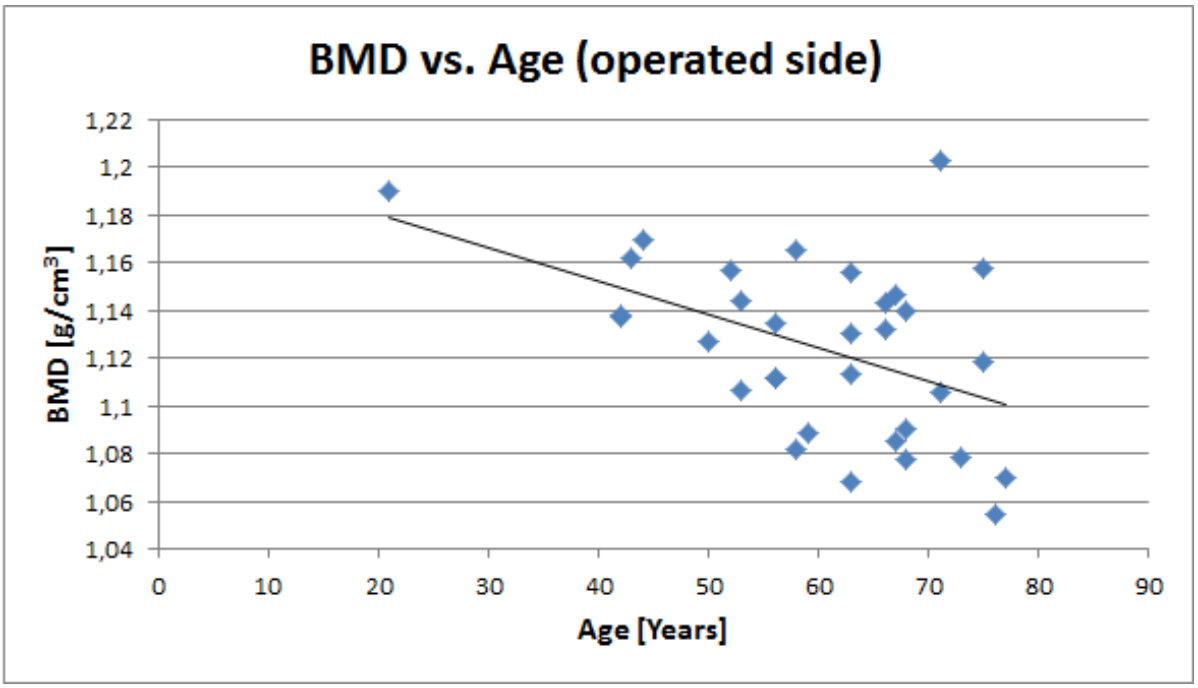

Figure 41: Bone Mineral Density calculated against age for the whole cohort.

According to the line of best fit, increase of one year in age is associated with a decrease in BMD of 0.0014 g/cm^3.

Comparison of cemented and cementless patients can be seen in figure 42. The average BMD of the operated leg for the cementless group was 1.131 g/cm^3 (±0.033%) and for the cemented 1.166 g/cm^3 (±0.040%). The difference was 1.32% (p=0.27). A power analysis indicated that at least 115 patients in each group are required to obtain statistically significant difference; given that the difference between the means and the standard deviation are the same and with a power of 0.8.

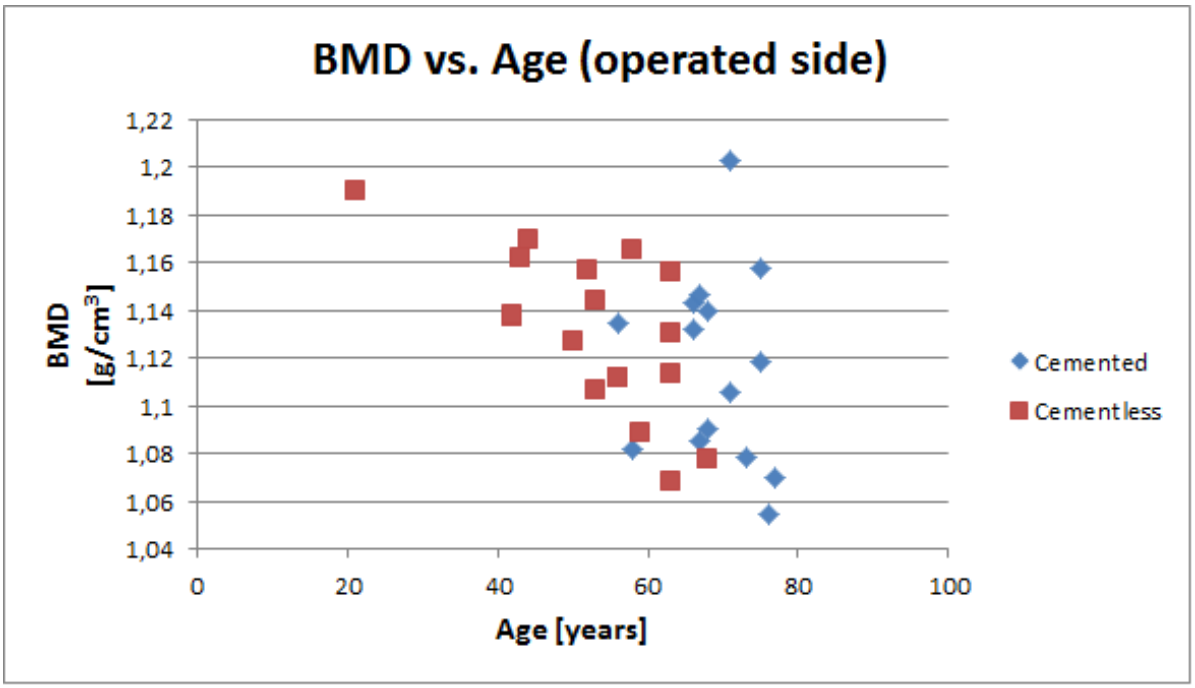

Figure 42: Bone Mineral Density plotted ageinst age for cemented and cementless patients seperately.

Average BMD for cementless female patients was 1.122 (±0.033) g/cm^3 and for cemented female patients 1.122 (±0.040) g/cm^3. The average BMD for the cementless males was 1.142 (±0.027) g/cm^3 and 1.098 (±0.038) g/cm^3 for the cemented males. The results can be seen in figure 43.

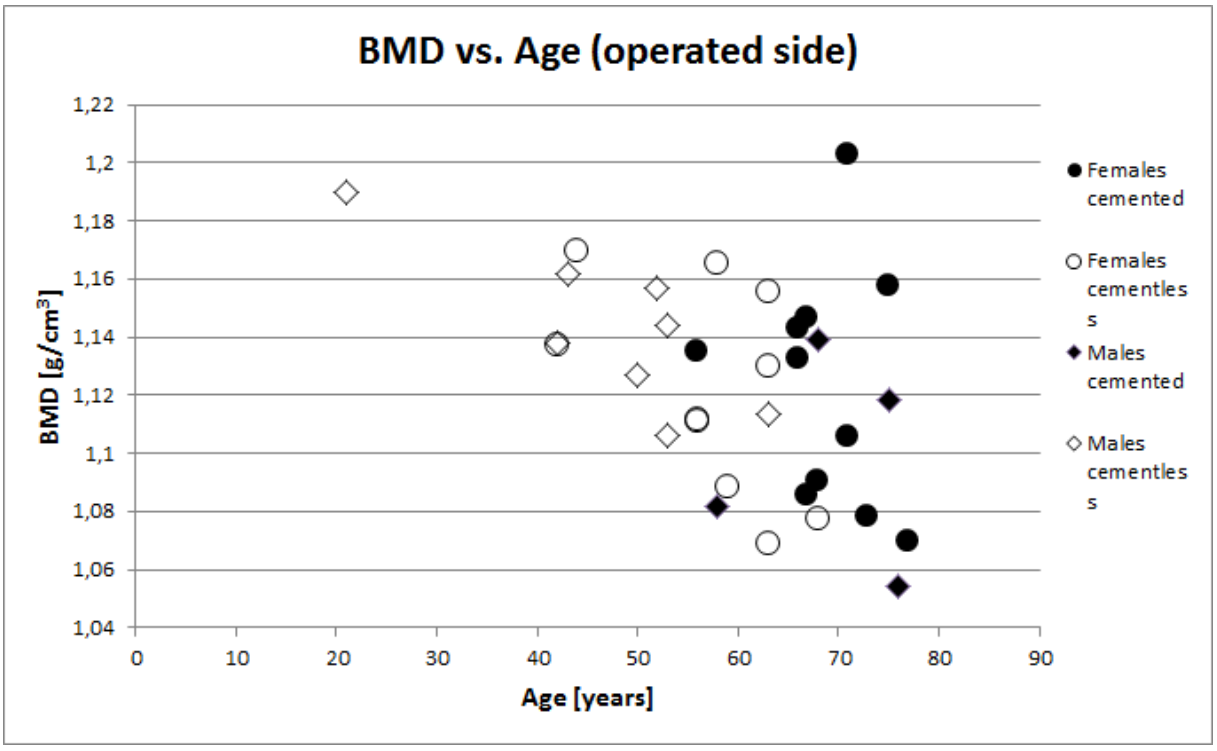

Figure 43: Bone Mineral Density plotted against age for four groups of patients, grouped according to gender and type of implant.

Table 10 collects all the results from the BMD measurements described by figure 41-43.

Table 10: An overview of average age and FRI for different groups, in the cohort. The last column displays the p-values from two-headed T-tests.

Bone Mineral Density

18 Cementless		15 Cemented		P-value
Average Age = 52.72 years		*Average Age = 68.93 years*		*p < 0.01*
Average BMD = 1.131 g/cm^3		Average BMD = 1.166 g/cm^3		*p = 0.27*
10 Females (55.6 %)	*Average Age = 57.2*	**11 Females (73.3 %)**	*Average Age = 68.82*	*p < 0.01*
	Average BMD = 1.122		*Average BMD = 1.122*	*p = 0.96*
8 Males (44.4 %)	*Average Age = 47.13*	**4 Males (26.7 %)**	*Average Age = 69.25*	*p < 0.01*
	Average BMD= 1.142		*Average BMD = 1.098*	*p = 0.1*
21 Females		**12 Males**		
Average Age = 63.29		*Average Age = 54.50*		*p = 0.09*
Average BMD = 1.122		Average BMD = 1.128		*p = 0.68*

4.3. Fracture Risk Index vs. Bone Mineral Density

In figure 44, Fracture Risk Index for cemented and cementless patients is plotted against their Bone Mineral Density.

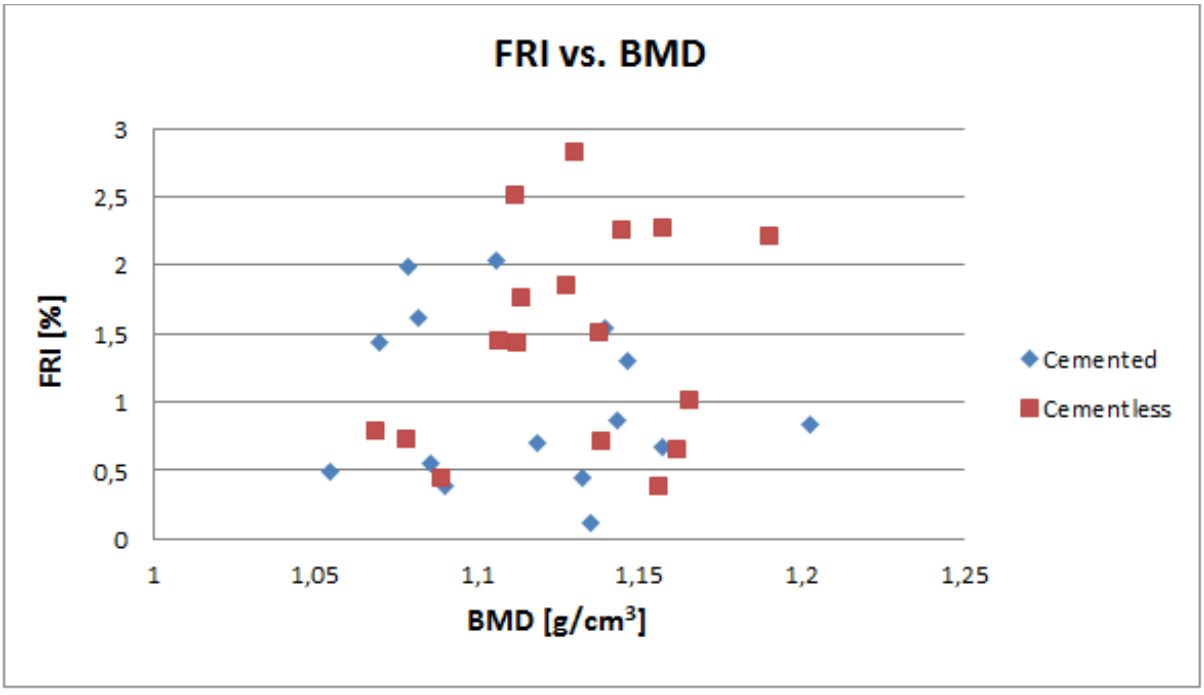

Figure 44: Fracture Risk Index plotted against Bone Mineral Density.

5. Discussions

Choosing between cemented and cementless techniques in total hip replacement is still debated. If the bone is of good quality, then cementless implants generally show superior outcomes compared to cemented ones; better long-term fixation. Hence, cementless techniques are used for younger and more active patients, while cement is used when operating older less active patients.

Although age and gender are known to give an idea of the bone quality, individual differences can be vast. Despite the importance of bone quality, there are currently no quantitative indicators in practice, to support the decision.

High costs are related to primary THA and even higher for revision surgeries which can include serious complications, especially in the case of bone cement. It is therefore important to choose the correct prosthesis for each patient from the beginning, to increase patient comfort, decrease rate of revision and avoid complications.

This study proposed bone mineral density measurements and finite element analysis which task was to estimate the risk of fracture during cementless surgery.

5.1. Fracture Risk Index

It is clear that the FRI values are very low, however, although the fracture risk cannot be considered to reflect real risk of fracture, it is possible to note the differences between patients and the difference reaches beyond their age and gender. One could play with the forces used in the simulations to acquire more realistic values, as figure 41 indicates, but the proportional differences will be the same. These results thus can be used to observe individual differences and indicate that every patient is different and do not follow an accurate trend.

It would be expected beforehand that FRI would increase with higher age and be higher for the cemented patients. According to the results, the cemented group presents lower FRI than the cementless, although it does not reach significance. The FRI results exhibit that differences between patients are relatively large although the fracture risk does not reflect real-life fracture risk. Furthermore, looking at specific patients, the five highest fracture risk indices occur in patients that received cementless implants and the lowest FRI occurs in a 56 year old cemented female patient who might have been suitable for a cementless stem. Additionally, many of the cemented patients present lower FRI than the average. This might mean that some of the patients which received cemented implants might have been suitable for a cementless operation.

One test simulation, where the strength of bones is considered to be dependent on their density, has been done. Implementing this method for all the patients would give more vigorous results. This way, every element of the model is considered, not only a few, chosen by hand. However, there are some very low density elements in the one model shown in figure 40. This could stem from the fact that every voxel in the image is considered bone, but might belong to air or other material. By building a model, where every voxel of the image represents an element in the model, and using known thresholds of bone to exclude every other material, would possible largely increase the accuracy of the model. A model of this type is under development as described in appendix A2.

There are some limits to the fracture risk calculations. First, the yield strength of bone is dependent on its bone mineral density, adding this feature would potentially increase the accuracy of the results. The first simulation taking this into account has been finished. Secondly, it can be hard to add the exactly same boundary conditions for all the models, so that introduces some error. A slightly different approach might prove to increase the reproducibility. Third, the 1000 N force is an estimate of the cumulative stresses introduced during the operation; although based on empirically measured force on the THR hammer. Conducting more precise analysis, perhaps on cadaveric femurs, with stress measurements inside the femoral canal, might improve this aspect. Fourth, material properties of cortical and trabecular bones are very different, mapping their properties separately would yield proper results.

5.2. Bone Mineral Density

The results from the BMD measurements underline the fact that BMD decreases with age (figure 41). BMD was higher for males than females overall, but the results are not significant. These results can be explained by that women in the study were older on average, although not significantly.

Comparing the cementless and cemented groups, the cementless group averaged higher than the cemented group. This can be considered normal, since the cemented group is significantly older. However, although the trend for both cemented and cementless patients is a decrease in BMD with increased age, there are some subjects that deviate from the trend. A good example is that the highest BMD is observed in a 71-year old female patient who received a cemented implant, averaging slightly over 1.2 g/cm3. There is a clear overlap between individuals that received cementless and cemented implants and age does not tell the whole story. This indicates that some of the cemented patients could, for example, have

received cementless implants and if they have to undergo a revision surgery. The bad thing about this is that success of the revision implant would be better if they did not have cemented THR. The goal of this research is to detect the stand-out patients and register them into the correct implant group.

The results are similar to what could have been expected beforehand, however differences between groups never reach a significant value. Recruiting additional patients undergoing THA and include their results, could give rise to significant results, as the power analysis indicated. Nonetheless, the results presented here indicate that quantitative CT-based assessment of BMD, of patients undergoing total hip replacement, can measure bone quality beyond their age and gender.

5.3. Fracture Risk Index and Bone Mineral Density

According the comparison of FRI and BMD, there is no trend which the patients follow; their BMD does not indicate their FRI. The results shown in figure 45 indicate that every patient is a specific case and the level of bone quality should be determined with factors reaching beyond their age and gender.

5.4. Future Work

This work will continue to develop in the near future. Recruitment of a larger group of patients is in progress. Additionally the first group will undergo a two-year post-surgical assessment.

The fracture risk analysis will be evaluated and ways to improve it will be explored. Collaboration with the Mechanical Department of Federico II University in Naples, Italy, has been agreed. The results of this collaboration already include a more accurate finite element model of the femur (appendix A2) following a different type of segmentation done in Matlab [162] (appendix A1) and the fracture risk analysis with these models is on the agenda. Moreover, an analysis of remodelling/resorption after the surgery has been discussed, where the bones will be analysed post-surgery. In order to be able to accurately analyse the femurs post-surgery, the metal artifacts have to be reduced. Artifact reduction is in progress at the moment (Appendix A3).

A contract of collaboration with Össur has also been agreed. The aim of the collaboration is to evaluate a new hip brace intended for pain relief before surgery. Some of the patients that are evaluated will have been using the brace for some time, and by acquiring gait parameters pre- and post-surgery a possible difference can be noted for those patients.

6. Conclusion

The-CT based fracture risk simulation introduced here demonstrates differences between patients, although it is unable to measure the real risk of fracture before cementless total hip replacement. However, the CT-based bone mineral density might prove to be a precise method of evaluating bone quality of patients and give indications for choice of implant.

References

[1] C. A. Engh, J. D. Bobyn, and A. H. Glassman, “Porous-coated hip replacement. The factors governing bone ingrowth, stress shielding, and clinical results,” *J Bone Joint Surg Br*, vol. 69, no. 1, pp. 45–55, Jan. 1987.

[2] L. A. Müller, N. Wenger, M. Schramm, D. Hohmann, R. Forst, and H.-D. Carl, “Seventeen-year survival of the cementless CLS Spotorno stem,” *Archives of Orthopaedic and Trauma Surgery*, vol. 130, no. 2, pp. 269–275, Sep. 2009.

[3] J. R. McLaughlin, “Total Hip Arthroplasty with an Uncemented Tapered Femoral Component,” *The Journal of Bone and Joint Surgery (American)*, vol. 90, no. 6, p. 1290, Jun. 2008.

[4] H. Jónsson Jr, “Skurðaðgerðir á Íslandi við slitgigt.”

[5] Hagdeild Landspítala Háskólasjúkrahúss, “DRG verðskrá.” .

[6] J. K. Gong, J. S. Arnold, and S. H. Cohn, “Composition of trabecular and cortical bone,” *Anat. Rec.*, vol. 149, pp. 325–331, Jul. 1964.

[7] H. A. Lowenstam, *On biomineralization*. New York: Oxford University Press, 1989.

[8] J.-Y. Rho, L. Kuhn-Spearing, and P. Zioupos, “Mechanical properties and the hierarchical structure of bone,” *Medical Engineering & Physics*, vol. 20, no. 2, pp. 92–102, Mar. 1998.

[9] S. Cowin, W. Buskirk Van, and R. Ashman, “The properties of bone,” in *Handbook of bioengineering*, R. Skalak and S. Chien, Eds. New York: McGraw Hill Companies, 1987, pp. 2.1–2.27.

[10] I. Singh, “The architecture of cancellous bone,” *Journal of Anatomy*, vol. 127, no. 2, pp. 305–310, 1978.

[11] Curry JD, “Differences in the Blood-supply of Bone of Different Histological Types,” *Q J Microsc Sci*, vol. 101, pp. 351–370, 1960.

[12] S. Cowin, “Mechanical properties of bones,” in *Mechanics of structured media*, A. Selvadurai, Ed. Philadelphia: Elsevier, 1981, pp. 151–184.

[13] S. C. Cowin, *Tissue mechanics*. New York: Springer, 2007.

[14] A. Ham, *Histology*, 6th ed. Philadelphia: Lippincott, 1969.

[15] J. W. T. Byrd, “Gross Anatomy,” in *Operative Hip Arthroscopy*, J. W. T. Byrd, Ed. New York: Springer-Verlag, 2005, pp. 100–109.

[16] K. L. Moore, Dalley, and Agur, *Clinically oriented anatomy*. 2014.

[17] B. Byrne, K. Mulhall, and F. Baker, “Anatomy & Biomechanics of the Hip,” *The Open Sports Medicine Journal*, vol. 4, pp. 51–57, 2010.

[18] J. J. Callaghan and A. G. Rosenberg, *The adult hip*, vol. Vol 2. Philadelphia [etc.]: Lippincott Williams & Wilkins, 2007.

[19] B. Young, *Wheater’s functional histology: a text and colour atlas*. [Edinburgh?]: Churchill Livingstone/Elsevier, 2006.

[20] S. Perez-Amodio, W. Beertsen, and V. Everts, “(Pre-)osteoclasts induce retraction of osteoblasts before their fusion to osteoclasts,” *J. Bone Miner. Res.*, vol. 19, no. 10, pp. 1722–1731, Oct. 2004.

[21] F. J. Hughes, W. Turner, G. Belibasakis, and G. Martuscelli, “Effects of growth factors and cytokines on osteoblast differentiation,” *Periodontol. 2000*, vol. 41, pp. 48–72, 2006.

[22] B. Clarke, “Normal Bone Anatomy and Physiology,” *Clinical Journal of the American Society of Nephrology*, vol. 3, no. Supplement 3, pp. S131–S139, Nov. 2008.

[23] B. F. Boyce, Z. Yao, and L. Xing, “Osteoclasts have multiple roles in bone in addition to bone resorption,” *Crit. Rev. Eukaryot. Gene Expr.*, vol. 19, no. 3, pp. 171–180, 2009.

[24] "Osteoclast," *Encyclopedia Britannica*. 2009.

[25] V. Everts and P. Saftig, "Degradation of Bone and the Role of Osteoclasts, Bone Lining Cells and Osteocytes," in *Extracellular Matrix Degradation*, vol. 2, W. C. Parks and R. P. Mecham, Eds. Springer Berlin Heidelberg, 2011, pp. 193–216.
[26] "Osteocyte," *Encyclopedia Britannica*. 2007.
[27] L. You, S. Temiyasathit, P. Lee, C. H. Kim, P. Tummala, W. Yao, W. Kingery, A. M. Malone, R. Y. Kwon, and C. R. Jacobs, "Osteocytes as mechanosensors in the inhibition of bone resorption due to mechanical loading," *Bone*, vol. 42, no. 1, pp. 172–179, Jan. 2008.
[28] P. S. Vezeridis, C. M. Semeins, Q. Chen, and J. Klein-Nulend, "Osteocytes subjected to pulsating fluid flow regulate osteoblast proliferation and differentiation," *Biochem. Biophys. Res. Commun.*, vol. 348, no. 3, pp. 1082–1088, Sep. 2006.
[29] J. Wolff, *Das Gesetz der Transformation der Knochen*. Berlin: Verlag von August Hirschwald, 1892.
[30] W. D. Bugbee, W. J. Culpepper 2nd, C. A. Engh Jr, and C. A. Engh Sr, "Long-term clinical consequences of stress-shielding after total hip arthroplasty without cement," *J Bone Joint Surg Am*, vol. 79, no. 7, pp. 1007–1012, Jul. 1997.
[31] Y. C. Fung, *Biomechanics: Mechanical Properties of Living Tissues*, 2nd ed. New York: Springer-Verlag, 1993.
[32] T. Goswami, *Human Musculoskeletal Biomechanics*, 1st ed. Rijeka, Croatia: InTech, 2011.
[33] A. D. P. Bankoff, *Morfologia e cinesiologia aplicada ao movimento humano*. Rio de Janeiro: Guanabara Koogan, 2007.
[34] D. T. Reilly and A. H. Burstein, "Review article. The mechanical properties of cortical bone," *J Bone Joint Surg Am*, vol. 56, no. 5, pp. 1001–1022, Jul. 1974.
[35] D. T. Reilly and A. H. Burstein, "The elastic and ultimate properties of compact bone tissue," *J Biomech*, vol. 8, no. 6, pp. 393–405, 1975.
[36] M. Nordin and V. H. Frankel, *Basic biomechanics of the musculoskeletal system*. Philadelphia: Wolters Kluwer Health/Lippincott Williams & Wilkins, 2012.
[37] A. H. Burstein, D. T. Reilly, and M. Martens, "Aging of bone tissue: mechanical properties," *J Bone Joint Surg Am*, vol. 58, no. 1, pp. 82–86, Jan. 1976.
[38] R. W. McCalden, J. A. McGeough, M. B. Barker, and C. M. Court-Brown, "Age-related changes in the tensile properties of cortical bone. The relative importance of changes in porosity, mineralization, and microstructure," *J Bone Joint Surg Am*, vol. 75, no. 8, pp. 1193–1205, Aug. 1993.
[39] J. McElhaney and E. Byars, "Dynamic response of biological materials," *American Society of Mechanical Engineers -- Papers*, p. 8, 1965.
[40] A. C. Courtney, W. C. Hayes, and L. J. Gibson, "Age-related differences in post-yield damage in human cortical bone. Experiment and model," *J Biomech*, vol. 29, no. 11, pp. 1463–1471, Nov. 1996.
[41] D. R. Carter, W. E. Caler, D. M. Spengler, and V. H. Frankel, "Fatigue behavior of adult cortical bone: the influence of mean strain and strain range," *Acta Orthop Scand*, vol. 52, no. 5, pp. 481–490, Oct. 1981.
[42] M. B. Schaffler, K. Choi, and C. Milgrom, "Aging and matrix microdamage accumulation in human compact bone," *Bone*, vol. 17, no. 6, pp. 521–525, Dec. 1995.
[43] T. M. Keaveny, E. F. Morgan, and Y. C. Oscar, "Bone Mechanics," in *Standard Handbook of Biomedical Engineering & Design*, M. Kutz, Ed. McGraw-Hill, 2003.

[44] T. M. Keaveny, X. E. Guo, E. F. Wachtel, T. A. McMahon, and W. C. Hayes, "Trabecular bone exhibits fully linear elastic behavior and yields at low strains," *J Biomech*, vol. 27, no. 9, pp. 1127–1136, Sep. 1994.
[45] E. F. Morgan, O. C. Yeh, W. C. Chang, and T. M. Keaveny, "Nonlinear Behavior of Trabecular Bone at Small Strains," *Journal of Biomechanical Engineering*, vol. 123, no. 1, p. 1, 2001.
[46] J. C. Rice, S. C. Cowin, and J. A. Bowman, "On the dependence of the elasticity and strength of cancellous bone on apparent density," *Journal of Biomechanics*, vol. 21, no. 2, pp. 155–168, Jan. 1988.
[47] S. A. Goldstein, D. L. Wilson, D. A. Sonstegard, and L. S. Matthews, "The mechanical properties of human tibial trabecular bone as a function of metaphyseal location," *J Biomech*, vol. 16, no. 12, pp. 965–969, 1983.
[48] M. J. Ciarelli, S. A. Goldstein, J. L. Kuhn, D. D. Cody, and M. B. Brown, "Evaluation of orthogonal mechanical properties and density of human trabecular bone from the major metaphyseal regions with materials testing and computed tomography," *J. Orthop. Res.*, vol. 9, no. 5, pp. 674–682, Sep. 1991.
[49] J. A. Hipp, A. E. Rosenberg, and W. C. Hayes, "Mechanical properties of trabecular bone within and adjacent to osseous metastases," *J. Bone Miner. Res.*, vol. 7, no. 10, pp. 1165–1171, Oct. 1992.
[50] L. Mosekilde, L. Mosekilde, and C. C. Danielsen, "Biomechanical competence of vertebral trabecular bone in relation to ash density and age in normal individuals," *Bone*, vol. 8, no. 2, pp. 79–85, 1987.
[51] J. C. Van Der Linden, J. A. Verhaar, and H. Weinans, "A three-dimensional simulation of age-related remodeling in trabecular bone," *J. Bone Miner. Res.*, vol. 16, no. 4, pp. 688–696, Apr. 2001.
[52] C. M. Ford and T. M. Keaveny, "The dependence of shear failure properties of trabecular bone on apparent density and trabecular orientation," *J Biomech*, vol. 29, no. 10, pp. 1309–1317, Oct. 1996.
[53] J. Ouyang, G. T. Yang, W. Z. Wu, Q. A. Zhu, and S. Z. Zhong, "Biomechanical characteristics of human trabecular bone," *Clin Biomech (Bristol, Avon)*, vol. 12, no. 7–8, pp. 522–524, Oct. 1997.
[54] D. L. Kopperdahl and T. M. Keaveny, "Yield strain behavior of trabecular bone," *J Biomech*, vol. 31, no. 7, pp. 601–608, Jul. 1998.
[55] R. B. Ashman and Jae Young Rho, "Elastic modulus of trabecular bone material," *Journal of Biomechanics*, vol. 21, no. 3, pp. 177–181, Jan. 1988.
[56] D. Ulrich, B. van Rietbergen, A. Laib, and P. Rüegsegger, "The ability of three-dimensional structural indices to reflect mechanical aspects of trabecular bone," *Bone*, vol. 25, no. 1, pp. 55–60, Jul. 1999.
[57] T. M. Keaveny, E. F. Wachtel, and D. L. Kopperdahl, "Mechanical behavior of human trabecular bone after overloading," *J. Orthop. Res.*, vol. 17, no. 3, pp. 346–353, May 1999.
[58] F. Linde, P. Nørgaard, I. Hvid, A. Odgaard, and K. Søballe, "Mechanical properties of trabecular bone. Dependency on strain rate," *J Biomech*, vol. 24, no. 9, pp. 803–809, 1991.
[59] W. N. Capello, J. A. D'Antonio, J. R. Feinberg, and M. T. Manley, "Ten-year results with hydroxyapatite-coated total hip femoral components in patients less than fifty years old. A concise follow-up of a previous report," *J Bone Joint Surg Am*, vol. 85-A, no. 5, pp. 885–889, May 2003.

[60] C. A. Engh Jr, W. J. Culpepper 2nd, and C. A. Engh, "Long-term results of use of the anatomic medullary locking prosthesis in total hip arthroplasty," *J Bone Joint Surg Am*, vol. 79, no. 2, pp. 177–184, Feb. 1997.
[61] J. B. Meding, E. M. Keating, M. A. Ritter, P. M. Faris, and M. E. Berend, "Minimum ten-year follow-up of a straight-stemmed, plasma-sprayed, titanium-alloy, uncemented femoral component in primary total hip arthroplasty," *J Bone Joint Surg Am*, vol. 86-A, no. 1, pp. 92–97, Jan. 2004.
[62] "Minimally Invasive Total Hip Replacement," *American Academy of Orthropaedic Surgeons*, 2007. [Online]. Available: http://orthoinfo.aaos.org/topic.cfm?topic=a00404. [Accessed: 25-Oct-2013].
[63] D. L. Green, "Complications of Total Hip Replacement," *Southern Medical Journal*, vol. 69, no. 12, 1976.
[64] "Components of a Hip Replacement — Exactech, Inc." [Online]. Available: http://www.exac.com/patients-caregivers/joint-replacement-surgery/hip-replacement/components-hip-replacement. [Accessed: 28-Nov-2013].
[65] U. Holzwarth and G. Cotogno, "Total Hip Arthroplasty: State of the Art, Challenges and Prospect," Institute for Health and Consumer Protection, Luxembourg: Publications Office of the European Union, Scientific and Policy, Jul. 2012.
[66] H. G. Willert, H. Bertram, and G. H. Buchhorn, "Osteolysis in alloarthroplasty of the hip. The role of ultra-high molecular weight polyethylene wear particles," *Clin. Orthop. Relat. Res.*, no. 258, pp. 95–107, Sep. 1990.
[67] P.-G. Ren, A. Irani, Z. Huang, T. Ma, S. Biswal, and S. B. Goodman, "Continuous infusion of UHMWPE particles induces increased bone macrophages and osteolysis," *Clin. Orthop. Relat. Res.*, vol. 469, no. 1, pp. 113–122, Jan. 2011.
[68] M. Meftah, G. G. Klingenstein, R. J. Yun, A. S. Ranawat, and C. S. Ranawat, "Long-term performance of ceramic and metal femoral heads on conventional polyethylene in young and active patients: a matched-pair analysis," *J Bone Joint Surg Am*, vol. 95, no. 13, pp. 1193–1197, Jul. 2013.
[69] M. Ihle, S. Mai, and W. Siebert, "Ceramic Versus Metal Femoral Heads in Combination With Polyethylene Cups," *Seminars in Arthroplasty*, vol. 22, no. 4, pp. 218–224, Dec. 2011.
[70] S. Glyn-Jones, S. Isaac, J. Hauptfleisch, P. McLardy-Smith, D. W. Murray, and H. S. Gill, "Does highly cross-linked polyethylene wear less than conventional polyethylene in total hip arthroplasty? A double-blind, randomized, and controlled trial using roentgen stereophotogrammetric analysis," *J Arthroplasty*, vol. 23, no. 3, pp. 337–343, Apr. 2008.
[71] C. A. Jacobs, C. P. Christensen, A. S. Greenwald, and H. McKellop, "Clinical performance of highly cross-linked polyethylenes in total hip arthroplasty," *J Bone Joint Surg Am*, vol. 89, no. 12, pp. 2779–2786, Dec. 2007.
[72] R. W. McCalden, S. J. MacDonald, C. H. Rorabeck, R. B. Bourne, D. G. Chess, and K. D. Charron, "Wear rate of highly cross-linked polyethylene in total hip arthroplasty. A randomized controlled trial," *J Bone Joint Surg Am*, vol. 91, no. 4, pp. 773–782, Apr. 2009.
[73] M. Wagner and H. Wagner, "Medium-term results of a modern metal-on-metal system in total hip replacement," *Clin. Orthop. Relat. Res.*, no. 379, pp. 123–133, Oct. 2000.
[74] "Concerns about Metal-on-Metal Hip Implants," *U.S. Food and Drug Administration*, 2013. [Online]. Available: http://www.fda.gov/MedicalDevices/ProductsandMedicalProcedures/ImplantsandProsthetics/MetalonMetalHipImplants/ucm241604.htm. [Accessed: 26-Nov-2013].

[75] D. Schroder, L. Bornstein, M. P. G. Bostrom, B. J. Nestor, D. E. Padgett, and G. H. Westrich, "Ceramic-on-ceramic total hip arthroplasty: incidence of instability and noise," *Clin. Orthop. Relat. Res.*, vol. 469, no. 2, pp. 437–442, Feb. 2011.

[76] M. Hasegawa, "Alumina ceramic-on-ceramic total hip replacement with a layered acetabular component," *Journal of Bone and Joint Surgery - British Volume*, vol. 88-B, no. 7, pp. 877–882, Jul. 2006.

[77] O. K. Muratoglu and S. M. Kurtz, "Alternate Bearing Surfaces in Hip Replacement," in *Hip replacement: current trends and controversies*, R. K. Sinha, Ed. New York: Marcel Dekker, 2002.

[78] S. M. Dellose, A. H. Kim, and R. K. Sinha, "Cemented Stems," in *Hip replacement: current trends and controversies*, R. K. Sinha, Ed. New York: Marcel Dekker, 2002.

[79] B. A. Goldberg, G. al-Habbal, P. C. Noble, M. Paravic, T. R. Liebs, and H. S. Tullos, "Proximal and distal femoral centralizers in modern cemented hip arthroplasty," Clin. Orthop. Relat. Res., no. 349, pp. 163–173, Apr. 1998.

[80] D. Ayers and K. Mann, "The importance of proximal cement filling of the calcar region: a biomechanical justification," *J Arthroplasty*, vol. 18, no. 7 Suppl 1, pp. 103–109, Oct. 2003.

[81] T. P. Harrigan and W. H. Harris, "A three-dimensional non-linear finite element study of the effect of cement-prosthesis debonding in cemented femoral total hip components," *J Biomech*, vol. 24, no. 11, pp. 1047–1058, 1991.

[82] K. T. Mäkelä, A. Eskelinen, P. Paavolainen, P. Pulkkinen, and V. Remes, "Cementless total hip arthroplasty for primary osteoarthritis in patients aged 55 years and older: Results of the 8 most common cementless designs compared to cemented reference implants in the Finnish Arthroplasty Register," Acta Orthopaedica, vol. 81, no. 1, pp. 42–52, Feb. 2010.

[83] "B. Braun Melsungen AG - Artificial Hip Joint - Hip Fixation." [Online]. Available: http://www.shorthip-patients.com/cps/rde/xchg/ae-methapat-en-int/hs.xsl/7225.html. [Accessed: 22-Oct-2013].

[84] D. J. Blaha and T. A. Borus, "Press-Fit Femoral Components," in *The Adult Hip*, 2nd ed., Lippincott Williams & Wilkins, 2007.

[85] *European instructional lectures: volume 13, 2013, 14th EFORT Congress, Istanbul, Turkey*. New York: Springer, 2013.

[86] S.-M. Lan and K.-A. Lai, "Reverse hybrid total hip arthroplasty in select patients," *Formosan Journal of Musculoskeletal Disorders*, vol. 1, no. 1, pp. 20–25, Nov. 2010.

[87] C. H. Rorabeck, R. B. Bourne, A. Laupacis, D. Feeny, C. Wong, P. Tugwell, K. Leslie, and R. Bullas, "A double-blind study of 250 cases comparing cemented with cementless total hip arthroplasty. Cost-effectiveness and its impact on health-related quality of life," *Clin. Orthop. Relat. Res.*, no. 298, pp. 156–164, Jan. 1994.

[88] C. H. Rorabeck, R. B. Bourne, B. D. Mulliken, N. Nayak, A. Laupacis, P. Tugwell, and D. Feeney, "The Nicolas Andry award: comparative results of cemented and cementless total hip arthroplasty," *Clin. Orthop. Relat. Res.*, no. 325, pp. 330–344, Apr. 1996.

[89] G. Hooper, M. Stringer, and A. Rothwell, "Early revision for cemented & cementless primary total hip arthroplasty: an analysis of the New Zealand Joint Registry," *Journal of Bone & Joint Surgery, British Volume*, vol. 91-B, no. SUPP II, pp. 336–337, May 2009.

[90] N. P. Hailer, G. Garellick, and J. Kärrholm, "Uncemented and cemented primary total hip arthroplasty in the Swedish Hip Arthroplasty Register: Evaluation of 170,413 operations," *Acta Orthopaedica*, vol. 81, no. 1, pp. 34–41, Feb. 2010.

[91] L. Wang, P. Lei, J. Xie, K. Li, Z. Dai, and Y. Hu, “Medium-term Outcomes of Cemented Prostheses and Cementless Modular Prostheses in Revision Total Hip Arthroplasty,” *Scientific Reports*, vol. 3, Sep. 2013.
[92] T. J. Liang, M. Z. You, P. F. Xing, S. Bin, Z. Z. Ke, and Y. Jing, “Uncemented Total Hip Arthroplasty in Patients Younger than 50 Years: A 6- to 10-Year Follow-Up Study,” *Orthopedics*, Apr. 2010.
[93] G. J. Hooper, A. G. Rothwell, M. Stringer, and C. Frampton, “Revision following cemented and uncemented primary total hip replacement: a seven-year analysis from the New Zealand Joint Registry,” *J Bone Joint Surg Br*, vol. 91, no. 4, pp. 451–458, Apr. 2009.
[94] G. X. Ni, W. W. Lu, K. Y. Chiu, and D. Y. Fong, “Cemented or uncemented femoral component in primary total hip replacement? A review from a clinical and radiological perspective,” *J Orthop Surg (Hong Kong)*, vol. 13, no. 1, pp. 96–105, Apr. 2005.
[95] D. D. D’Lima, C. S. Oishi, W. J. Petersilge, C. W. Colwell Jr, and R. H. Walker, “100 cemented versus 100 noncemented stems with comparison of 25 matched pairs,” *Clin. Orthop. Relat. Res.*, no. 348, pp. 140–148, Mar. 1998.
[96] W. J. Hozack, R. H. Rothman, R. E. Booth Jr, and R. A. Balderston, “Cemented versus cementless total hip arthroplasty. A comparative study of equivalent patient populations,” *Clin. Orthop. Relat. Res.*, no. 289, pp. 161–165, Apr. 1993.
[97] D. R. Taaffe, J. A. Cauley, M. Danielson, M. C. Nevitt, T. F. Lang, D. C. Bauer, and T. B. Harris, “Race and sex effects on the association between muscle strength, soft tissue, and bone mineral density in healthy elders: the Health, Aging, and Body Composition Study,” *J. Bone Miner. Res.*, vol. 16, no. 7, pp. 1343–1352, Jul. 2001.
[98] N. N. Mahomed, J. A. Barrett, J. N. Katz, C. B. Phillips, E. Losina, R. A. Lew, E. Guadagnoli, W. H. Harris, R. Poss, and J. A. Baron, “Rates and outcomes of primary and revision total hip replacement in the United States medicare population,” *J Bone Joint Surg Am*, vol. 85-A, no. 1, pp. 27–32, Jan. 2003.
[99] R. K. Sinha, “Revision of the Femoral Component,” in *Hip replacement: current trends and controversies*, R. K. Sinha, Ed. New York: Marcel Dekker, 2002.
[100] “The CLS® Spotorno® Stem.” Zimmer, 2008.
[101] A. S. Hoffman, “Metals,” in *Biomaterials science: an introduction to materials in medicine*, B. D. Ratner, A. S. Hoffman, F. J. Schoen, and J. E. Lemons, Eds. San Diego, California, USA: ACADEMIC PRESS, 1996.
[102] R. Boyer, G. Welsch, and E. W. Collings, *Materials properties handbook titanium alloys*. Materials Park, OH: ASM International, 1994.
[103] M. Long and H. J. Rack, “Titanium alloys in total joint replacement--a materials science perspective,” *Biomaterials*, vol. 19, no. 18, pp. 1621–1639, Sep. 1998.
[104] P. R. Aldinger, A. W. Jung, S. J. Breusch, V. Ewerbeck, and D. Parsch, “Survival of the Cementless Spotorno® Stem in the Second Decade,” *Clinical Orthopaedics and Related Research®*, vol. 467, no. 9, pp. 2297–2304, Jun. 2009.
[105] P. J. Yates, B. J. Burston, E. Whitley, and G. C. Bannister, “Collarless polished tapered stem: clinical and radiological results at a minimum of ten years’ follow-up,” *J Bone Joint Surg Br*, vol. 90, no. 1, pp. 16–22, Jan. 2008.
[106] A. J. C. Lee, R. D. Perkins, and R. S. M. Ling, “Time-Dependent Properties of Polymethylmethacrylate Bone Cement,” in *Implant Bone Interface*, J. Older, Ed. London: Springer London, 1990, pp. 85–90.
[107] “CPT® 12/14 HIP SYSTEM.” Zimmer, 2008.
[108] B. J. Burston, A. J. Barnett, R. Amirfeyz, P. J. Yates, and G. C. Bannister, “Clinical and radiological results of the collarless polished tapered stem at 15 years follow-up,” *J Bone Joint Surg Br*, vol. 94, no. 7, pp. 889–894, Jul. 2012.

[109] P. Yates, D. Gobel, and G. Bannister, “Collarless polished tapered stem,” *The Journal of Arthroplasty*, vol. 17, no. 2, pp. 189–195, Feb. 2002.
[110] “Spectron EF Hip System.” Smith & Nephew.
[111] G. Garellick, H. Malchau, and P. Herberts, “The Charnley versus the Spectron hip prosthesis: clinical evaluation of a randomized, prospective study of 2 different hip implants,” *J Arthroplasty*, vol. 14, no. 4, pp. 407–413, Jun. 1999.
[112] P. S. Issack, H. G. Botero, R. N. Hiebert, M. R. Bong, S. A. Stuchin, J. D. Zuckerman, and P. E. Di Cesare, “Sixteen-year follow-up of the cemented spectron femoral stem for hip arthroplasty,” *J Arthroplasty*, vol. 18, no. 7, pp. 925–930, Oct. 2003.
[113] D. J. Berry, “Epidemiology,” *Orthopedic Clinics of North America*, vol. 30, no. 2, pp. 183–190, Apr. 1999.
[114] C. P. Duncan and B. A. Masri, “Fractures of the femur after hip replacement,” *Instr Course Lect*, vol. 44, pp. 293–304, 1995.
[115] K. J. Egan and P. E. Di Cesare, “Intraoperative complications of revision hip arthroplasty using a fully porous-coated straight cobalt—chrome femoral stem,” *The Journal of Arthroplasty*, vol. 10, pp. S45–S51, Nov. 1995.
[116] A. Moroni, C. Faldini, F. Piras, and S. Giannini, “Risk factors for intraoperative femoral fractures during total hip replacement,” *Ann Chir Gynaecol*, vol. 89, no. 2, pp. 113–118, 2000.
[117] J. Franklin and H. Malchau, “Risk factors for periprosthetic femoral fracture,” *Injury*, vol. 38, no. 6, pp. 655–660, Jun. 2007.
[118] H. Lindahl, “Three Hundred and Twenty-one Periprosthetic Femoral Fractures,” *The Journal of Bone and Joint Surgery (American)*, vol. 88, no. 6, p. 1215, Jun. 2006.
[119] R. Saluja and B. L. Bargar, “A Five-Step Approach to Preoperative Planning in Total Hip Arthroplasty,” in *Hip Replacement: Current Trends and Controversies*, R. K. Sinha, Ed. New York: Marcel Dekker, 2002, pp. 403–424.
[120] “Dr. Thomas Gross, South Carolina Joint Replacement Center,” *http://www.grossortho.com/*. [Online]. Available: http://www.grossortho.com/. [Accessed: 01-Nov-2013].
[121] P. C. Noble, “Biomechanical Advances in Total Hip Replacement,” in *Biomechanics in Orthopedics*, S. Niwa, S. M. Perren, and T. Hattori, Eds. Tokyo: Springer Japan, 1992, pp. 46–75.
[122] E. De Thomasson, C. Mazel, O. Guingand, and R. Terracher, “Value of preoperative planning in total hip arthroplasty,” *Rev Chir Orthop Reparatrice Appar Mot*, vol. 88, no. 3, pp. 229–235, May 2002.
[123] S. Eggli, M. Pisan, and M. E. Müller, “The value of preoperative planning for total hip arthroplasty,” *Journal of Bone & Joint Surgery, British Volume*, vol. 80-B, no. 3, pp. 382–390, May 1998.
[124] J. L. Knight and R. D. Atwater, “Preoperative planning for total hip arthroplasty. Quantitating its utility and precision,” *J Arthroplasty*, vol. 7 Suppl, pp. 403–409, 1992.
[125] A. G. Della Valle, D. E. Padgett, and E. A. Salvati, “Preoperative planning for primary total hip arthroplasty,” *J Am Acad Orthop Surg*, vol. 13, no. 7, pp. 455–462, Nov. 2005.
[126] R. Iorio, J. Siegel, L. M. Specht, J. F. Tilzey, A. Hartman, and W. L. Healy, “A Comparison of Acetate vs Digital Templating for Preoperative Planning of Total Hip Arthroplasty,” *The Journal of Arthroplasty*, vol. 24, no. 2, pp. 175–179, Feb. 2009.
[127] H. J. A. Crooijmans, A. M. R. P. Laumen, C. Pul, and J. B. A. Mourik, “A New Digital Preoperative Planning Method for Total Hip Arthroplasties,” *Clinical Orthopaedics and Related Research*, vol. 467, no. 4, pp. 909–916, Sep. 2008.

[128] Y. Kosashvili, N. Shasha, E. Olschewski, O. Safir, L. White, A. Gross, and D. Backstein, "Digital versus conventional templating techniques in preoperative planning for total hip arthroplasty," *Can J Surg*, vol. 52, no. 1, pp. 6–11, Feb. 2009.
[129] M. Viceconti, R. Lattanzi, B. Antonietti, S. Paderni, R. Olmi, A. Sudanese, and A. Toni, "CT-based surgical planning software improves the accuracy of total hip replacement preoperative planning," *Medical Engineering & Physics*, vol. 25, no. 5, pp. 371–377, Jun. 2003.
[130] E. Sariali, R. Mauprivez, F. Khiami, H. Pascal-Mousselard, and Y. Catonné, "Accuracy of the preoperative planning for cementless total hip arthroplasty. A randomised comparison between three-dimensional computerised planning and conventional templating," *Orthop Traumatol Surg Res*, vol. 98, no. 2, pp. 151–158, Apr. 2012.
[131] C. Eingartner, "Current trends in total hip arthroplasty," *Ortop Traumatol Rehabil*, vol. 9, no. 1, pp. 8–14, Feb. 2007.
[132] M. Honl, K. Schwieger, C. H. Gauck, F. Lampe, M. M. Morlock, M. A. Wimmer, and E. Hille, "[Comparison of total hip replacements cup orientation and position. Navigation vs. conventional manual implantation of hip prostheses]," *Orthopade*, vol. 34, no. 11, pp. 1131–1136, Nov. 2005.
[133] T. Leenders, D. Vandevelde, G. Mahieu, and R. Nuyts, "Reduction in variability of acetabular cup abduction using computer assisted surgery: a prospective and randomized study," *Comput. Aided Surg.*, vol. 7, no. 2, pp. 99–106, 2002.
[134] T. S. Keller, "Predicting the compressive mechanical behavior of bone," *Journal of Biomechanics*, vol. 27, no. 9, pp. 1159–1168, Sep. 1994.
[135] J. J. Schreiber, P. A. Anderson, H. G. Rosas, A. L. Buchholz, and A. G. Au, "Hounsfield units for assessing bone mineral density and strength: a tool for osteoporosis management," *J Bone Joint Surg Am*, vol. 93, no. 11, pp. 1057–1063, Jun. 2011.
[136] F. Taddei, L. Cristofolini, S. Martelli, H. S. Gill, and M. Viceconti, "Subject-specific finite element models of long bones: An in vitro evaluation of the overall accuracy," *Journal of Biomechanics*, vol. 39, no. 13, pp. 2457–2467, Jan. 2006.
[137] F. Taddei, E. Schileo, B. Helgason, L. Cristofolini, and M. Viceconti, "The material mapping strategy influences the accuracy of CT-based finite element models of bones: An evaluation against experimental measurements," *Medical Engineering & Physics*, vol. 29, no. 9, pp. 973–979, Nov. 2007.
[138] C. Zannoni, R. Mantovani, and M. Viceconti, "Material properties assignment to finite element models of bone structures: a new method," *Medical Engineering & Physics*, vol. 20, no. 10, pp. 735–740, Feb. 1999.
[139] E. Schileo, F. Taddei, A. Malandrino, L. Cristofolini, and M. Viceconti, "Subject-specific finite element models can accurately predict strain levels in long bones," *Journal of Biomechanics*, vol. 40, no. 13, pp. 2982–2989, Jan. 2007.
[140] X.-W. Zheng, "Finite Element Analysis of Stress Distribution of Cemented Stem After Total Hip Replacement," 2009, pp. 1–4.
[141] P. Colombi and L. Sgambi, "Non-linear finite element analysis of bone-cement interface condition in cemented total hip replacement," *Engineering Transactions*, vol. 47, pp. 99–115, 1999.
[142] R. D. Crowninshield, R. A. Brand, R. C. Johnston, and J. C. Milroy, "An analysis of femoral component stem design in total hip arthroplasty," *J Bone Joint Surg Am*, vol. 62, no. 1, pp. 68–78, Jan. 1980.

[143] A. H. Abdullah, M. N. M. Asri, M. S. Alias, and T. Giha, "Finite Element Analysis of Cemented Hip Arthroplasty: Influence of Stem Tapers," in *Proceedings of International MultiConference of Engineers and Computer Scientists*, Hong Kong, 2010, vol. 3.
[144] P. Beulah, S. Sivarasu, and L. Mathew, "Design optimization of skeletal hip implant cross-sections using finite-element analysis.," *J Long Term Eff Med Implants*, vol. 19, no. 4, pp. 271–278, 2009.
[145] W. Li, H. Lu, K. Sun, and X. Qiao, "Three-dimensional finite-element analysis and biomechanical design of femoral prosthesis," *Sheng Wu Yi Xue Gong Cheng Xue Za Zhi*, vol. 24, no. 6, pp. 1385–1389, 1393, Dec. 2007.
[146] A. A. Oshkour, N. A. Abu Osman, Y. H. Yau, F. Tarlochan, and W. A. B. W. Abas, "Design of new generation femoral prostheses using functionally graded materials: a finite element analysis," *Proc Inst Mech Eng H*, vol. 227, no. 1, pp. 3–17, Jan. 2013.
[147] A. S. Wong, A. M. R. New, G. Isaacs, and M. Taylor, "Effect of bone material properties on the initial stability of a cementless hip stem: a finite element study," *Proc Inst Mech Eng H*, vol. 219, no. 4, pp. 265–275, Jul. 2005.
[148] T. Otani, L. A. Whiteside, S. E. White, and D. S. McCarthy, "Effects of femoral component material properties on cementless fixation in total hip arthroplasty," *The Journal of Arthroplasty*, vol. 8, no. 1, pp. 67–74, Feb. 1993.
[149] E. J. Cheal, M. Spector, and W. C. Hayes, "Role of loads and prosthesis material properties on the mechanics of the proximal femur after total hip arthroplasty," *J. Orthop. Res.*, vol. 10, no. 3, pp. 405–422, May 1992.
[150] Y. K. Kang, H. C. Park, Y. Youm, I. K. Lee, M. H. Ahn, and J. C. Ihn, "Three dimensional shape reconstruction and finite element analysis of femur before and after the cementless type of total hip replacement," *J Biomed Eng*, vol. 15, no. 6, pp. 497–504, Nov. 1993.
[151] M. Lengsfeld, R. Burchard, D. Günther, T. Pressel, J. Schmitt, R. Leppek, and P. Griss, "Femoral strain changes after total hip arthroplasty — patient-specific finite element analyses 12 years after operation," *Medical Engineering & Physics*, vol. 27, no. 8, pp. 649–654, Oct. 2005.
[152] S. H. Teoh, W. H. Chan, and R. Thampuran, "An elasto-plastic finite element model for polyethylene wear in total hip arthroplasty," *J Biomech*, vol. 35, no. 3, pp. 323–330, Mar. 2002.
[153] M. E. Nadzadi, D. R. Pedersen, H. J. Yack, J. J. Callaghan, and T. D. Brown, "Kinematics, kinetics, and finite element analysis of commonplace maneuvers at risk for total hip dislocation," *J Biomech*, vol. 36, no. 4, pp. 577–591, Apr. 2003.
[154] D. Janssen, J. van Aken, T. Scheerlinck, and N. Verdonschot, "Finite element analysis of the effect of cementing concepts on implant stability and cement fatigue failure," *Acta Orthop*, vol. 80, no. 3, pp. 319–324, Jun. 2009.
[155] M. Pekedis, "Comparison of fatigue behaviour of eight different hip stems: a numerical and experimental study," *Journal of Biomedical Science and Engineering*, vol. 04, no. 10, pp. 643–650, 2011.
[156] S. L. Bevill, G. R. Bevill, J. R. Penmetsa, A. J. Petrella, and P. J. Rullkoetter, "Finite element simulation of early creep and wear in total hip arthroplasty," *Journal of Biomechanics*, vol. 38, no. 12, pp. 2365–2374, Dec. 2005.
[157] S. Agarwal, "Osteolysis—basic science, incidence and diagnosis," *Current Orthopaedics*, vol. 18, no. 3, pp. 220–231, Jun. 2004.
[158] L. W. Goldman, "Principles of CT and CT Technology," *Journal of Nuclear Medicine Technology*, vol. 35, no. 3, pp. 115–128, Sep. 2007.
[159] "Mimics - Materialise ©." [Online]. Available: http://biomedical.materialise.com/mimics. [Accessed: 05-Nov-2013].

[160] "ANSYS - ANSYS, Inc." [Online]. Available: http://www.ansys.com/. [Accessed: 06-Nov-2013].
[161] M. Bessho, I. Ohnishi, J. Matsuyama, T. Matsumoto, K. Imai, and K. Nakamura, "Prediction of strength and strain of the proximal femur by a CT-based finite element method," *Journal of Biomechanics*, vol. 40, no. 8, pp. 1745–1753, Jan. 2007.
[162] "MATLAB - © The MathWorks, Inc." [Online]. Available: http://www.mathworks.se/products/matlab/. [Accessed: 05-Nov-2013].
[163] I. Mori, Y. Machida, M. Osanai, and K. Iinuma, "Photon starvation artifacts of X-ray CT: their true cause and a solution," *Radiol Phys Technol*, vol. 6, no. 1, pp. 130–141, Jan. 2013.
[164] "Metal Deletion Technique (MDT) - ReVision Radiology," *ReVision Radiology*. [Online]. Available: http://www.revisionrads.com/. [Accessed: 05-Nov-2013]

7. Appendices

7.1. A1 – Matlab Segmentation Code

In order to be able to import the CT-data into Ansys all the images were segmented with a programmed script in Matlab. The script implements a semi-automatic process of segmenting the femur bone from other pixels in the image. This has to be done to every 2D slice comprising the CT-data. A polyline is used to surround the femoral bone (figure 45) and everything inside the enclosed line is excluded from the final picture (figure 46). The program works is the way, that is asks they user if he wants automatic segmentation or manual segmentation. Automatic segmentation is only usable below the femoral neck, where the cortical shell is thicker because the polyline searches for sudden rise in values in the image. This sudden rise is the difference between cortical bone and the surroundings. Where the cortical bone is not as solid as at the femoral shaft, the polyline will erase everything, so manual segmentation is necessary. In manual segmentation, the user selects the position and number of points to create the polyline, then the polyline moves between slides but can be adjusted for each of them.

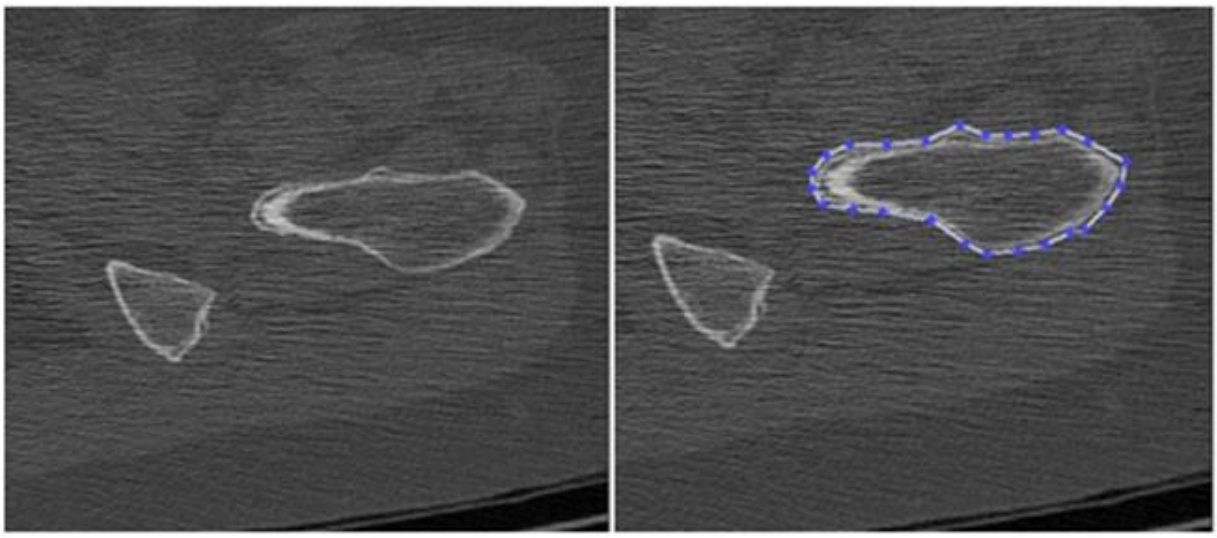

Figure 45: A polyline surrounds the femur bone

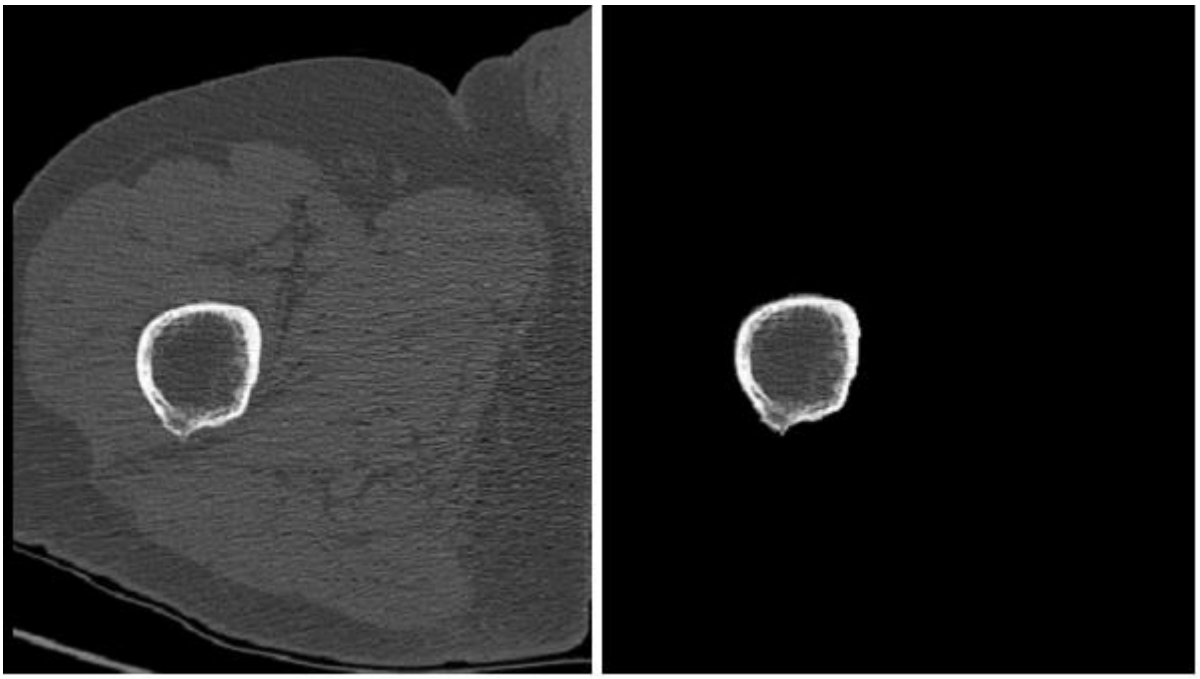

Figure 46: Everything outside of the closed polyline is excluded from the segmented image.

The following code is used to implement the methods described above. The code was developed in Matlab mathematical programming software. At the end is the graphical user interface that appears when the program is run (figure 47).

Face.m – a function to segment images.

```
function varargout = Face(varargin)
% FACE M-file for Face.fig

% Begin initialization code
gui_Singleton = 1;
gui_State = struct('gui_Name',       mfilename, ...
   'gui_Singleton',  gui_Singleton, ...
   'gui_OpeningFcn', @Face_OpeningFcn, ...
   'gui_OutputFcn',  @Face_OutputFcn, ...
   'gui_LayoutFcn',  [] , ...
   'gui_Callback',   []);
if nargin && ischar(varargin{1})
   gui_State.gui_Callback = str2func(varargin{1});
end

if nargout
   [varargout{1:nargout}] = gui_mainfcn(gui_State, varargin{:});
else
   gui_mainfcn(gui_State, varargin{:});
end
% End initialization code - DO NOT EDIT


% --- Executes just before Face is made visible.
```

```
function Face_OpeningFcn(hObject, eventdata, handles, varargin)
% This function has no output args, see OutputFcn.
% hObject    handle to figure
% eventdata  reserved - to be defined in a future version of MATLAB
% handles    structure with handles and user data (see GUIDATA)
% varargin   command line arguments to Face (see VARARGIN)

% Choose default command line output for Face
handles.output = hObject;

% Update handles structure
guidata(hObject, handles);


% --- Outputs from this function are returned to the command line.
function varargout = Face_OutputFcn(hObject, eventdata, handles)
% varargout  cell array for returning output args (see VARARGOUT);
% hObject    handle to figure
% eventdata  reserved - to be defined in a future version of MATLAB
% handles    structure with handles and user data (see GUIDATA)

% Get default command line output from handles structure
varargout{1} = handles.output;


% --- Executes on button press in pushbutton1.
function pushbutton1_Callback(hObject, eventdata, handles)
% hObject    handle to pushbutton1 (see GCBO)
% eventdata  reserved - to be defined in a future version of MATLAB
% handles    structure with handles and user data (see GUIDATA)

prompt={'Name','Surname','Weight'};
name='Patient Data';
numlines=1;
defaultanswer={'...','...','0'};
options.Resize='off';
options.WindowStyle='normal';
options.Interpreter='tex';
answer=inputdlg(prompt,name,numlines,defaultanswer,options);
namep= answer{1};
surname= answer{2};
weight= (answer{3});

errorstringa='...';
errorstringb='..';
errorstringc='.';
TFa = strcmp(namep(1:3),errorstringa);
TFb = strcmp(namep(1:2),errorstringb);
TFc = strcmp(namep(1),errorstringc);
TF1a= strcmp(surname(1:3),errorstringa);
TF1b= strcmp(surname(1:2),errorstringb);
TF1c= strcmp(surname(1:1),errorstringc);
N=str2double(weight);

if N>120
    error('You might mistake for patient weight')
else if N<40
```

```
        error('You might mistake for patient weight')
    end
end

if TFa==1
    error('Wrong name')
else if TFb==1
        error('Wrong name')
    else if TFc==1
            error('Wrong name')
        end
    end
end

if TF1a==1
    error('Wrong surname')
else if TF1b==1
        error('Wrong surname')
    else if TF1c==1
            error('Wrong surname')
        end
    end
end

K = menu('Patient Class','Uncemented','Cemented');
H = menu('Operated side','Left','Right');
D = menu('Acquisition','PREop','POSTop','ONEyear');

if K==1
    pclass= 'U';
else
    pclass= 'C';
end

if D==1
    pdata= 'pre';
else if D==2
        pdata= 'pos';
    else
        pdata= '1ye';
    end
end

if H==1
    side= 'L';
else
    side= 'R';
end

ini1= namep(1:2);
ini2= surname(1:2);
dicomname = strcat(ini1, ini2, weight, pclass, pdata,side);



set(handles.text78,'String',dicomname);
set(handles.pushbutton2, 'enable', 'on')
```

```
handles.dicomname=dicomname;
guidata(hObject,handles)

% --- Executes on button press in pushbutton2.
function pushbutton2_Callback(hObject, eventdata, handles)
% hObject    handle to pushbutton2 (see GCBO)
% eventdata  reserved - to be defined in a future version of MATLAB
% handles    structure with handles and user data (see GUIDATA)
DIM_X=512; %our images are all 512x512
DIM_Y=512;

dicomname = handles.dicomname;

prompt={'Insert Images Directory','First Slice to Segment','Number of Slices'};
name='Program Initialization';
numlines=1;
defaultanswer={'path','file name','0'};
options.Resize='off';
options.WindowStyle='normal';
options.Interpreter='tex';
answer=inputdlg(prompt,name,numlines,defaultanswer,options);
img_dir= answer{1};
strfile= answer{2};
N = str2double(answer{3});
ii=1;
done=0;

set(handles.text19,'String',img_dir);
set(handles.text20,'String',strfile);
set(handles.text21,'String',N);
set(handles.text22,'String',done);

% first image to start the segmentation
example= dicomread(fullfile(img_dir, strfile));
example=double(example);
figure('name','Manual or Automatic??')
imagesc(example)
colormap(gray)

K = menu('Choose Segmentation Method','Automatic', 'Manual');

% Manual Segmentaion:
if K==2
   set(Face, 'HandleVisibility', 'off');
   close all;
   set(Face, 'HandleVisibility', 'on');
   while ii<=N % run through all the images in a specified dir
      ind1= strfile(2:length(strfile));
      index1= str2double(ind1);
      new_index=index1+((ii-1)*20); % take every other slice, for non-overlap
      ind2= num2str(new_index);
      strfile1= strcat('I',ind2);
      image= dicomread(fullfile(img_dir, strfile1));
      info=dicominfo(fullfile(img_dir, strfile1));
      strfile2= sprintf('%s %s', 'Select the Roi of', strfile1);
      image=double(image);
```

```
        figure('name',strfile2,'Units','normalized','Position',[0 0 1 1])
        imagesc(image)
        colormap(gray)

        if ii==1
           h=impoly();
        else
           h=impoly(gca,h);
        end

        h=round(wait(h));
        mask=poly2mask(h(:,1)',h(:,2)',DIM_X,DIM_Y);
        close 1
        imagenew= image.*mask;
        imagenew= uint16(imagenew);

        figure('name','segmented','Units','normalized','Position',[0 0 1 1])
        imagesc(imagenew)
        colormap(gray)

        Default = 'Yes';
        button = questdlg('Do you like it?','AREA SELECTION','Yes','No',Default);

        switch button
           case 'Yes'
              set(Face, 'HandleVisibility', 'off');
              close all;
              set(Face, 'HandleVisibility', 'on');
              name_file=strcat(dicomname,strfile1(2:end),'.dcm');
              dicomwrite(imagenew,name_file,info)
              done=done+1;
              set(handles.text22,'String',done);
              ii=ii+1;
           case 'No'
              set(Face, 'HandleVisibility', 'off');
              close all;
              set(Face, 'HandleVisibility', 'on');
              ii=ii+0;
        end

    end

% Automatic segmentation
else if K==1
        set(Face, 'HandleVisibility', 'off');
        close all;
        set(Face, 'HandleVisibility', 'on');
        figure('name','Surround widely the Femur(to separate from the other)')
        imagesc(example)
        colormap(gray)
        h=impoly();
        h=round(wait(h));
        mask=poly2mask(h(:,1)',h(:,2)',DIM_X,DIM_Y);
        set(Face, 'HandleVisibility', 'off');
        close all;
        set(Face, 'HandleVisibility', 'on');
```

```
        while ii<=N
            ind1= strfile(2:length(strfile));
            index1= str2double(ind1);
            new_index=index1+((ii-1)*20); % slices overlapped then take half
            ind2= num2str(new_index);
            strfile1= strcat('I',ind2);
            image= dicomread(fullfile(img_dir, strfile1));
            info=dicominfo(fullfile(img_dir, strfile1));
            strfile2= sprintf('%s %s', 'Segmentation of ', strfile1);
            image=double(image);
            % IMlp=medfilt2(image,[4 4]);
            % A median filter is more effective than convolution when the goal
            % is to simultaneously reduce noise and preserve edges.
            H = fspecial('gaussian',[4 4],2.5);
            IMlp = imfilter(image,H); % apply a filter
            IMlp(IMlp<225)=0; % to isolate the bone
            BW = edge(IMlp,'log',[]);
            BW2 = imfill(BW,'hole');% to fill the hole inside the bone
            BW2=double(BW2); % mask

            aa=1;
            while aa==1
                R=1;
                se = strel('disk',R);
                BW2 = imopen(BW2,se);
                imagenew= BW2.*mask;
                imagenew=double(imagenew);
                a = image.*(imagenew);
                a = uint16(a);

                set(Face, 'HandleVisibility', 'off');
                close all;
                set(Face, 'HandleVisibility', 'on');
                name_file=strcat(dicomname,strfile1(2:end),'.dcm');
                dicomwrite(a,name_file,info)
                done=done+1;
                set(handles.text22,'String',done);
                ii=ii+1;
                aa=2;
            end
        end
    end
end
clc
guidata(hObject,handles)
```

Face.fig - Graphical User Interface for the function Face.m

Figure 47: Graphical user interface from the function Face.m

7.2. A2 – A New Modelling Method

When the two-dimensional medical images have been segmented to exclude everything except the femurs of the patients, they are imported into Ansys mechanical APDL to where a model is made. The first step is to create text files from the Dicom images, then the text files are used to create an array, including positional- and density information. With this information cube-shaped elements are created from the array. Figure 48 shows the top part of an Ansys Mechanical APDL-created model.

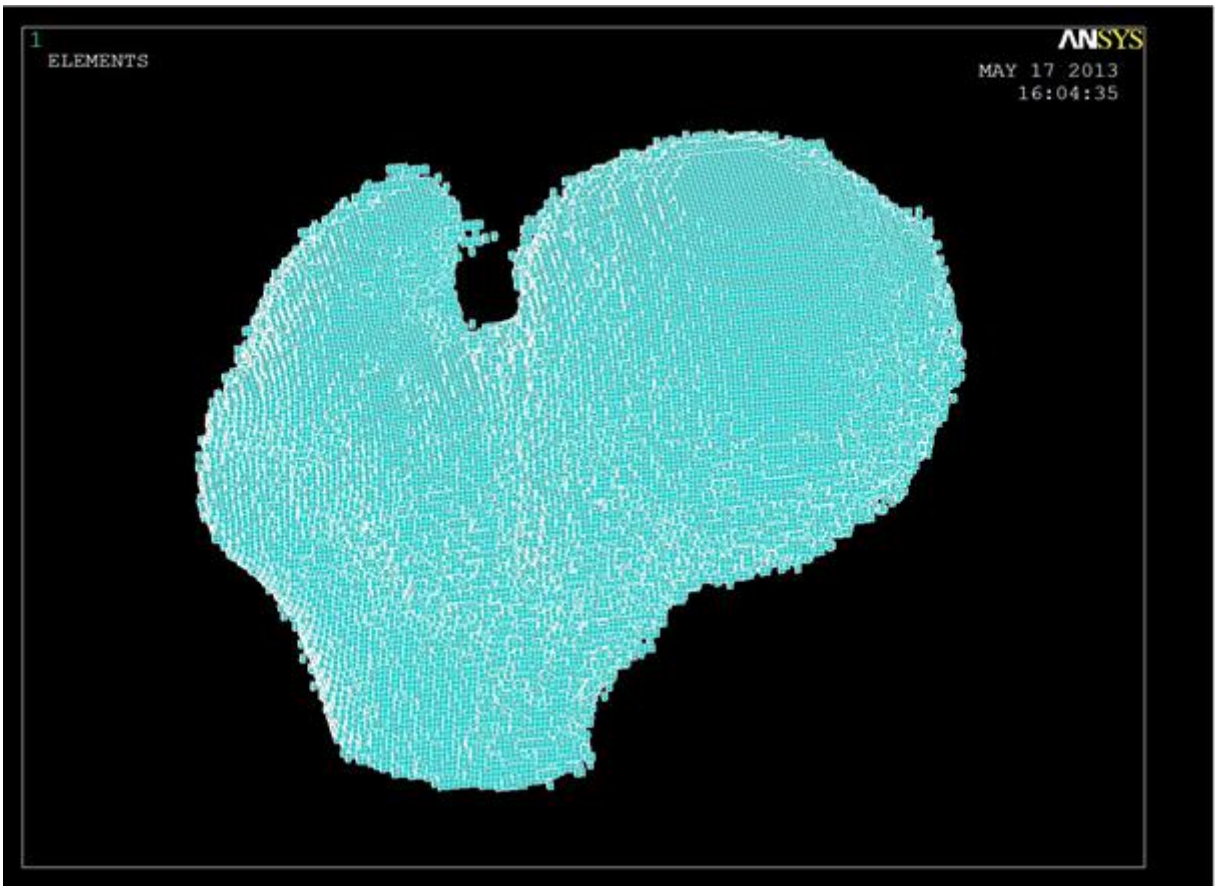

Figure 48: A 3D model built in Ansys mechanical APDL, from a pre-operative femur.

The model in figure 47 includes some isolated and unstable elements. Unstable elements are elements that are connected on only one or two nodes. These elements have to be erased to produce a model capable of transmitting load through it, based on boundary conditions.

Fracture risk index is still to be included in the simulations, but it is a work in progress. Models created in this way are more precise than the ones used in this study, however the process is more time-consuming. Although not calculating fracture risk, simulations, using this model, are publish-ready. They are based on boundary conditions mimicking the gait, similar to the biomechanical model described in chapter "biomechanical properties of bone.

When artifacts have been reduced from the post-data, modelling of this type can be used to evaluate bone addition or absorption around the prosthetic stem. This could add a new vital parameter to the assessment and monitoring of patients undergoing THA.

7.3. A3 – Artifact Reduction

Direct comparison between pre- and post-operation images is not possible due to image artifacts that stem from the metal prostheses (black and bright areas in image 49A). Image

artifacts stem from mechanisms such as scattering of photons, beam hardening, motion during imaging and photon starvation. If photons are scattered, not only attenuated, they are not sensed by the sensor. Stem hardening means that the mean energy of the photon beam is increased due to absorbed low-energy photons. Photon starvation occurs in the case of dense materials, where energy of photons is attenuated so rapidly that too few photons reach the detector. Photon starvation introduces strong streaks in images and can make them useless [163].

With the artifact reduction software *Metal Deletion Technique* from ReVision Radiology [164] the artifacts can be reduced to allow comparison (figure 49B). The MDT software reduces metal artifacts due to beam hardening, motion and photon scattering and starvation. The MDT software uses forward back projection to get an estimation of the raw scanner data. Then all projected data are used to reconstruct the pixels representing the metal. To reconstruct the soft tissue and bone, only non-metal data are used; the software looks around the metal, instead of trying to look through it when reconstructing everything besides the metal. With the metal pixels deleted, the reconstructed image is forward projected and used to replace the inaccurate metal data. Performing this iteratively improves the results.

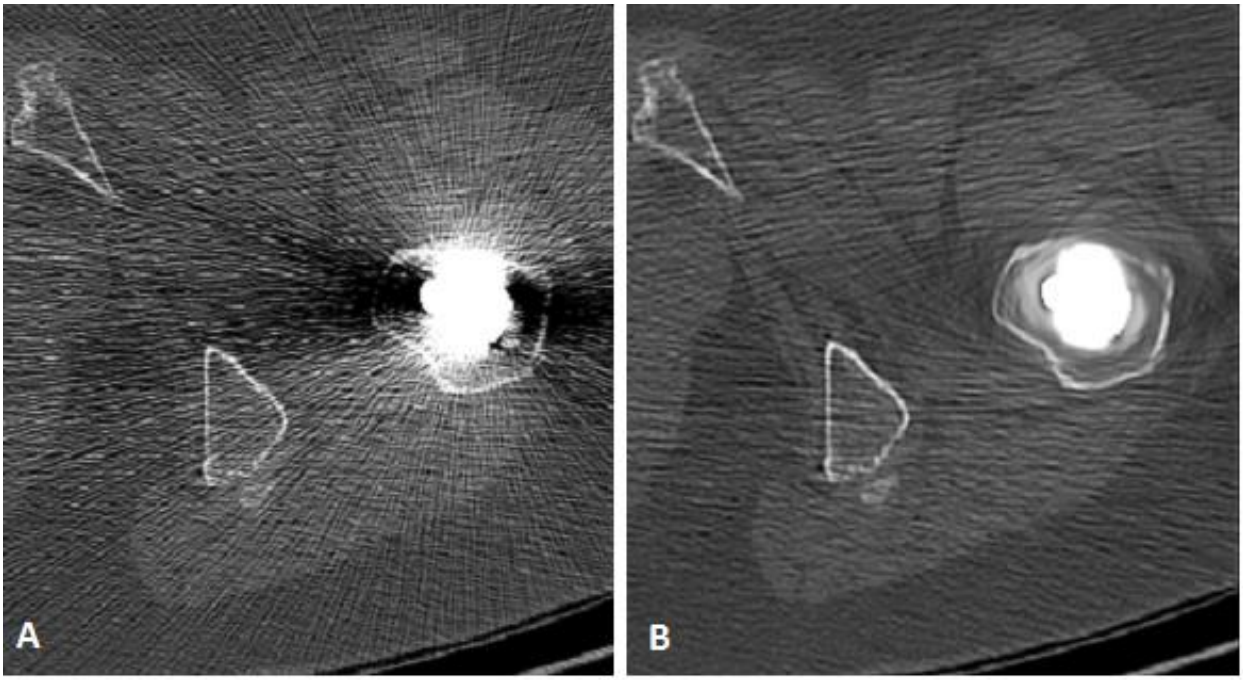

Figure 49: A) CT-slice of a THA patient post-surgery, filled with artifacts from the metal hip stem. B) After the reduction the artifact streaks are no longer there.